NASA CR-114623
Available to the Public

DESIGN INTEGRATION AND NOISE STUDIES FOR JET STOL AIRCRAFT

Task VIIC
Augmentor Wing Cruise Blowing Valveless System

Volume II—Small-Scale Development Testing of Augmentor Wing Critical Ducting Components

By J. N. Runnels and A. Gupta

November 1973

Prepared under Contract NAS2-6344 by

BOEING COMMERCIAL AIRPLANE COMPANY
P.O. Box 3707
Seattle, Washington 98124

for

Ames Research Center
NATIONAL AERONAUTICS AND SPACE ADMINISTRATION

1. Report No.	2. Government Accession No.	3. Recipient's Catalog No.
NASA CR-114623		

4. Title and Subtitle	5. Report Date
Design Integration and Noise Studies for Jet STOL Aircraft; Task VIIC, Volume II–Small-Scale Development Testing of Augmentor Wing Critical Ducting Components	November 1973
	6. Performing Organization Code
7. Author(s)	8. Performing Organization Report No.
J. N. Runnels and A. Gupta	D6-40879
	10. Work Unit No.
9. Performing Organization Name and Address	11. Contract or Grant No.
Boeing Commercial Airplane Company P.O. Box 3707 Seattle, Washington 98124	NAS2-6344
	13. Type of Report and Period Covered
12. Sponsoring Agency Name and Address	Contractor Report
National Aeronautics and Space Administration Washington, D.C. 20546	14. Sponsoring Agency Code

15. Supplementary Notes

16. Abstract

Experimental pressure loss data of:

- A unique strut-wing duct Y-junction incorporating flow convergence along the flow path
- A family of lobe-type blowing nozzles fed by flush-type flow offtakes

are presented over a range of operating conditions, compatible with current augmentor wing airplane system design studies. This development program was conducted to provide a firm technical base to conduct airplane performance analysis for the augmentor wing airplane configuration.

17. Key Words (Suggested by Author(s))	18. Distribution Statement
Augmentor wing Duct system Pressure loss Turbulent level Duct junction	Unclassified – Unlimited

19. Security Classif. (of this report)	20. Security Classif. (of this page)	21. No. of Pages	22. Price*
Unclassified	Unclassified	~~75~~ 78	7.00

*For sale by the National Technical Information Service, Springfield, Virginia 22151

CONTENTS

DESIGN INTEGRATION AND NOISE STUDIES FOR JET STOL AIRCRAFT

Volume II—Small-Scale Development Testing of Augmentor Wing Critical Ducting Components

By J. N. Runnels and A. Gupta

1.0 SUMMARY

The objectives of this test program were to:

- Investigate the flow characteristics of ducting components that have relatively high pressure loss coefficients
- Investigate turbulent pressure fluctuations associated with flows at high Mach numbers to evaluate potential duct fatigue problems

The overall program objectives for the design integration and noise studies for jet STOL aircraft are discussed in detail in reference 1.

Augmentor wing ducting-system studies conducted on a valveless system configuration that provides cruise thrust from the augmentor nozzles (fig. 1) have shown that most of the duct-system pressure loss would occur in the strut-wing duct Y-junction and the wing duct-augmentor lobe nozzles. These components were consequently selected for development testing over a range of duct Mach numbers and pressure ratios to provide a firm technical basis for predicting installed wing thrust loading and for evaluating design wing loading of particular wing aspect ratios.

The following significant conclusions were obtained from the test results:

1) The pressure loss in the strut-wing duct Y-junction is considerably lower in the inboard outlet than in the outboard outlet due primarily to the smaller angle turned relative to the strut duct (70° versus 110°). The installation of turning vanes in the Y-junction provides no significant improvement in pressure loss above inlet flow Mach numbers of 0.30. The average total pressure loss of the strut-wing duct Y-junction, at an inlet Mach number of 0.35, is approximately 2.6%, nearly 1% lower than anticipated. The pressure loss for this component is shown in figures 2 and 3.

2) Pressure loss from the wing duct to the nozzle exit is shown in figures 4 and 5. The data indicate that the flow losses

   - Increase with increase in nozzle turn angle (θ_N) and duct flow Mach number (M_D), but

- Decrease with increase in nozzle turn radius ratio (R_c/w) and nozzle spacing ratio (S/w^*),

as expected.

3) An axial wing-duct total pressure loss, resulting from the adverse pressure gradient imposed by offtaking air with discrete nozzles, was identified in this test. This characteristic, shown in figure 6, is a function of the individual nozzle area to duct flow area ratio.

4) The Y-junction without integral turning vanes (configuration Y-3) amplies the acoustic pressure level of the duct system by approximately 35 dB at an inlet flow Mach number of 0.32 (fig. 7). The design of large, thin-wall augmentor ducting will have to consider duct fatigue resulting from acoustic pressure levels.

2.0 INTRODUCTION

The potential for application of the augmentor wing concept to commercial STOL airplanes has been shown (refs. 1 and 2) to depend on achieving large noise suppressions while maintaining a high level of installed thrust in augmentors that fit within wing envelopes.

Augmentor air-ducting systems impose a thrust loss penalty on the aircraft due to pressure losses in the system (see fig. 8) and a weight and space penalty dependent on the physical size of the system. Weight and volume penalties of such systems can obviously be minimized by designing smaller diameter duct systems with higher flow velocities (fig. 9), but eventually the attendant pressure loss (fig. 10) overbalances other savings. A desirable balance between these penalties can be investigated for a specific design only if sufficient information is available to define the pressure loss characteristics of all system components over a wide range of operating conditions.

Current augmentor wing airplane air-ducting systems trade and optimization studies have not obtained adequate test data on the pressure loss characteristics of critical augmentor ducting-system components such as the strut-wing duct Y-junction and the wing-duct-lobe nozzle assemblies. System analysts have generally assigned pressure loss coefficients to these critical components based on limited low flow Mach number test data (refs. 3 and 4) derived from approximating the flow geometries of these components. The potential error in the overall pressure (or thrust) loss that is inherent in this method of analyzing ducting systems is considered too large for adequate analysis of the augmentor wing air-ducting systems being considered. Large overestimates or underestimates of pressure loss significantly affect airplane design (ref. 5); thus, the present small-scale development testing program was undertaken.

The main aims of this program were to:

1) Develop a low-pressure-loss strut-wing duct Y-junction with a 50% flow split suitable for installation in an augmentor wing airplane of wing aspect ratio up to 7.5 and engines located at 45% and 25% semispan.

2) Study the effect of various lobe nozzle design parameters on the overall wing-duct-lobe nozzle total pressure loss. Pertinent parameters are nozzle turn angle (θ_N), turn radius ratio (R_c/w), spacing ratio (S/w^*), and aspect ratio (h^*/w^*).

3) Establish the pressure loss characteristics of the test components over a wide range of operating conditions to facilitate augmentor wing airplane air-ducting system analysis and optimization studies. Significant operating variables are wing-duct Mach number and pressure ratio.

4) Investigate turbulent pressure fluctuations associated with flows at high Mach numbers to evaluate potential duct fatigue problems.

3.0 SYMBOLS AND ABBREVIATIONS

A	area, sq in.
A*	area at Mach 1.0, sq in.
c	chord
dB	decibel
F	thrust, lb
h*	lobe nozzle height at Mach 1.0, in.
M	Mach number
N	number of nozzles
NPR	nozzle pressure ratio
OASPL	overall sound pressure level, dB re 0.0002 μbar
P	pressure, psia
q	dynamic pressure, psi
R_C	nozzle offtake turn radius, in.
RSS	root sum square
S	nozzle centerline spacing, in.
T	temperature, °R
TP	tangent point
w	nozzle offtake passage width, in.
w*	lobe nozzle width at Mach 1.0, in.
w_A	airflow, lb/sec
x	distance, in.
γ	ratio of specific heats
δ	P/14.7, pressure ratio

Δ	differential
θ	T/520, temperature ratio
θ_N	nozzle rotation with respect to duct, deg
ξ	compressibility correction factor

Subscripts:

amb	ambient
D	duct
E	entry
in	inlet
L	local
N	lobe nozzle
NE	offtake entry
O	total
R	rake
S	static

4.0 DISCUSSION

The selection of the test facility, the establishment of model designs, and the implementation of test procedures were aimed at providing the most rapid and versatile test program, while exercising sufficient care to ensure confidence in test results. A reasonable balance between model costs and testing time was desired. Selection of the number and variety of wing-duct-lobe nozzle assemblies and strut-wing duct Y-junction configurations was based on a balance between model fabrication costs and the requirement for evaluating a representative number of configurations.

4.1 FACILITY

The Boeing North Field Mechanical Laboratories in Seattle, Washington, were chosen as the test location. The laboratories have a facility especially suitable for testing ducting components at high operating pressures and flows. An acoustically treated muffler plenum (fig. 11a), located upstream of the test model air-supply duct, prevents noise generated by the air-supply lines and control valves from reaching the test components.

4.2 TEST SETUP

Figure 12 shows a schematic of the test setup, which consists of an acoustically treated muffler plenum supplied from a bank of 300-psig compressed-air bottles at ambient temperature. The muffler plenum, located downstream of the main supply and flow-control valves, reduces the turbulent pressure fluctuations, generated by the air-supply lines and control valves, that propagate downstream to the test components. Microphones (Photocon) installed upstream and downstream of the muffler allow turbulent pressure fluctuations to be monitored. Burst disks (fig. 11a) are provided in the plenum to safeguard test components from overpressurization in the event the flow-control valve malfunctions or fails. The flow-control valve is a remotely controlled hydraulic-fluid-actuated valve and can be operated in both position and pressure control modes (fig. 11b). This test facility is capable of providing up to 30 lb/sec of compressed air for intermittent test runs of up to 5 min duration with no noticeable change in set test conditions.

4.3 TEST MODEL

The test model, shown in figure 13, consists of the two critical augmentor wing airplane air-ducting system components:

- Strut-wing duct Y-junction
- Wing-duct-lobe nozzle assembly

The following paragraphs discuss details of the test components, design variables, design philosophy, and instrumentation.

4.3.1 Strut-Wing Duct Y-Junction

All engine bleed air passes through the strut-wing duct Y-junction and can experience a high pressure loss. The design of this component is governed by the available space envelope as determined by detailed ducting system layouts of various competitive augmentor wing airplane studies, such as those presented in reference 2.

4.3.1.1 Design

The strut-wing duct Y-junction developed and tested in this program is shown in figure 14. It is comprised of a tight, 90° turn (centerline radius/duct diameter = 0.5), followed by two diverging passages (included angle = 60°), wherein the flow splits into two streams (fig. 15). The diverging passages turn the flow through 60° such that the flow exhausts out of the Y in a horizontal plane. The two exhaust ducts of the Y are turned 70° and 110° in the horizontal plane to match the orientation of the inboard and outboard wing ducts of an augmentor wing of wing sweep equal to 20°. This scale model (characteristic length, inlet diameter) represents the prototypes that can be installed in the available space of an augmentor wing airplane of wing aspect ratio up to 7.5, with wing sweep of 20° and with engines located at 25% and 45% semi-wingspan (ref. 2). The test model is approximately 1/4 scale of the airplane design Y-junction.

The test model was designed such that the flow continuously accelerates along the various turns to allow a favorable pressure gradient along the flow path. This flow convergence has been introduced in the design because of space limitations and to avoid adverse pressure-gradient-induced flow separation common in constant-flow-area turns.

Adverse pressure gradient is the cause of high pressure losses in conventional constant-flow-area turns. Its minimization or elimination in the present design is expected to lead to low pressure losses. For the test model, the flow area convergence along the turn is 25% of the turn inlet flow area. This results in an outlet Mach number of 0.50 for an inlet Mach equal to 0.35. The test model was designed for a 50% flow split in the two outlets based on the studies reported in reference 2. An included angle of 60° between the two outlets allows airplane structural clearance in the vicinity of the Y-junction.

Sheet metal turning vanes are provided in the various turns to facilitate the turning of the flow by increasing the effective mean turn radius/flow width ratio.

4.3.1.2 Test Configurations

The strut-wing Y-junction was tested with various combinations of turning vanes to determine their effectiveness. The configurations are identified in figure 16, and the turning vane shapes are shown in figure 17.

4.3.1.3 Instrumentation

The strut-wing duct Y-junction was instrumented with cruciform-type pressure rakes (fig. 17) at the inlet and outlets. Each rake had 29 total pressure probes and one static pressure tap.

Internal noise generated by the Y-junction was measured by a Photocon microphone installed flush with the wing-duct inner surface approximately 1 in. downstream of the Y-junction right outlet (fig. 12).

4.3.2 Wing-Duct-Lobe Nozzle Assembly

The wing-duct-lobe nozzle assemblies bolt to the Y-junction outlet (fig. 13). Six nozzle assemblies were tested, divided into two sets of three based on the nozzle spacing/width (S/w) ratio. Figures 18 and 19 give a plan view of the nozzles. Design details of these assemblies are shown in figures 20 through 25.

4.3.2.1 Design

The wing-duct nozzle assemblies were designed based on the system layout studies reported in reference 2. Each wing duct is a constant-diameter (inside diameter = 4.25 in.) and constant-length (length = 48.0 in.) duct with eight lobe nozzles equally spaced along its length. The total installed nozzle area on each duct is 10.55 sq in. This nozzle area, with operating pressures above critical pressure, yields a flow Mach number in the duct from 0 to 0.5, a range that is compatible with the flow Mach number range currently being considered for augmentor wing airplane air-ducting systems. In the test model, a constant-diameter duct rather than a tapered duct (airplane design) was selected to provide parametric pressure loss data relative to axial duct flow Mach numbers. The constant-diameter duct provides more gradually decreasing duct flow Mach numbers at measuring stations than does a tapered duct.

The nozzle offtakes for each nozzle assembly (figs. 20 through 25) are similar. They are set in the duct such that they act as flush scoops. The offtake turn is a constant-area turn. However, the turn radius/passage width (R_c/w) ratio and turn angle (θ_N) vary between the assemblies of a set. The offtakes feed the flow to the lobe nozzles, which converge linearly along their length. The convergence is one-dimensional, along the nozzle width, and the nozzle exit area is 56% of the nozzle inlet area. For operating pressure above critical pressure, this area ratio yields an offtake entry and turn Mach number of 0.35 and a flow acceleration from Mach 0.35 to 1 in the nozzle.

Studies of augmentor wing airplane air-ducting systems (ref. 2) have indicated that in major sections of the ducting system, flow Mach numbers in the 0.25 to 0.40 range are necessary to achieve relatively high thrust loading within the limited space available or ducting-system installation. The designed offtake inlet Mach number (0.35) of the present nozzle assemblies, over the above-mentioned typical flow Mach number range, provides an offtake inlet velocity ratio (M_{NE}/M_D) from 0.875 to 1.40, a range that provides low offtake pressure losses (ref. 5).

Wedge-shaped slotted nozzle shims, shown in figure 17, were designed for quick installation and removal to change the nozzle flow area. There are two sets of nozzle shims for each set of nozzle assemblies. The nozzle shims allow study of the effect of nozzle aspect ratio (defined as nozzle height/width [h*/w*]) on overall nozzle performance. They have the effect of changing the offtake inlet and turn Mach number and the rate of flow acceleration in the nozzle. The two sets of nozzle shims yield offtake inlet Mach numbers of

0.25 and 0.20. The corresponding duct flow Mach number ranges with the shims installed are approximately 0 to 0.390 and 0 to 0.300.

4.3.2.2 Test Configurations

The wing-duct-lobe nozzle assemblies were tested with and without nozzle shims. The various configurations are identified in table 1.

TABLE 1.—WING-DUCT-LOBE NOZZLE ASSEMBLY TEST CONFIGURATIONS

Nozzle assembly	S/w*	R_c/w	θ_N	N	h*/w* (a)	M_{NE} (a)	A_N* (a)
Set I							
DNA-1	12.0	3.0	90°	8	8.0, 6.54, 5.30	0.35, 0.25, 0.20	10.55, 8.60, 7.00
DNA-3	12.0	3.0	110°	8	8.0, 6.54, 5.30	0.35, 0.25, 0.20	10.55, 8.60, 7.00
DNA-5	12.0	2.0	110°	8	8.0, 6.54, 5.30	0.35, 0.25, 0.20	10.55, 8.60, 7.00
Set II							
DNA-2	9.0	3.0	90°	8	6.0, 4.91, 3.98	0.35, 0.25, 0.20	10.55, 8.60, 7.00
DNA-4	9.0	3.0	70°	8	6.0, 4.91, 3.98	0.35, 0.25, 0.20	10.55, 8.60, 7.00
DNA-6	9.0	2.0	70°	8	6.0, 4.91, 3.98	0.35, 0.25, 0.20	10.55, 8.60, 7.00

[a]First value is the design value; other values obtained by installation of nozzle shims.

4.3.2.3 Instrumentation

Four total and static pressure probes were located in each duct to determine duct flow conditions. The measuring stations were placed midway between two consecutive nozzles and upstream of nozzles 2, 4, 6, and 8. Wing-duct inlet conditions (conditions upstream of nozzle 1) were determined from the Y-junction outlet instrumentation (cruciform rake, fig. 17).

The nozzle exit plane was surveyed by a pressure rake consisting of 27 pressure probes arranged in nine rows of three (fig. 26). A minimum of five (15 probes) and a maximum of nine (27 probes) rows were used, depending on nozzle height.

4.4 DATA SYSTEM

Data were recorded using a Boeing-assembled standard digital data system, shown in figure 27. Four scanivalves and cutoff valves were used to sample the pressures to the Statham (50 psid) model PM131TC pressure transducers at the rate of two channels per second. NLS model 1400 signal conditioning units were used to balance and span pressure transducer signals. The resulting pressure readout was in engineering units.

A Tally model P120 paper punch and a Franklin model 1640 printer recorded the data simultaneously. The printer output was used for visual check of the data system operation and as a cross-check for the punch tape output.

The instrumentation equipment calibrations are traceable through the Flight Test Calibration Laboratory (FTCL) to the National Bureau of Standards (NBS). The accuracy of the data system is given in table 2.

TABLE 2.—DATA SYSTEM ACCURACY

Equipment	Accuracy, % of full scale
Transducer	±1
Mansfield and Green calibrator	±0.1
Hewlett-Packard 2402A DVM analog-to-digital converter	±0.1
Power and balance amplifier	±0.2
Pressure measuring system (RSS[a])	±1.3

[a]Root sum square value of independent errors

4.5 TEST PROCEDURE

The following test procedure was followed for each test run:

1) One wing-duct nozzle assembly from each set was attached to the Y-junction outlets (fig. 13). Care was taken to ensure that each assembly had essentially the same installed nozzle area to cause 50% flow split in the Y-junction. Nozzle exit plane pressure survey rakes were located at the exit of the nozzles under investigation. One nozzle on each duct was surveyed at a time (fig. 26), and nozzles 1, 2, 4, 6, and 8 were surveyed.

2) The remotely controlled flow-control valve was adjusted such that the desired supply pressure (36, 42, or 48 psia) was recorded by the Y-junction inlet cruciform pressure rake's central probe.

3) After the flow conditions had stabilized, the cutoff valves were closed and the pressure data were scanned and recorded at the rate of two channels per second. A total of 178 data items (including test constants, zero readings) were recorded for each run.

The above procedure was repeated to obtain data for various operating conditions and model configurations. A total of 135 test runs were made.

Strut-duct Y-junction internal noise at the three test points (fig. 12) was recorded on magnetic tape for selected configurations and operating conditions.

4.6 DATA REDUCTION AND TEST RESULTS

4.6.1 Strut-Wing Duct Y-Junction

Pressure loss and internal noise data reduction and test results are given in the following sections for the strut-wing duct Y-junction.

4.6.1.1 Pressure Loss Data Reduction

The strut-wing duct Y-junction average inlet and outlet total pressures were calculated from the pressures recorded by the total pressure probes of the respective cruciform rakes by an area-average method, which can be mathematically represented by the relation:

$$\overline{P} = \frac{\sum_{1}^{n} P_n (dA)_n}{\sum_{1}^{n} (dA)_n}$$

where:

$\overline{P}$ = average pressure (psia)

P_n = n^{th} probe recorded pressure (psia)

$(dA)_n$ = n^{th} probe domain area (sq in.)

n = number of probes

The inlet flow Mach number, M_{in}, was determined from the average inlet total pressure and the recorded inlet static pressure by the isentropic flow relation:

$$M = \left\{ \left(\frac{2}{\gamma - 1} \right) \left[(P_o/P_S)^{\frac{\gamma-1}{\gamma}} - 1 \right] \right\}^{0.5}$$

where:

M = flow Mach number

P_o = total pressure (psia)

P_S = static pressure (psia)

γ = ratio of specific heats (-)

The inlet flow dynamic pressure, q_{in}, was determined from the average inlet total and recorded static pressure by arithmetic difference. The pressure loss experienced by the flow

between inlet and outlet stations was found by the arithmetic difference of inlet and outlet average total pressures. The turbulent pressure fluctuation power spectral density was determined by analyzing the recorded acoustic data with a 20-Hz bandwidth and 512 degrees of freedom.

4.6.1.2 Pressure Loss Test Results

The pressure loss experienced by the flow in flowing from the inlet to the right and left outlets is shown in figures 28 through 30 for the three Y-configurations tested. The loss data have been presented as a function of inlet flow Mach number, both as a percentage pressure loss and as a pressure loss coefficient.

The data indicate that the flow experiences a higher pressure loss in flowing from the inlet to the outboard outlet than to the inboard outlet. Installation of flow turning vanes decreases substantially the pressure loss of the right outlet at low inlet flow Mach numbers (0.2 to 0.3), but at higher flow Mach numbers there is essentially no improvement in the pressure loss characteristics.

The observed unbalanced pressure loss of the two outlets is due primarily to the lack of symmetry of the Y-junction about its centerline. A close examination of figures 14 and 15 reveals that there is a sharper turn radius at the junction of the right outlet and inlet duct than at the junction of the left outlet. This lack of symmetry is introduced by the sweep of the outlets. The sharper inlet turn of the right outlet most probably causes the higher pressure drop.

The pressure loss exhibited by the strut-wing duct Y-junction is lower than the loss expected of a similar component whose design is based on existing technology that uses constant-flow area along the turns. The data meet the low pressure loss performance objectives and validate the design concept discussed in section 4.3.1.1.

4.6.1.3 Internal Noise Data Reduction

During the tests, the acoustic data were recorded in analog form on magnetic tape. At the conclusion of the test series, the magnetic tape analog data were reduced to 500 frequency bands, each 20 Hz wide. These data were then plotted (see figs. 31 through 36) as power spectral density (PSD) (psi^2/Hz versus frequency). Since the analysis was performed in 20-Hz-wide bands, the scale of the PSD plots is reduced by dividing the band level by the effective bandwidth. This technique may result in a pure tone being plotted as only 70% of its true level.

Please note: The symbol ◆ is plotted at the same value in figures 31 through 36 as an aid in comparing the six PSD plots.

4.6.1.4 Internal Noise Test Results

To ensure that the data taken at the Y-junction outlet (test point 3) are meaningful, data were recorded at two upstream locations. Figures 33 and 35 show the power spectral densities at the inlet of the muffler (test point 1) at two pressures, 22 and 34 psig; figures 34

and 36 show the corresponding at the outlet of the muffler (test point 2). Above 400 cycles, the outlet PSD is at least one order of magnitude below the inlet PSD. A comparison of figure 34 with figure 31 (test point 3) shows the rise in turbulence of the flow through the Y-junction.

Figure 31 demonstrates the strong dependence of the power spectral density on inlet Mach number, and figure 32 shows the relative insensitivity of the power spectral density changes in inlet pressure. These effects can be seen in the two curves of figure 37 labeled "Outlet microphone (test point 3), configuration Y-1."

Figure 37 presents the noise levels in terms of overall sound pressure levels rather than in psi^2/Hz. As such, these levels are independent of the energy in those frequency bands whose amplitude is one order of magnitude lower than the peak shown in the PSDs. In effect, figure 37 shows only the effect of energy below 400 Hz. Since the Y-junction is roughly 1/4 scale of an aircraft installation, the OASPL magnitude is indicative of energies below 100 Hz in an aircraft. The Y-junction amplifies the inlet noise by about 30 dB. Since the structure of the model is not exact, these data should be used with some caution in computing turbulent-flow-induced pressure loads for structurally safe design.

4.6.2 Wing-Duct-Lobe Nozzle Assembly

Pressure loss data reduction and test results are given below for the wing-duct-lobe nozzle assembly.

4.6.2.1 Data Reduction

The wing-duct total and static pressures were determined from the pressure probes located in the duct (see sec. 4.3.2.3). These pressures were used to determine duct flow Mach number (M_D).

The calculation of the nozzle exit plane total pressure is a two-step procedure, as described below:

1) Recorded average pressure is calculated from the total pressure probes of the nozzle rake by the area-average method described in section 4.6.1.1.

2) The nozzle rake recorded average pressure is lower than the actual nozzle exit plane pressure due to the modification of the rake probe's pressure recovery by the presence of a shock wave ahead of the probe (ref. 6). A compressibility correction is made for all measurements taken in a supersonic stream.

The recorded average nozzle pressure was corrected using the correction factors shown in figure 38. These correction factors were derived based on the assumption that the curved shock waves, ahead of the rake measuring probes, may be approximated by plane shock waves—an accepted practice.

The overall nozzle pressure loss was determined by the arithmetic difference between the duct total pressure (P_{T_1}) just upstream of the nozzle and the calculated nozzle exit plane pressure.

4.6.2.2 Test Results

The pressure loss characteristics of the test nozzle assemblies are shown in figures 39 through 50. The data are presented in terms of percentage duct total pressure drop as a function of duct flow Mach number. Percentage pressure loss ($\Delta P/P$) rather than pressure loss coefficient ($\Delta P/q$) was chosen as the significant parameter because:

- Pressure loss can be easily correlated to the thrust loss (fig. 8)
- Augmentor thrust loss is critical to airplane performance

If desired, the pressure loss data can be converted to pressure loss coefficients by use of the correlation curves shown in figure 51.

The pressure loss values shown in figures 39 through 50 account for the following losses:

- Offtake entry or nozzle capture loss
- Flow turning loss
- Nozzle frictional loss

and represent the overall loss that occurs between a point midway in the duct just upstream of the nozzle offtake and the nozzle exit plane.

In the paragraphs that follow, the effects of operating and design parameters on the pressure loss characteristics of the nozzle assemblies are discussed.

Effect of operating (or duct) pressure.—Figures 39, 41, 43, 45, 47, and 49 show that pressure loss varies with duct pressure. The observed variation does not show any clear trend, and this scatter is most probably due to instrumentation error and errors introduced due to the flow velocity profile and compressibility effects discussed below.

The root sum square (RSS) value of independent errors for the data system (sec. 4.4) is ±1.3% full scale. This RSS value, though representative of a good data system, can contribute data scatter ($\Delta P/P$) of up to 0.1%.

The data are referenced to the duct midpoint total pressure just upstream of the nozzle under investigation (sec. 4.3.2.3), with the duct midpoint total pressure measured by a single probe. The data recorded by this probe are influenced by the flow velocity profile and the data may exhibit some scatter. Variations in velocity profile are introduced by wall separation effects due to sudden expansion at upstream nozzle offtakes.

The nozzle exit plane total pressure was determined from the nozzle rake recorded total pressure (sec. 4.6.2.1) by applying compressibility correction factors; see figure 38. This method of calculating total pressures in supersonic flow is an accepted practice for single probes. However, in these tests, a rake consisting of multiple probes was used to

survey the nozzle exit, and interaction of multiple bow shock waves upstream of the rake probes could influence the compressibility correction factors, and hence cause data scatter.

Effect of duct flow Mach number.—Figures 39 through 50 show that the pressure loss for all nozzle assemblies increases with increase of duct flow Mach number, M_D. This is primarily due to offtake entry or nozzle capture loss. As the duct flow Mach number and flow dynamic pressure increase, the offtake entry (or nozzle capture) loss increases.

The various losses (sec. 4.6.2.2) that contribute to the overall pressure loss cannot be distinctively separated from the overall pressure loss at all operating conditions. However, a rough estimate of these losses can be made by investigating the pressure loss data as discussed below.

1) Duct Flow Mach Number Approaching Zero
As the duct flow Mach number approaches zero, the duct nozzle assembly reduces to the classical plenum nozzle combination. The overall loss exhibited is contributed solely by the offtake turn flow contraction and nozzle friction.

Close examination of the data showing duct flow Mach number approaching zero reveals:

- Nozzle turning and friction loss vary between 1.5% and 2.5% of the duct total pressure for all nozzle assemblies tested (figs. 39, 41, 43, 45, 47, and 49).

- Nozzle turning and friction loss show a trend that is indicative of decreasing loss with decreasing nozzle offtake (or nozzle entry) flow Mach number (figs. 39, 41, 43, 45, 47, and 49).

  The effect of nozzle offtake flow Mach number on the turning pressure loss cannot be explicitly determined from the present data due to the simultaneous presence of one or more design variables such as:
  Nozzle aspect ratio (h*/w*)
  Nozzle spacing/width ratio (S/w*)
  Offtake turn angle (θ_N)
  Offtake turn radius/width ratio (R_c/w)

- Nozzle turning and friction loss data suggest that the overall pressure loss is influenced by the offtake turn angle. At constant values of h*/w*, S/w*, and R_c/w, set I nozzle assemblies DNA-1 and DNA-3 (figs. 39 and 43) show a higher pressure loss for higher values of offtake turn angle, θ_N. However, set II nozzle assemblies DNA-2 and DNA-4 (figs. 41 and 45) indicate a reverse trend. This conflict of trends between the two sets of nozzle assemblies cannot be explained based on the limited available data. In view of small differences that exist, it is believed that the discrepancy is most probably due to instrumentation errors and/or manufacturing imperfections. In general, for identical nozzle and offtake combinations, the overall pressure loss decreases with decrease in turn angle due to lower pressure loss experienced in the negotiation of the turn.

- Nozzle turning and friction loss (figs. 43 and 47 and figs. 45 and 49) show a trend that suggests that the loss decreases with an increase in the turn radius/width ratio from 2.0 to 3.0. The decrease in loss is fairly small and variable (0 to 0.5%), thus indicating that other nozzle design parameters such as offtake entry Mach number (M_{NE}), θ_N, S/w, and h*/w* influence the change in pressure loss. In general, the pressure loss for turns decreases with an increase of turn radius/width ratio. However, increasing the turn radius/width ratio from 2.0 to 3.0 has an insignificant effect on the turn pressure loss coefficient.

2) Duct Flow Mach Number Greater than Zero

The pressure loss exhibited by the duct nozzle assemblies at all duct flow Mach numbers greater than zero is a combination of offtake entry, nozzle turning, and friction loss.

The nozzle turning and friction loss can be determined from the loss values at duct flow Mach number equal to zero (plenum condition). The offtake entry (or nozzle capture) loss, at any duct flow Mach number, can thus be approximated by:

$$(\Delta P/P)_{NE} = (\Delta P/P)_{M_D} = M_D - (\Delta P/P)_{M_D \to 0}$$

The offtake entry pressure loss is found to be strongly dependent (discounting for data scatter due to pressure) on the duct flow Mach number. As the duct flow Mach number and dynamic pressure increase, this loss increases progressively. At high duct flow Mach numbers, it contributes a substantial part to the overall pressure loss.

In theory, this loss should be independent of nozzle design parameters such as R_c/w, S/w*, θ_N, and h*/w* and should depend only on the offtake entry Mach number (hence, inlet velocity ratio M_{NE}/M_D). The test data, however, indicate slight variations for constant offtake entry Mach numbers (see figs. 40, 42, 44, 46, 48, and 50). The maximum variation observed for duct Mach number equal to 0.4 is approximately 1.5%.

The offtake entry pressure loss at constant duct Mach number is found to depend on the offtake entry Mach number. For low values of offtake entry Mach number, the pressure loss is smaller. This results from lower friction losses in the nozzle. The data also indicate that duct flow Mach number is a more significant parameter than inlet velocity ratio (M_{NE}/M_D) relative to offtake pressure loss (figs. 40, 42, 44, 46, 48, and 50).

4.6.2.3 Test Data Summary

The pressure loss exhibited by the test wing-duct nozzle assemblies varies from approximately 1.0% to 6.0% of the duct total pressure for duct flow Mach numbers in the 0 to 0.516 range. This loss of pressure is contributed by offtake entry, nozzle turning, and nozzle frictional losses.

Because of the numerous design and operating variables, empirical formulas for depicting pressure loss characteristics of nozzle assemblies outside the domain of this test must be developed for each specific nozzle assembly design. The use of curves shown in figures 4 and 5 is recommended for system evaluation studies. The data have been presented both as percentage pressure losses and pressure loss coefficients. The curves of figures 4 and 5 have been obtained by curve fitting the test data of respective nozzle assemblies using the method of least squares. All data points have been weighted equally. The data lend themselves to a good curve fit by a cubic algebraic equation.

4.6.3 Axial Pressure

Wing-duct axial pressure losses and Mach number distribution are correlated below, and the significance of flow offtake on axial pressure loss is discussed briefly.

4.6.3.1 Wing-Duct Axial Pressure Data Reduction

The axial pressure in the ducts was determined from the total and static pressure probes (four each) located in the ducts midway between two consecutive nozzles and upstream of nozzles 2, 4, 6, and 8. The flow conditions at the duct inlet were determined from the strut-wing duct Y-junction outlet cruciform rake.

4.6.3.2 Wing-Duct Axial Pressure and Mach Number Distribution

The axial pressure and flow Mach number distribution for ducts of set I (DNA-1, -3, and -5) are shown in figure 52 for three values of installed nozzle area. The data presented are the arithmetic mean of all test runs for the respective nozzle areas. Among individual test runs, data scatter was observed to be due to instrumentation system resolution limits and flow velocity profile effects. The degree of scatter was lower near the end of the duct than at the entry. Ducts of set II (DNA-2, -4, and -6) showed essentially the same axial pressure and flow Mach number distribution.

Figure 52 indicates that the axial pressure loss is a strong function of installed nozzle area (A_N*). The overall pressure loss decreases with decrease in nozzle area. Overall axial pressure loss changes from 5.0% to 2.0% when installed nozzle area is decreased from 10.55 to 7.00 sq in. This change arises due to lower flow Mach numbers in the duct system that correspond with lower values of installed nozzle area.

The axial pressure loss observed for all conditions is significantly greater than the calculated loss caused by friction and axial sudden expansions. This higher axial pressure loss is caused by the offtaking of flow, which introduces a sudden increase of axial static pressure and hence dissipation of axial pressure energy. The static pressure rise due to the offtaking of flow is far greater than the static pressure rise due only to the axial geometric area change at nozzle offtakes.

The static pressure rise from the offtaking of flow can be correlated to equivalent sudden expansion (upstream flow area/downstream flow area) based on isentropic flow equations. Analysis indicates that the equivalent sudden expansion due to flow exhausting

out of the nozzles is a variable for each nozzle and is independent of the total installed nozzle area. The values for the respective nozzles are tabulated below:

Nozzle no.	1	2	3	4	5	6	7	8
Equivalent sudden expansion	0.875	0.857	0.833	0.800	0.750	0.667	0.50	∞

The geometric axial area change, however, is constant for each nozzle but it depends on the total installed nozzle area. The respective values of axial geometric sudden expansions are:

Installed nozzle area (sq in.)	10.55	8.60	7.00
Geometric sudden expansion	0.915	0.928	0.940

The above indicates the significance of flow offtake on axial pressure loss. Investigation of offtake flow losses was not a part of the test program, and the duct was not instrumented to investigate these losses in detail. However, limited data were extracted from the test runs, as discussed below.

4.6.3.3 Nozzle Offtake Axial Pressure Loss Coefficient

The pressure drop in the wing duct between a station upstream of nozzle 1 (strut-wing duct Y-junction outlet cruciform rake data) and a station downstream of nozzle 1 provides a value for the pressure drop in a segment of the duct that consists of a single nozzle offtake. The pressure drop between these two measuring stations is due to:

- Duct friction
- Axial geometric area change
- Offtake flow

From these data, the pressure loss due to duct friction and axial geometric area change can be separated based on flow conditions, duct geometry, and friction factor; hence, the loss due to offtake flow can be determined.

Figure 53 shows the axial pressure loss coefficient, based on upstream flow dynamic pressure, as a function of local areas at nozzle offtake. This loss is due to the offtake flow. The data represent the mean for the three test values of installed nozzle area. The data indicate that the offtake axial pressure loss is a function of the local nozzle area/local duct area ratio $(A_N^*/A_D)_L$ or the local exhaust flow. The loss coefficient increases as $(A_N^*/A_D)_L$ increases, due to the rapid rise of duct static pressure.

The plot of axial pressure loss coefficient as a function of fractional duct area at nozzle offtake, $[A_D/(A_D + A_N^*)]_L$, also indicates that the loss coefficient is a function of offtake flow. The correlating empirical relation for the tested offtakes over the range of test variables is determined to be parabolic of the approximate form:

$$\frac{\Delta P}{q_D} = 5.9 \left[1 - \left(\frac{A_D}{A_D + A_N^*} \right)_L \right]^2$$

5.0 CONCLUSIONS AND RECOMMENDATIONS

The test program has resulted in performance data of augmentor wing airplane critical ducting components. The data, which have been presented in terms of percentage pressure drop and pressure loss coefficient as a function of flow Mach numbers, can be readily used in both manual and computerized calculations for the evaluation and optimization of ducting systems.

The pressure loss data on the strut-wing duct Y-junction indicate that the main program objective—development of a low-pressure-loss Y-junction—has been satisfactorily met. For its critical outlet leg (right), the Y-junction at its highest test operating inlet flow Mach number (0.35) shows a pressure loss of 2.8% (pressure loss coefficient = 0.35). The corresponding pressure loss for the inboard outlet is approximately 1.85% (pressure loss coefficient = 0.21). This unbalanced pressure loss of the two outlets is due to different turn radii at the entrance of the two Y outlets. The pressure loss exhibited by this component is lower than the pressure loss expected of a similar component,based on available test data on turns, and is well within the acceptable pressure loss limit. The data validate the design concept and illustrate that introduction of flow convergence along the turn suppresses adverse pressure-gradient-induced flow separation. Reduction of Y-junction outboard outlet pressure loss by additional development is feasible.

The Y-junction outlet turbulent-flow power spectral density traces indicate the presence of high, fluctuating pressure loads. These loads can contribute to premature system or component failure due to fatigue or resonance. Consideration of these loads in the early design stage is recommended for a structurally safe design.

The lobe nozzle pressure loss, at a duct flow Mach number approaching zero, is found to vary between approximately 1.5% to 2.5% of the nozzle upstream (duct) total pressure. This loss, which is comprised of nozzle turning and nozzle friction loss, is essentially insensitive to design parameters such as nozzle spacing/width ratio (S/w*) and nozzle aspect ratio (h*/w*) over the range of design parameters tested. This pressure loss is found to vary with nozzle turn angle (θ_N) and nozzle turn radius/width ratio (R_c/w). Conclusions on the effect of θ_N on the pressure loss cannot be drawn from the limited test data, which show conflicting trends. The pressure loss for identical nozzles increases with a decrease in R_c/w.

The strut-wing turning loss and lobe nozzle pressure loss data, discussed above, suggest the following guidelines for the design of low-pressure-loss lobe nozzles:

- High turn radius/width ratio
- Low turn flow Mach number
- Flow convergence along the turn

Test of manufactured lobe nozzles based on the above design guidelines is recommended to optimize lobe nozzle performance. A decrease of from 20% to 30% of the recorded lobe nozzle pressure loss is considered feasible by the above design guidelines.

The nozzle offtake entry pressure loss is found to depend strongly on the duct flow Mach number. This pressure loss, determined by the arithmetic difference of the overall wing-duct-lobe nozzle assembly loss at flow Mach number M_D and at zero, increases with increase of duct flow Mach number. Typically, this loss has been determined to contribute from 1.8% to 3.0% of the overall wing-duct-lobe nozzle assembly pressure loss at a duct flow Mach number equal to 0.45. This represents a nozzle offtake, duct flow dynamic pressure recovery of from 85% to 75%, which agrees fairly well with the dynamic pressure recovery of flush-type scoops.

The nozzle offtake entry pressure loss is found to depend on the offtake inlet Mach number. The data suggest that the nozzle offtakes for low pressure loss should be designed such that they operate at an entry Mach number of approximately 0.25.

The wing-duct axial pressure loss (offtake axial pressure loss) coefficient is determined to depend on the local nozzle flow area. It increases as the local nozzle area or offtake flow increases. The data suggest that this loss can be minimized by decreasing individual offtake flows, i.e., by distributing the required nozzle area over a larger number of lobe nozzles.

In the present program, investigation of this loss was not a part of the study, and the duct was not instrumented to investigate the loss in detail. The limited test data obtained, however, indicate that this loss can be significant. It is recommended that further tests be conducted on lobe nozzle configurations to minimize the axial pressure loss resulting from offtaking air from wing ducts. A continuous-slot nozzle would presumably not have as high an axial pressure loss as that exhibited by the test lobe nozzle arrangement.

Generally, while component losses varied significantly from previously assumed values, losses for the complete distribution system were essentially as predicted. Table 3 compares previously assumed loss coefficients with results from this test at a nominal operating flow Mach number equal to 0.35.

TABLE 3.–PRESSURE LOSS COEFFICIENT COMPARISON

Component	Total pressure loss coefficient, $\Delta P_T/q_D$	
	Assumed	Test results
Strut-wing duct Y-junction	0.45 ($\Delta P/P$ = 3.7%)	0.32 ($\Delta P/P$ = 2.6%); figures 28-30
Wing-duct-lobe nozzle	0.50 ($\Delta P/P$ = 4.10%)	0.40 ($\Delta P/P$ = 3.3%); figures 39-50
Wing duct (axial)	Friction loss as a function of Reynolds number	Friction as a function of Reynolds number plus nozzle offtake pressure loss, a function of $(A_N^*/A_D)_L$; figure 53

Boeing Commercial Airplane Company
P.O. Box 3707
Seattle, Washington 98124, November 30, 1973

6.0 REFERENCES

1. O'Keefe, J. V.; and Kelley, G. S.: *Design Integration and Noise Studies for Jet STOL Aircraft,* Vol. I–"Program Summary." NASA CR-114471 (originally issued as CR-114283), May 1972.

2. Roepcke, F. A.; and Kelley, G. S.: *Design Integration and Noise Studies for Jet STOL Aircraft,* Task VIIA, Augmentor Wing Cruise Blowing Valveless System; Vol. II–"Design Exploration." NASA CR-114570 (originally issued as NASA CR-114284), April 1973.

3. Society of Automotive Engineers, *SAE Aerospace Applied Thermodynamics Manual,* Society of Automotive Engineers, Inc., New York.

4. Gupta, A.; and Angrisani, S.: *Wing Duct-Nozzle Turning Pressure Loss Characteristics Applicable to Augmentor Wing STOL Airplane Design.* D6-54343 TN, The Boeing Company, 1971.

5. Gupta, A.; and Runnels, J. N.: *Analytical Techniques for Augmentor Wing Airplane Design Gross Weight Optimization.* D6-40376 TN, The Boeing Company, 1972.

6. Houghton, E. L.; and Brock, A. E.: *Tables for the Compressible Flow of Dry Air,* Edward Arnold (Publishers), Ltd., 1961.

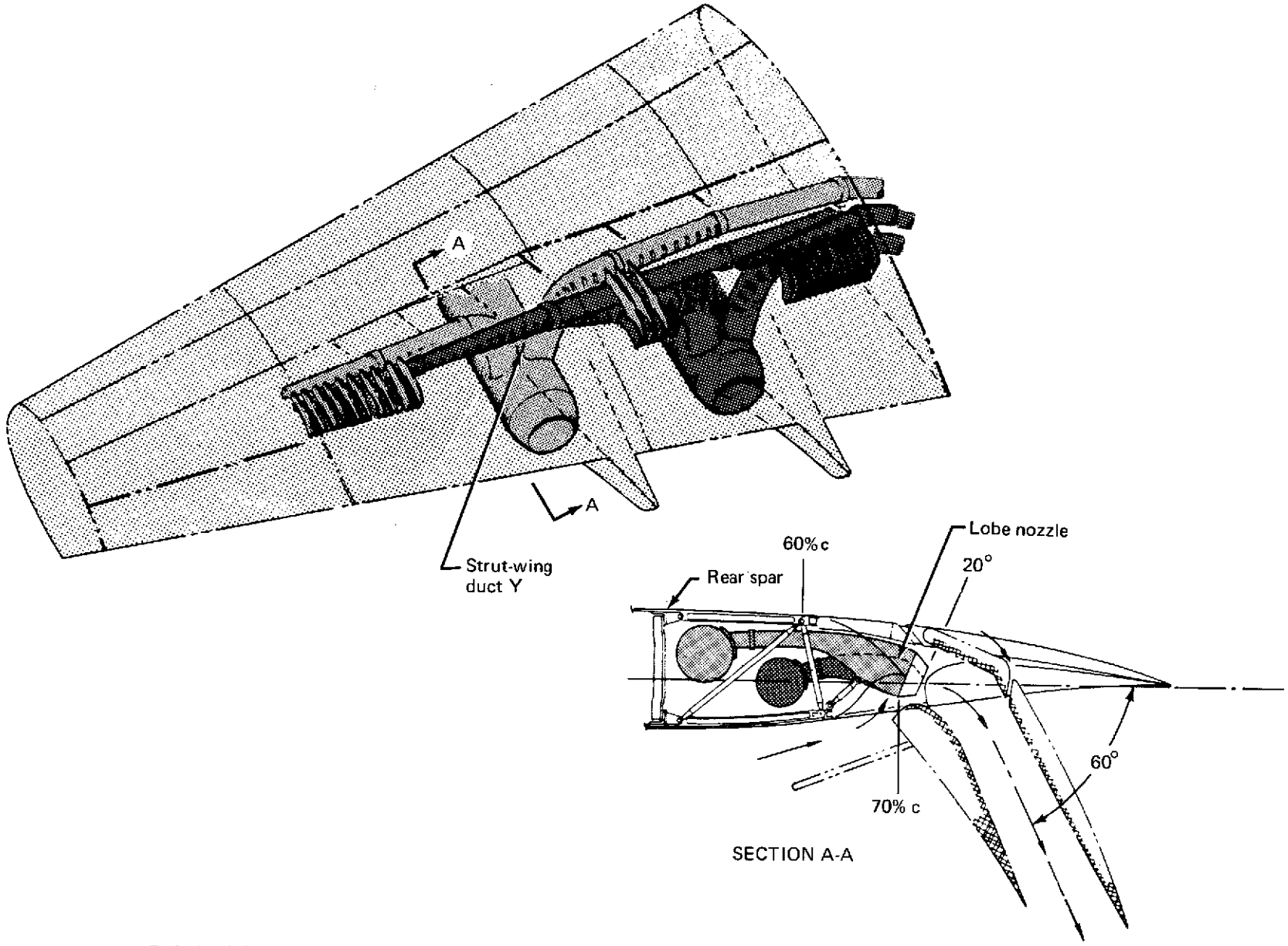

FIGURE 1.—AUGMENTOR WING DUCTING SYSTEM CONFIGURATION (VALVELESS DESIGN)

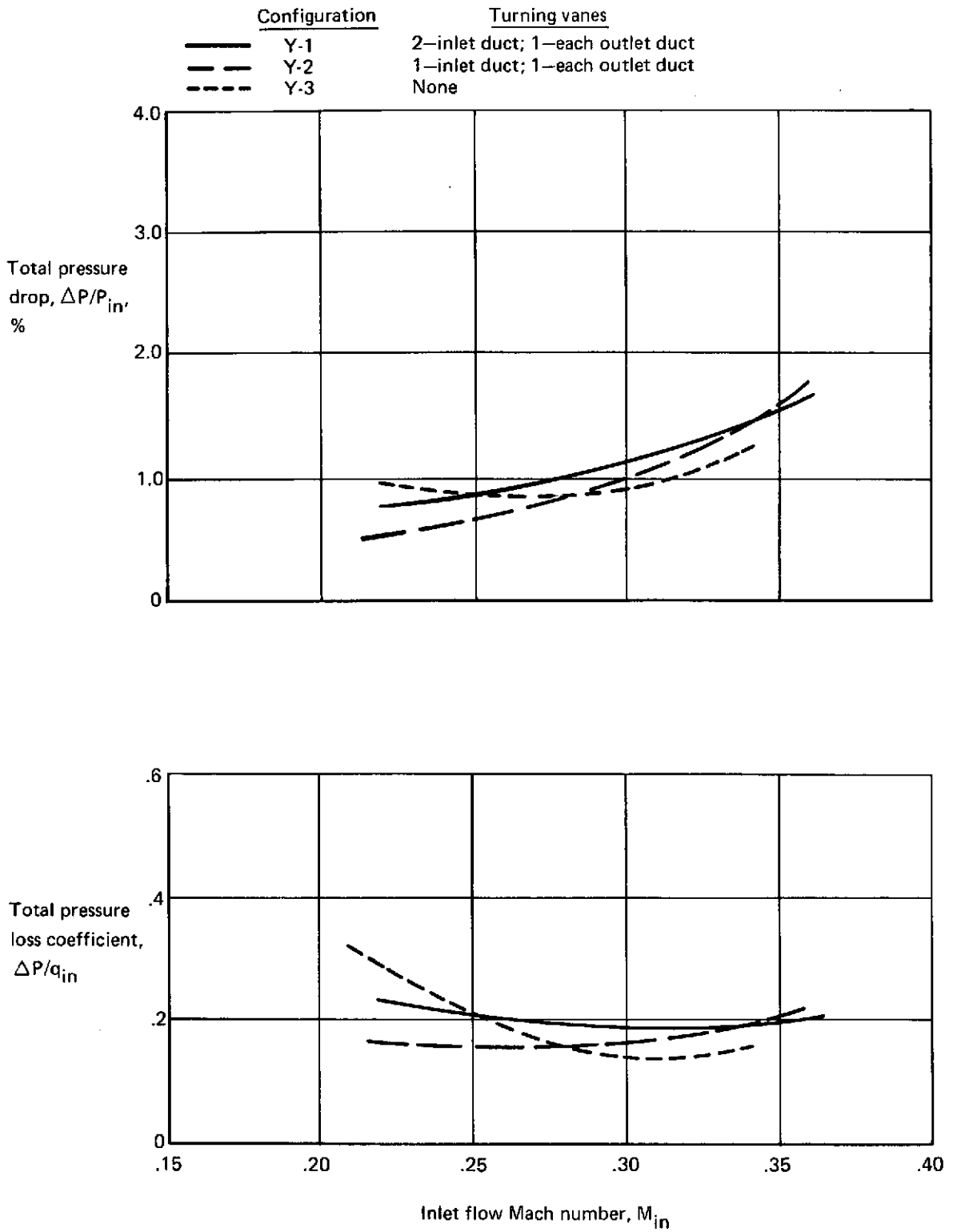

FIGURE 2.—INBOARD OUTLET PRESSURE LOSS, CONFIGURATIONS Y-1, Y-2, AND Y-3

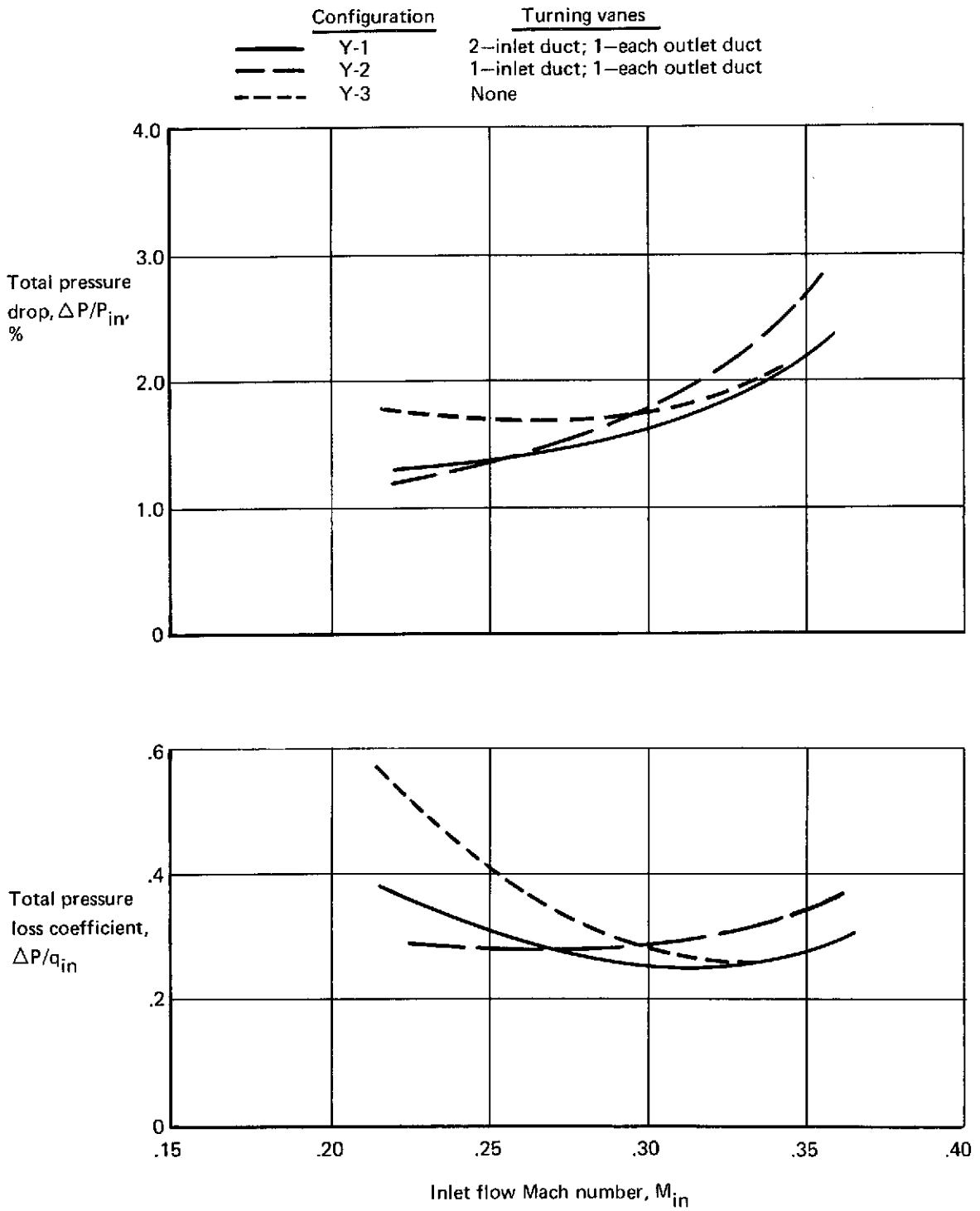

FIGURE 3.—OUTBOARD OUTLET PRESSURE LOSS, CONFIGURATIONS Y-1, Y-2, AND Y-3

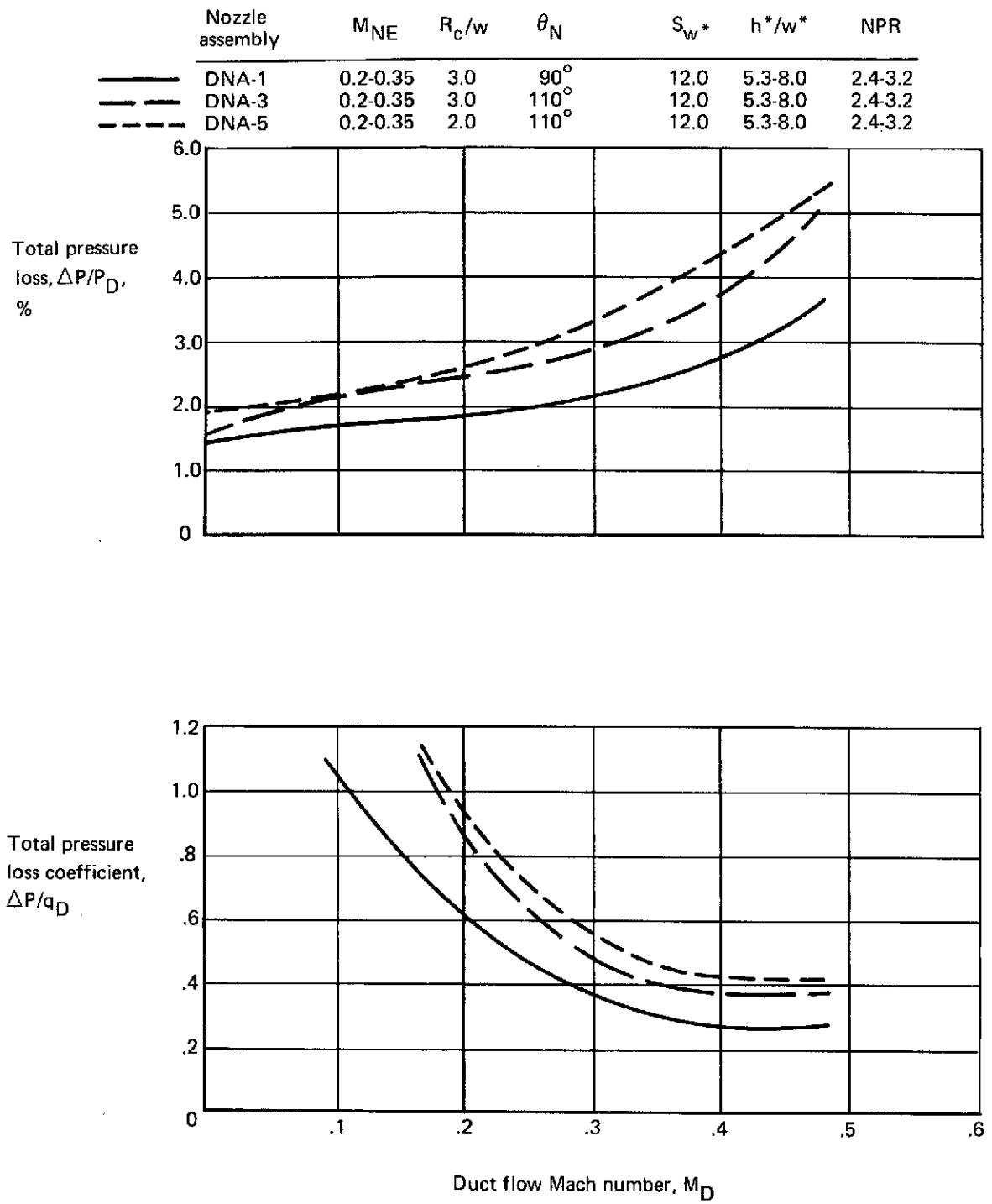

FIGURE 4.–PRESSURE LOSS, SET I LOBE NOZZLE ASSEMBLIES

	Nozzle assembly	M_{NE}	R_c/w	θ_N	S/w*	h*/w*	NPR
———	DNA-2	0.2-0.35	3.0	90°	9.0	3.98-6.0	2.4-3.2
— —	DNA-4	0.2-0.35	3.0	70°	9.0	3.98-6.0	2.4-3.2
– – – –	DNA-6	0.2-0.35	2.0	70°	9.0	3.98-6.0	2.4-3.2

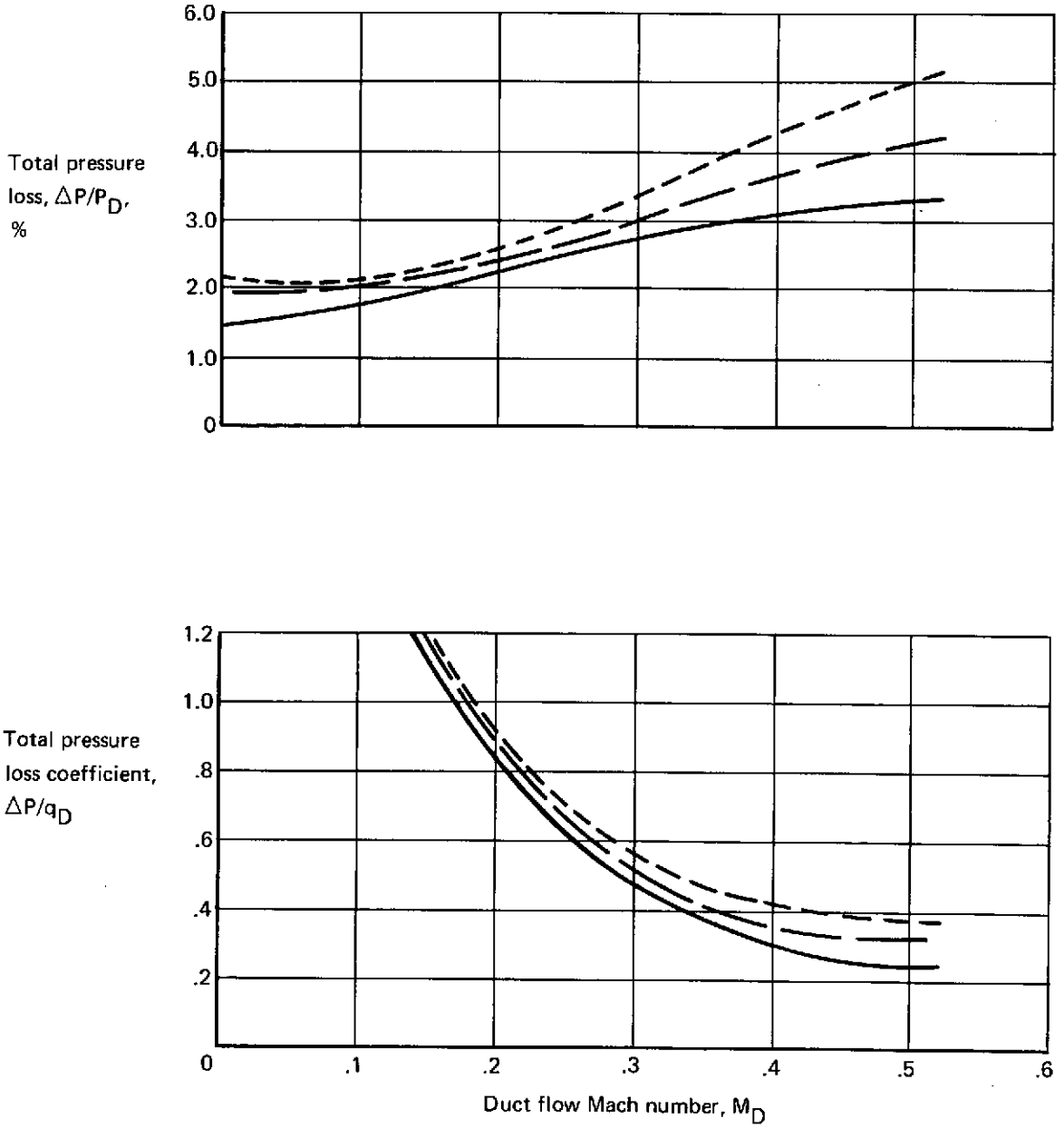

FIGURE 5.—PRESSURE LOSS, SET II LOBE NOZZLE ASSEMBLIES

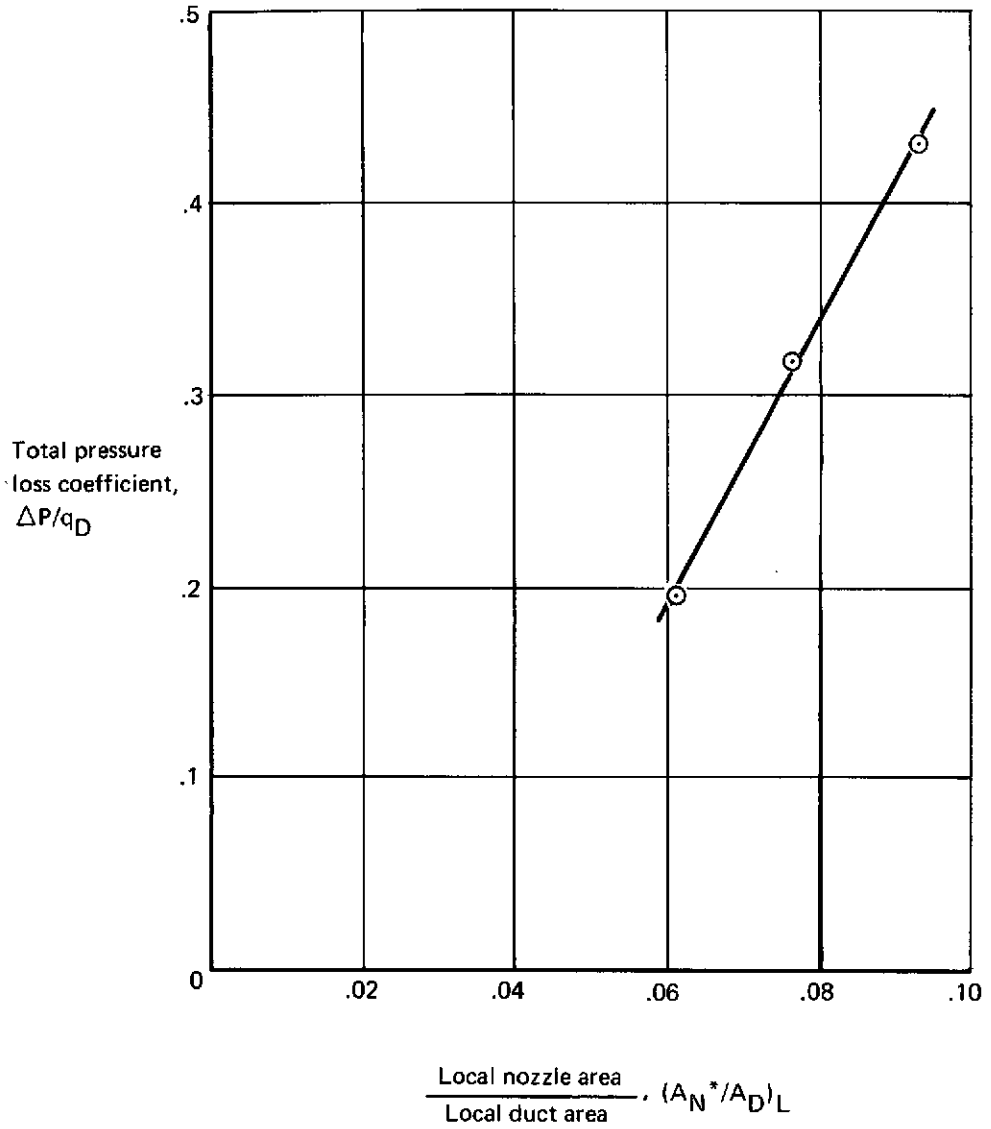

FIGURE 6.—DUCT AXIAL PRESSURE LOSS COEFFICIENT, SINGLE-NOZZLE OFFTAKE

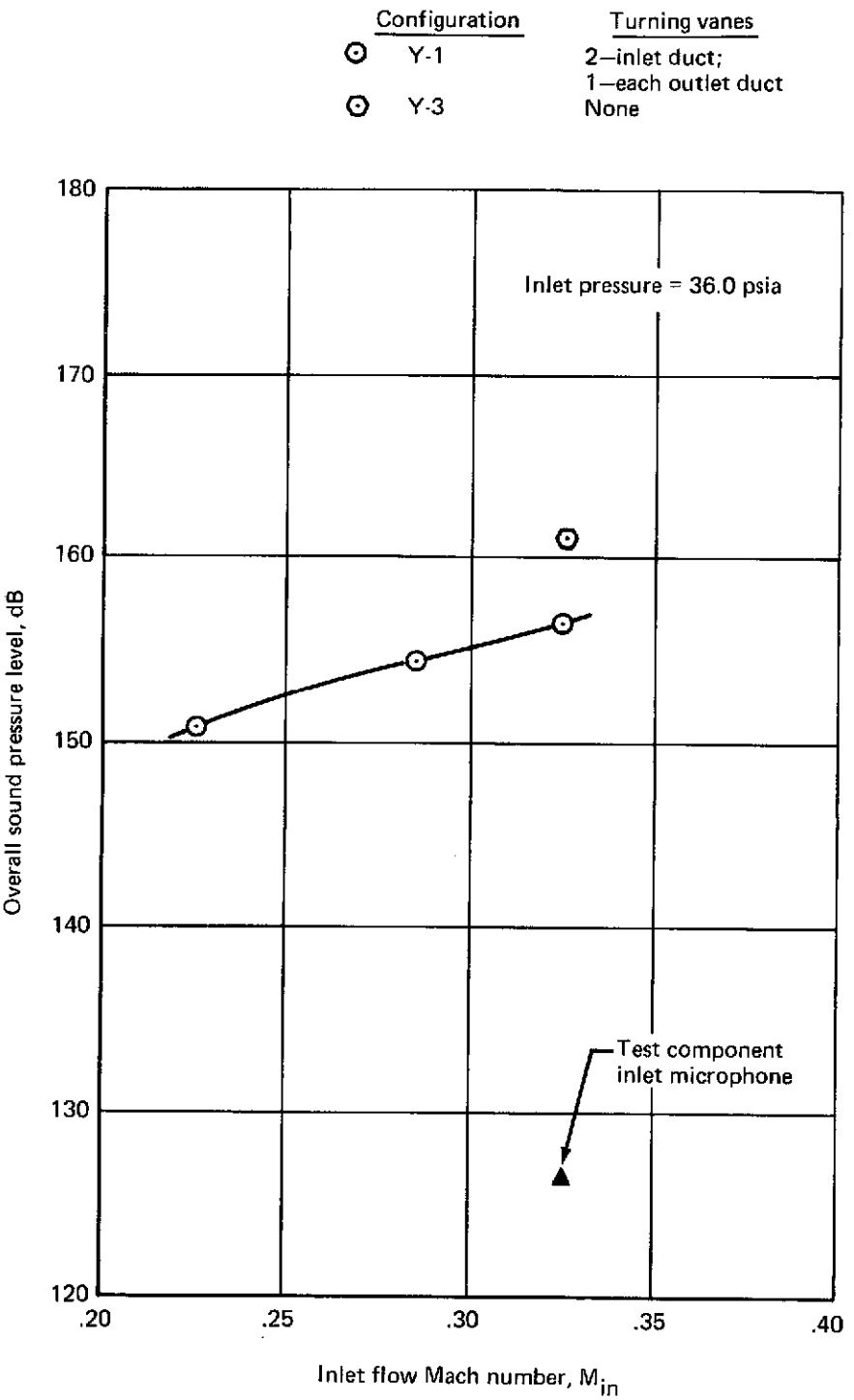

FIGURE 7.—OUTLET DUCT OVERALL SOUND PRESSURE LEVEL

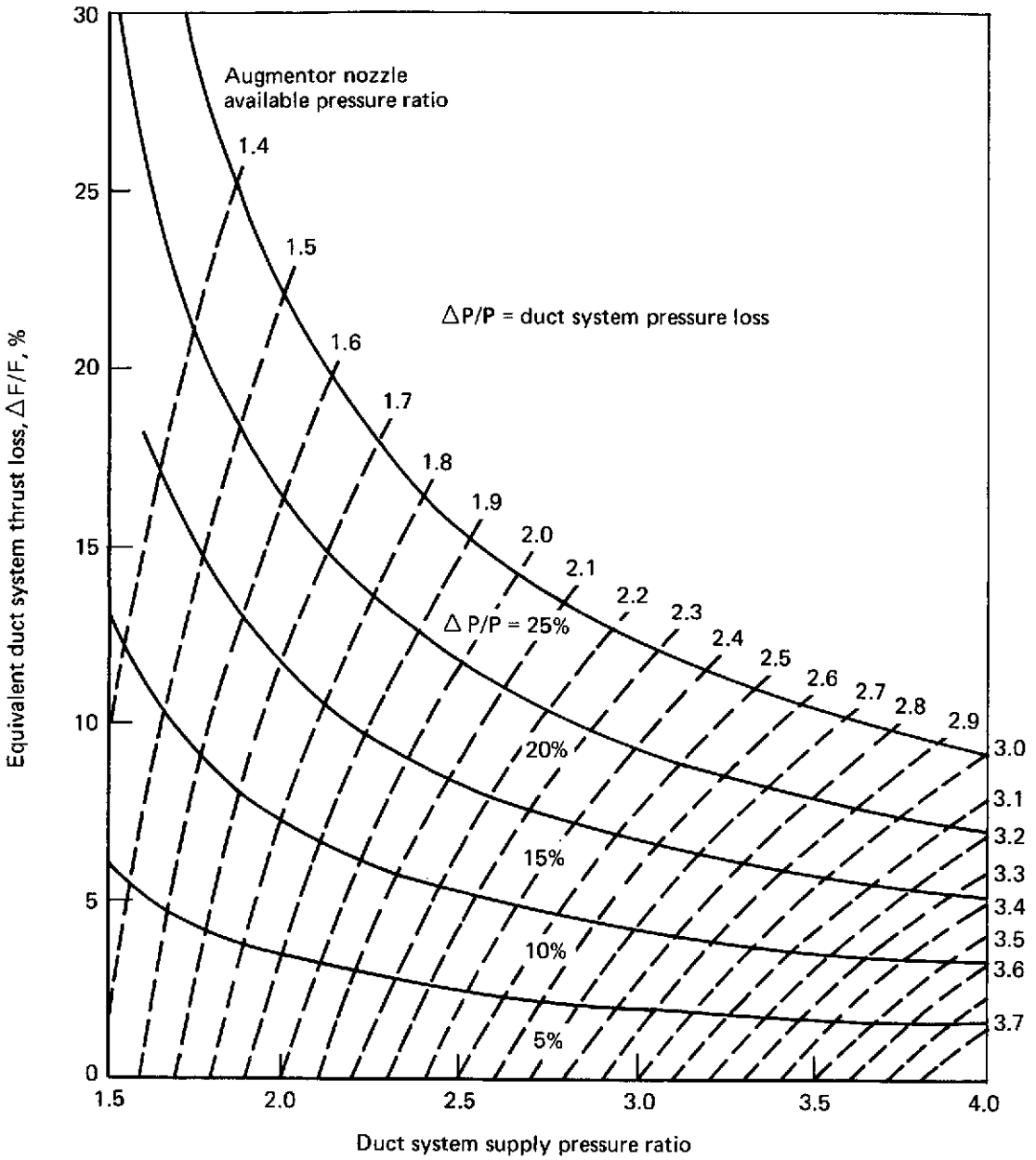

FIGURE 8.–PRESSURE LOSS/THRUST LOSS CORRELATION

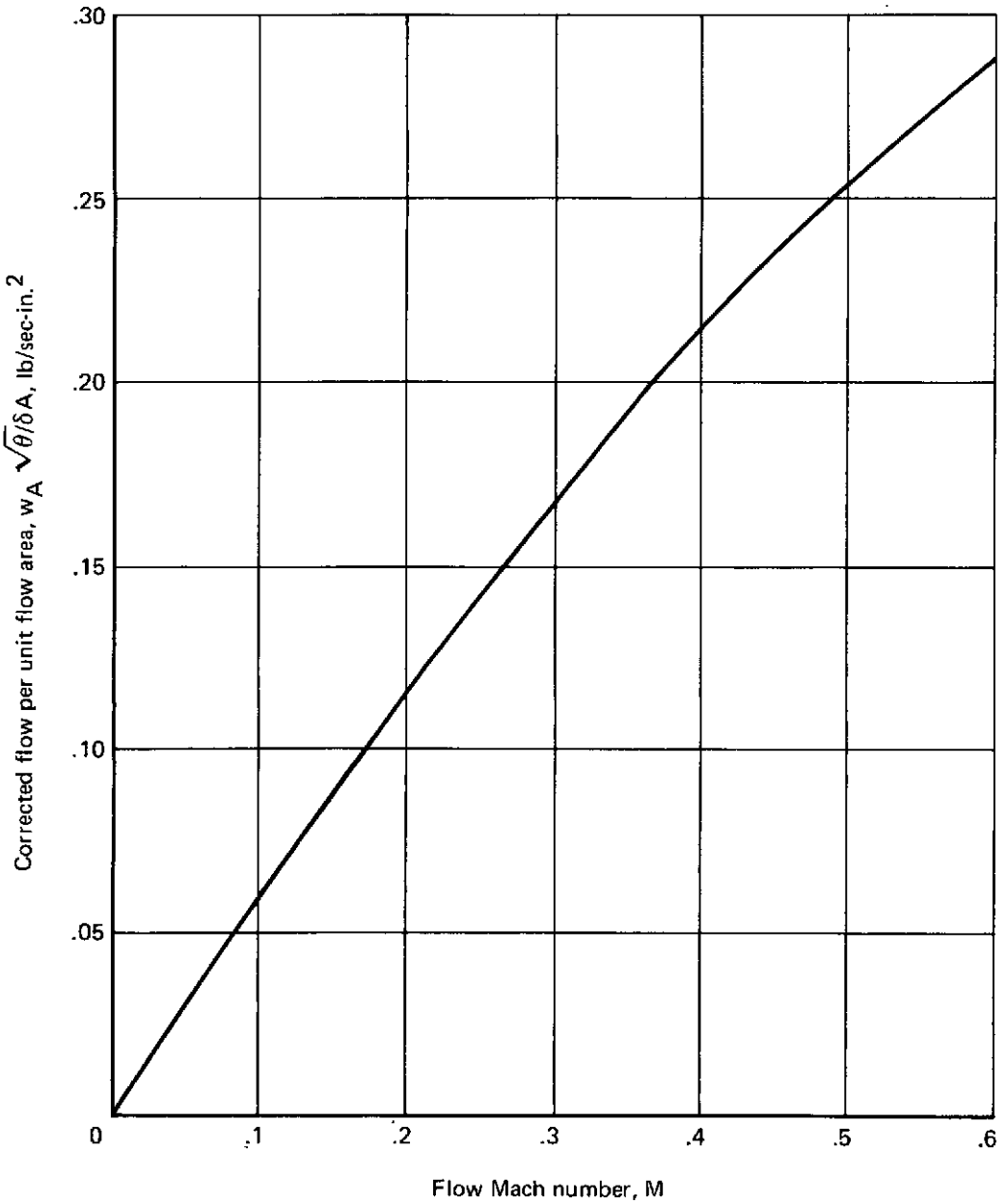

FIGURE 9.–CORRECTED FLOW PER UNIT FLOW AREA VERSUS FLOW MACH NUMBER

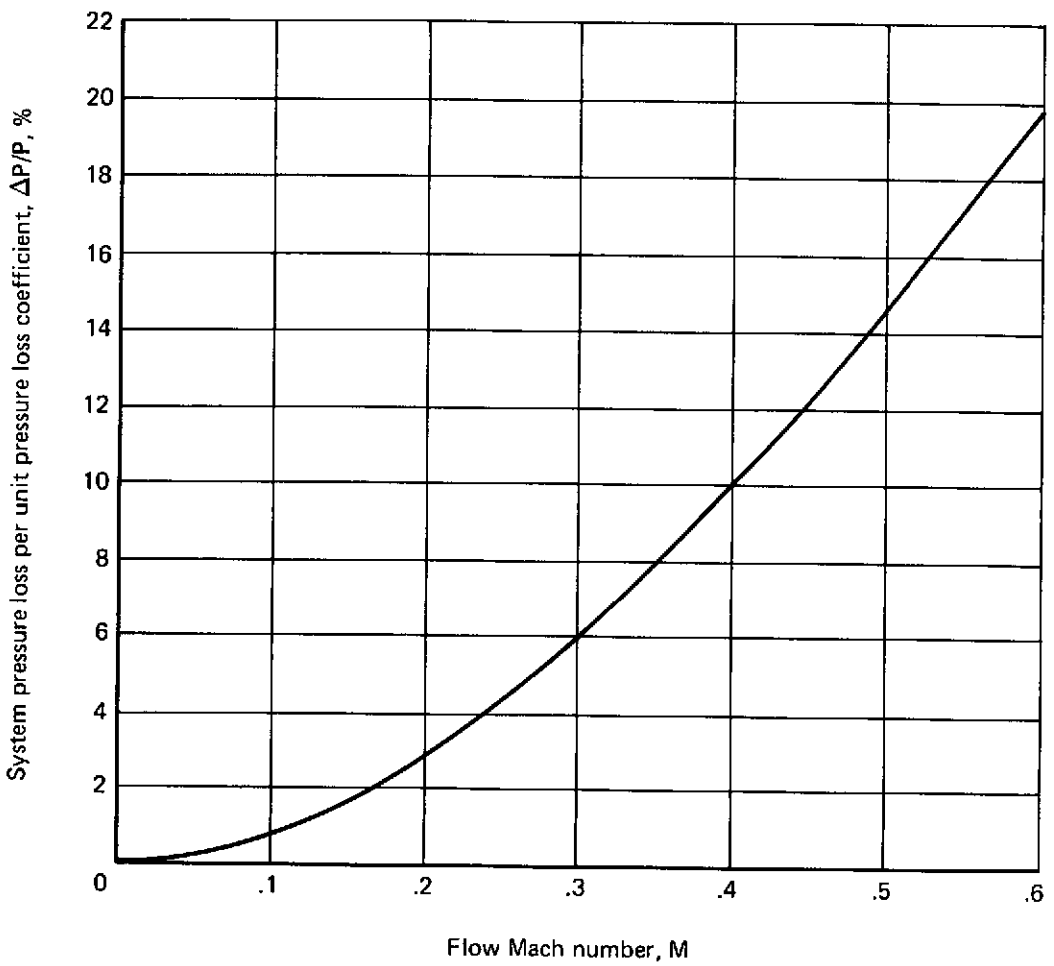

FIGURE 10.–SYSTEM PRESSURE LOSS PER UNIT PRESSURE LOSS COEFFICIENT VERSUS FLOW MACH NUMBER

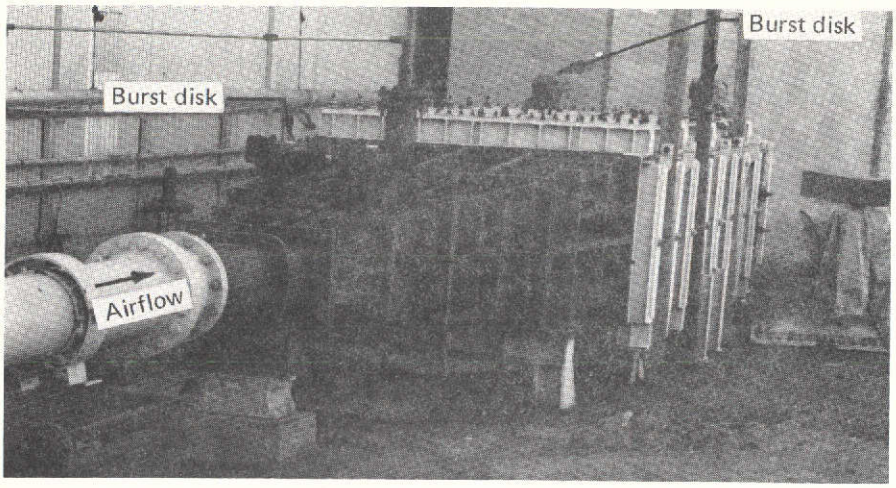

a. ACOUSTICALLY TREATED MUFFLER PLENUM

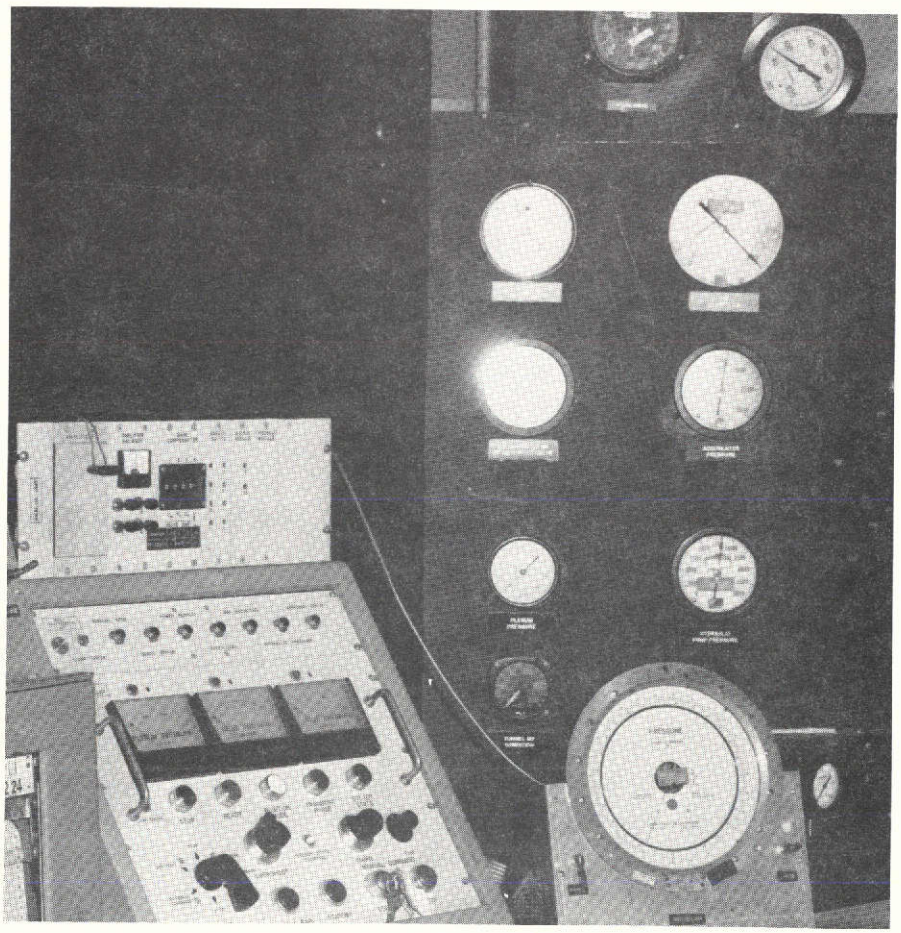

b. SUPPLY CONTROL VALVE–CONTROL CONSOLE

FIGURE 11.–FLOW LABORATORY COMPONENTS

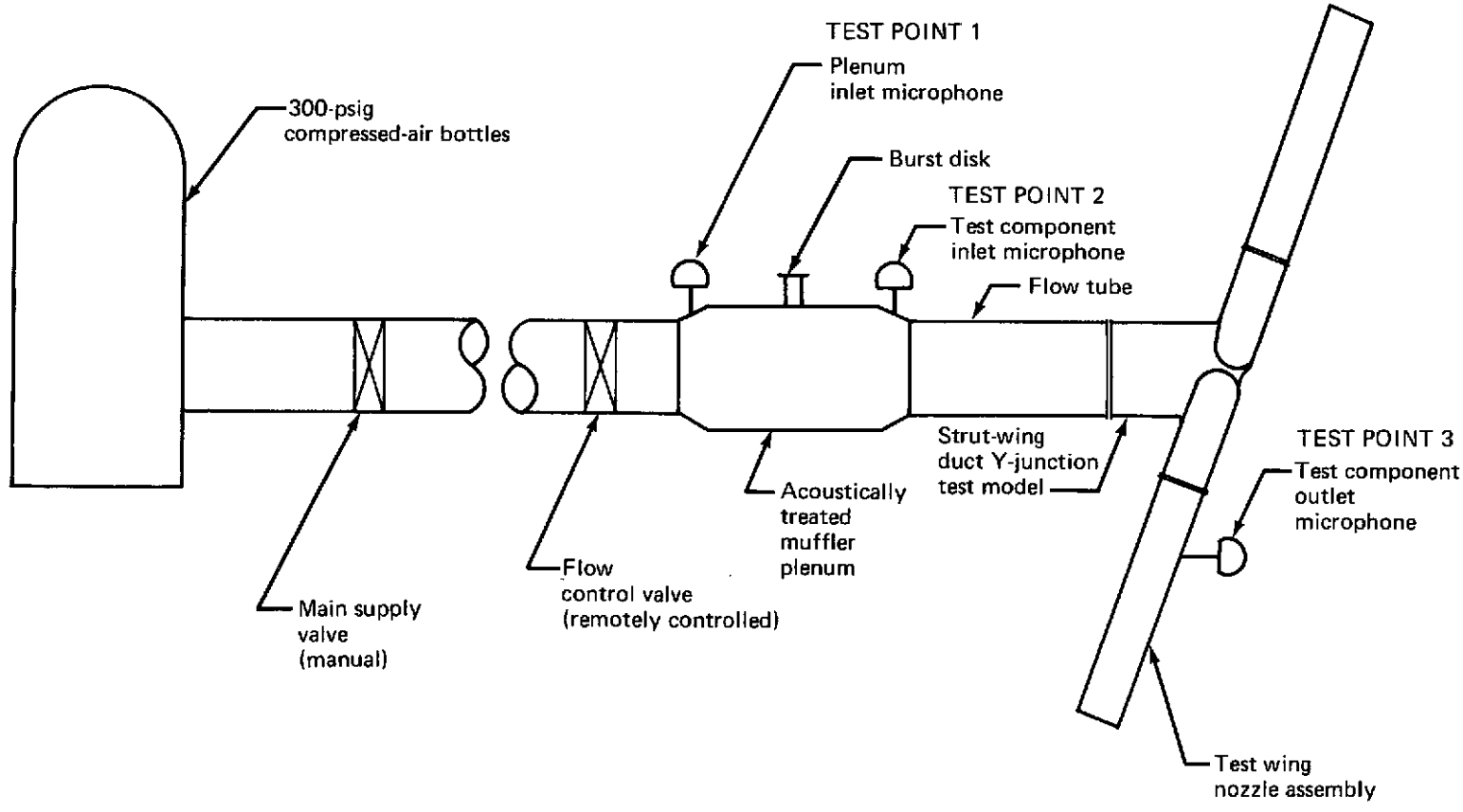

FIGURE 12.—TEST SETUP SCHEMATIC

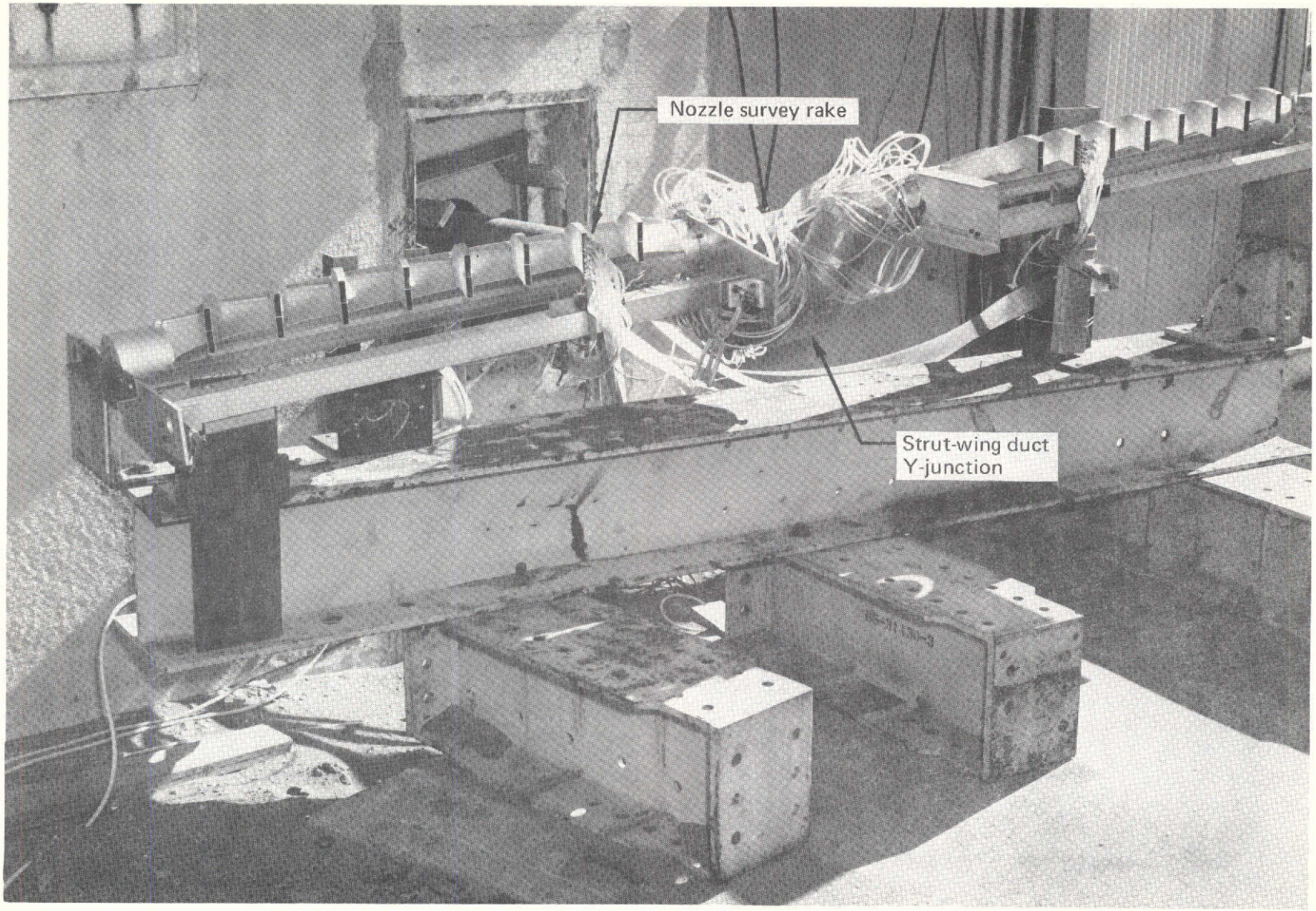

FIGURE 13.–TEST SETUP

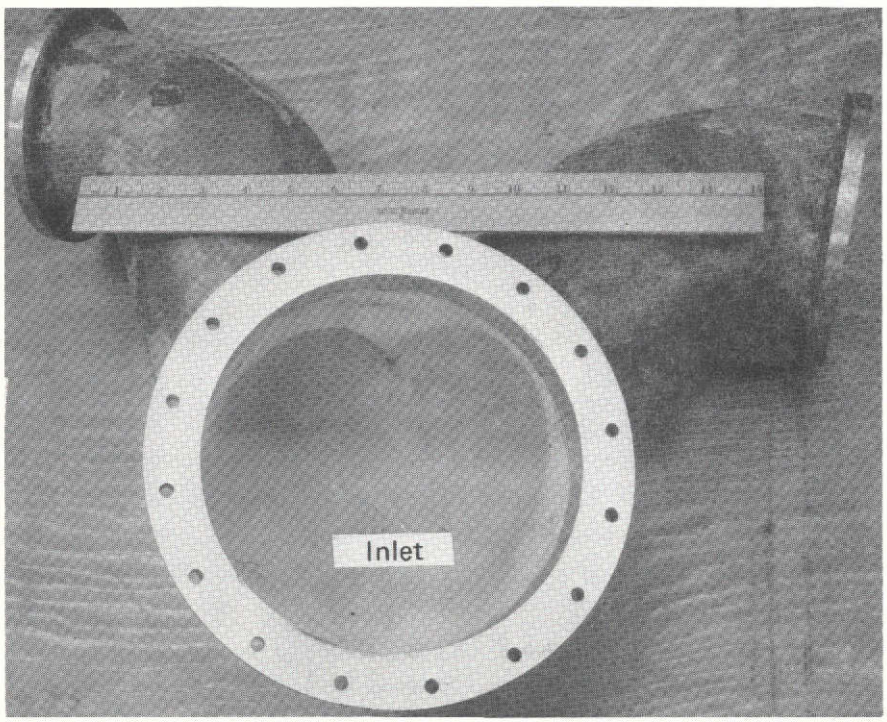

Y-JUNCTION FRONT VIEW

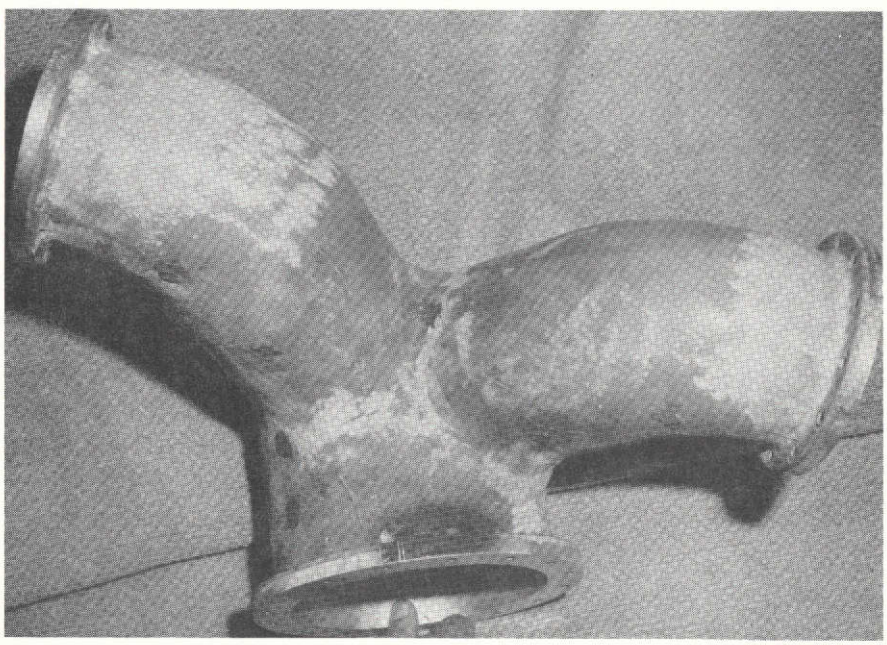

Y-JUNCTION TOP VIEW

FIGURE 14.—STRUT-WING DUCT Y-JUNCTION

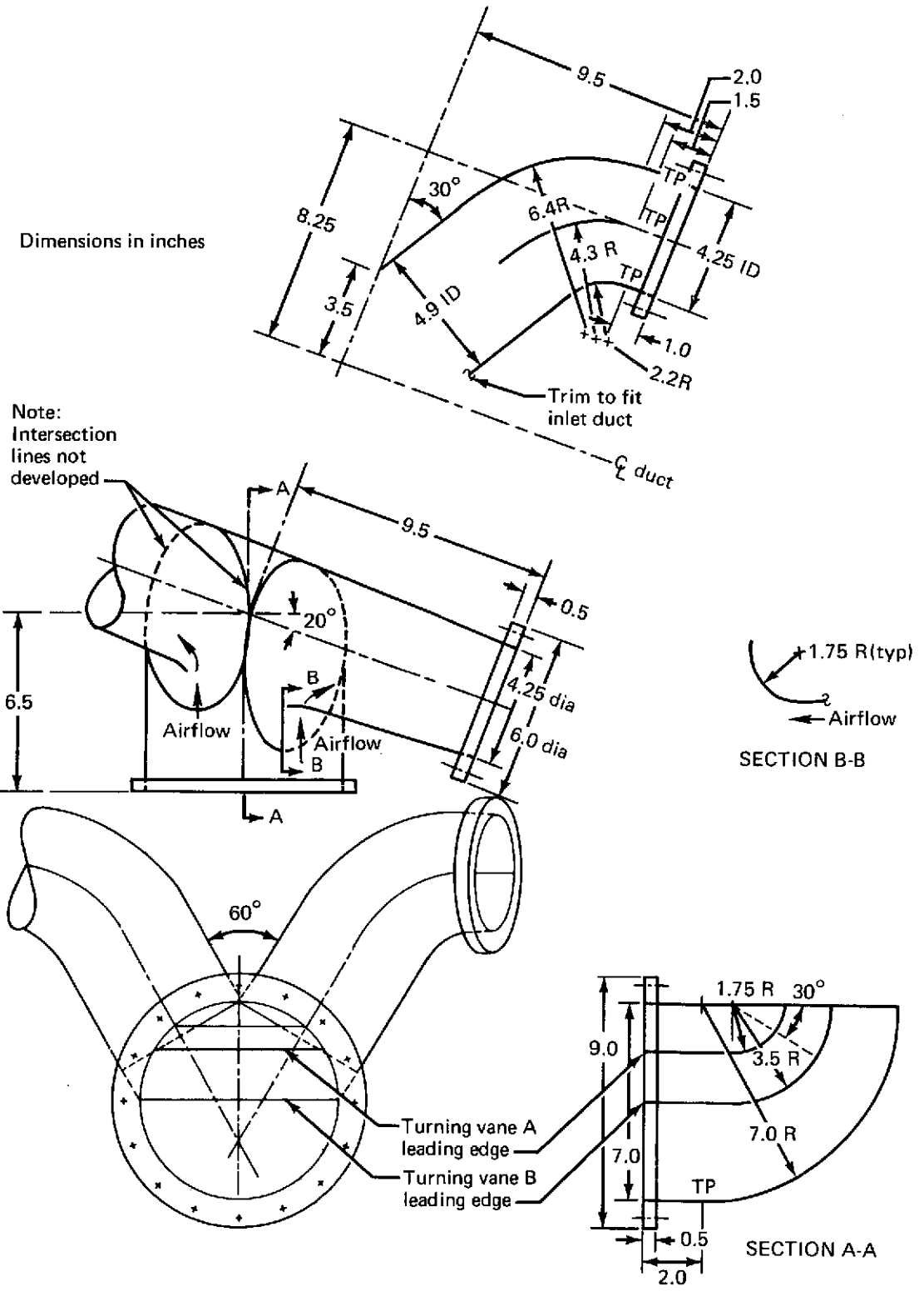

FIGURE 15.–STRUT-WING DUCT Y-JUNCTION DESIGN DETAILS

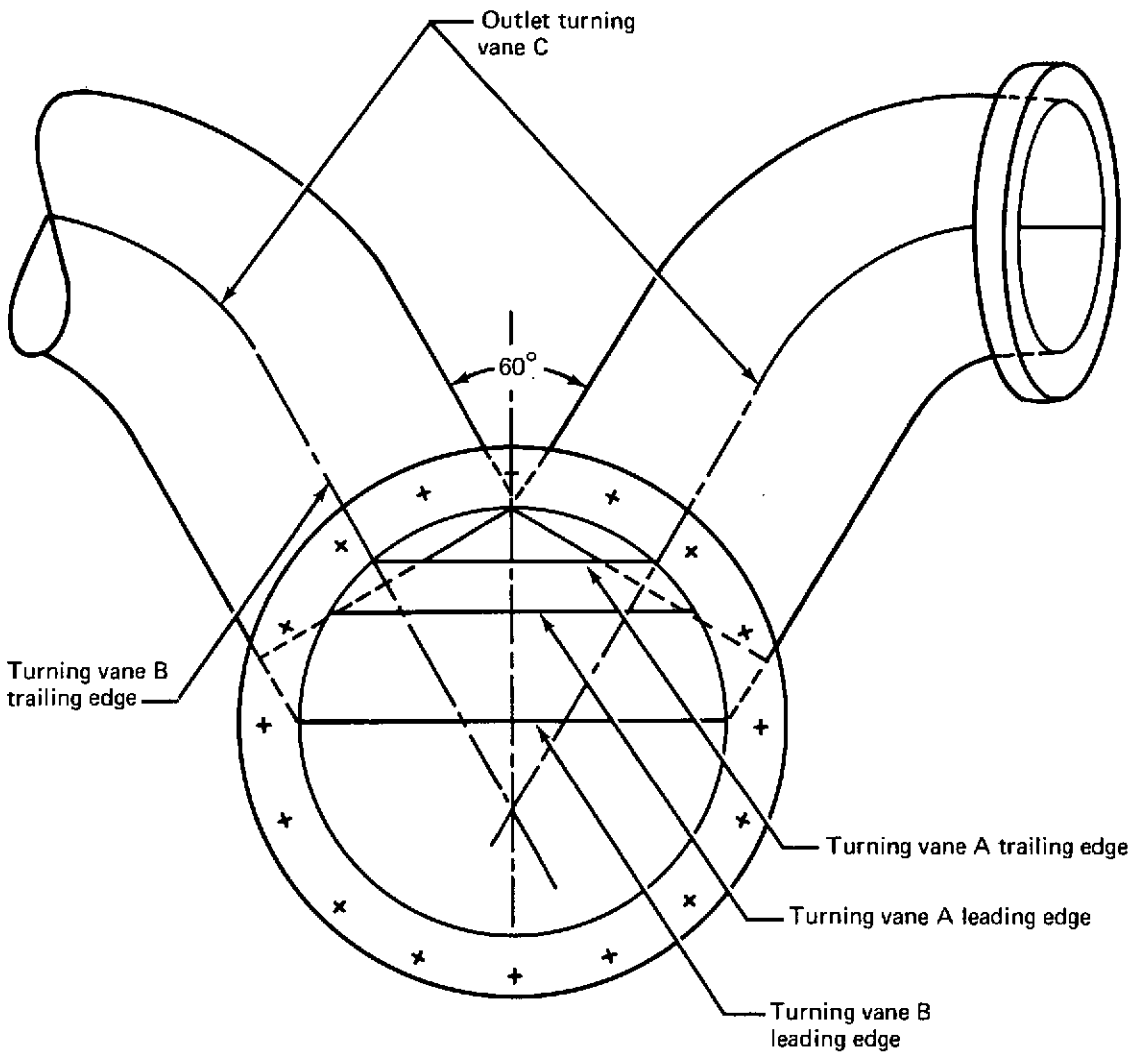

Configuration	Inlet turning vane	Outlet turning vane
Y-1	A,B	C
Y-2	B	C
Y-3	None	None

FIGURE 16.–STRUT-WING DUCT Y-JUNCTION TEST CONFIGURATIONS

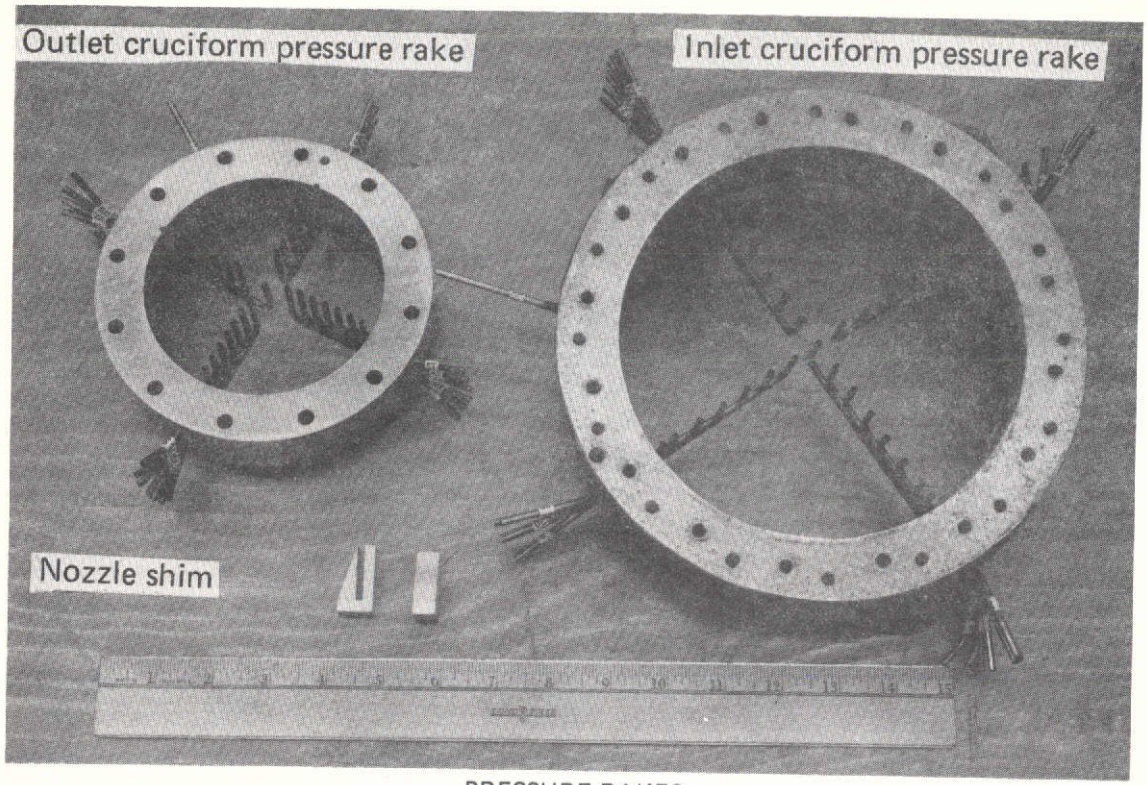

PRESSURE RAKES

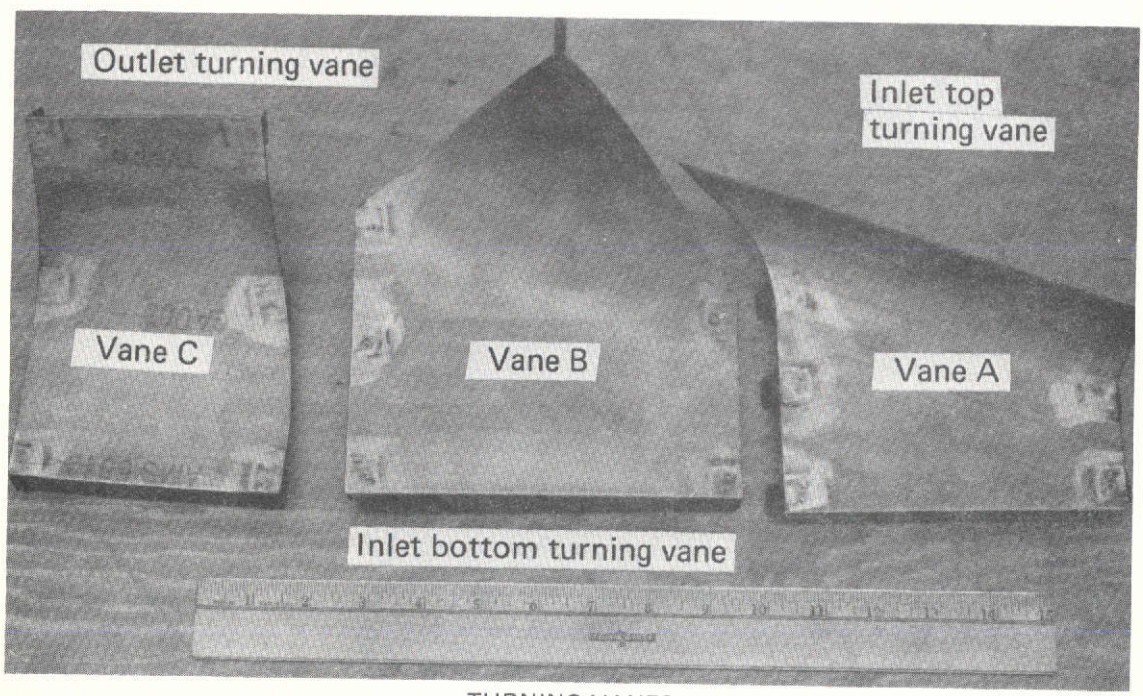

TURNING VANES

FIGURE 17.—PRESSURE RAKES AND TURNING VANES

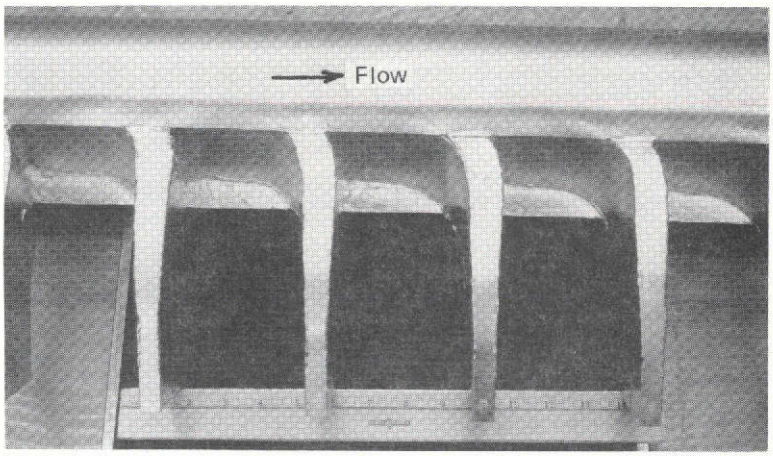

R_c/w = 3.0
S/w^* = 12.0
θ_N = 90°

NOZZLE ASSEMBLY DNA-1

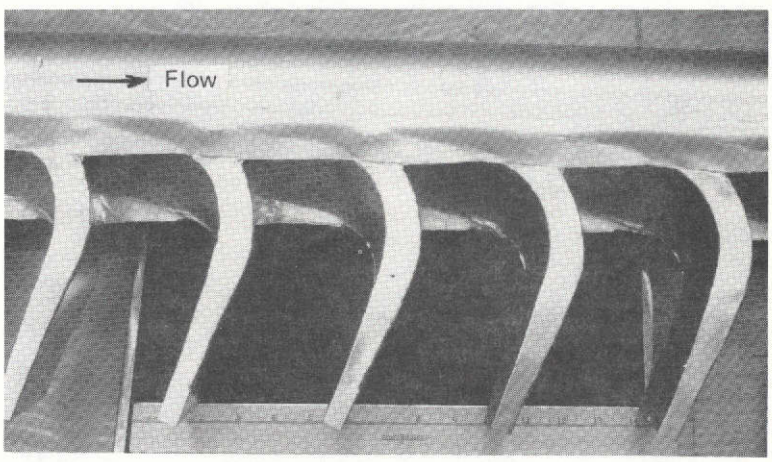

R_c/w = 3.0
S/w^* = 12.0
θ_N = 110°

NOZZLE ASSEMBLY DNA-3

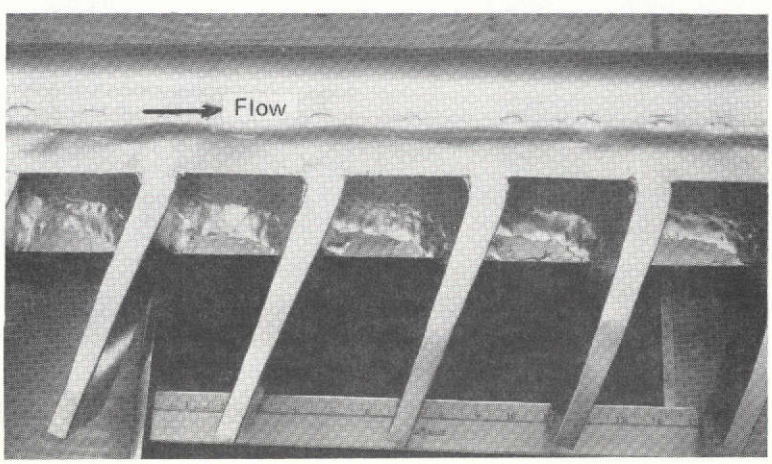

R_c/w = 2.0
S/w^* = 12.0
θ_N = 110°

NOZZLE ASSEMBLY DNA-5

FIGURE 18.–SET 1 NOZZLE ASSEMBLIES

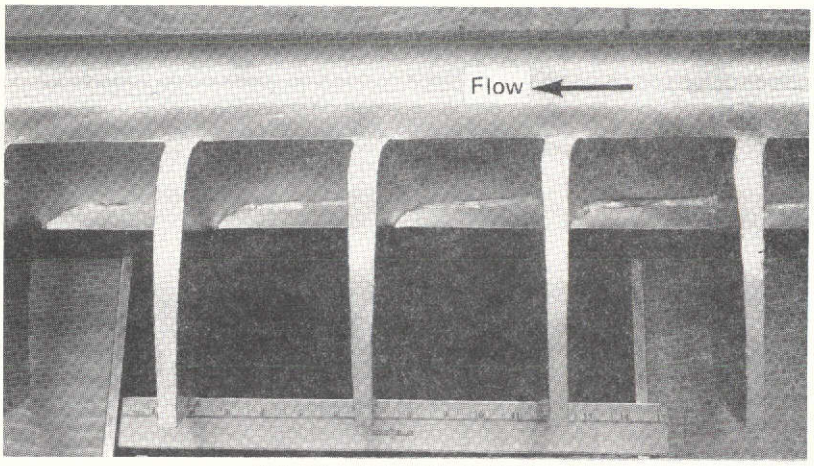

NOZZLE ASSEMBLY DNA-2

R_c/w = 3.0
S/w^* = 9.0
θ_N = 90°

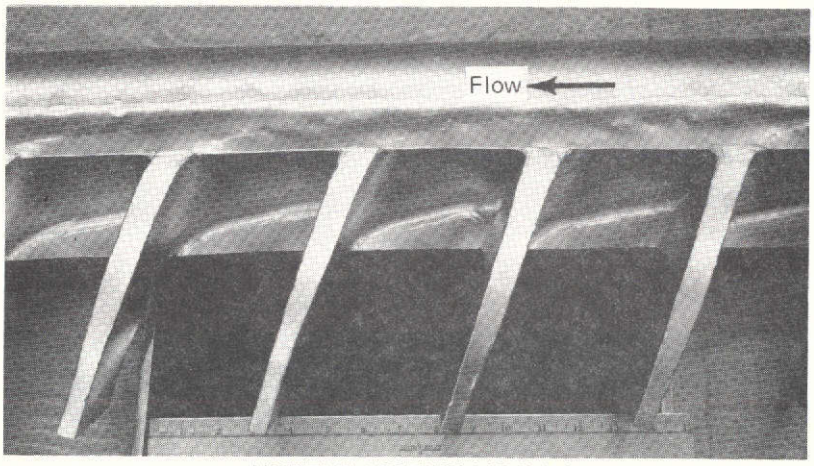

NOZZLE ASSEMBLY DNA-4

R_c/w = 3.0
S/w^* = 9.0
θ_N = 90°

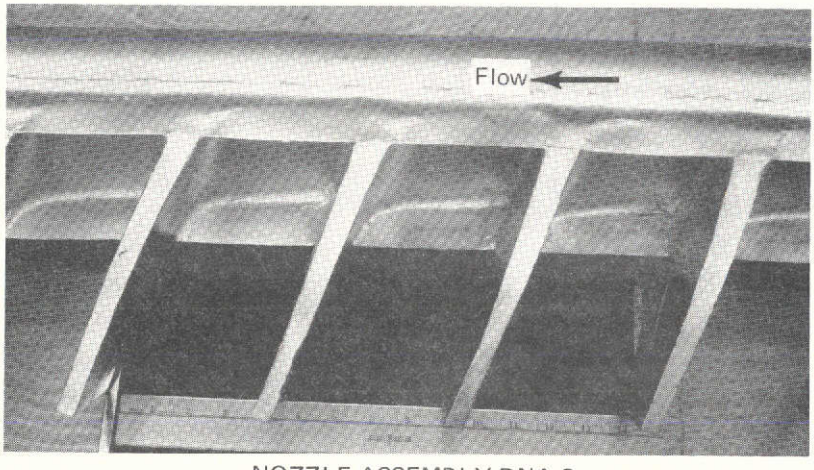

NOZZLE ASSEMBLY DNA-6

R_c/w = 2.0
S/w^* = 9.0
θ_N = 70°

FIGURE 19.—SET 2 NOZZLE ASSEMBLIES

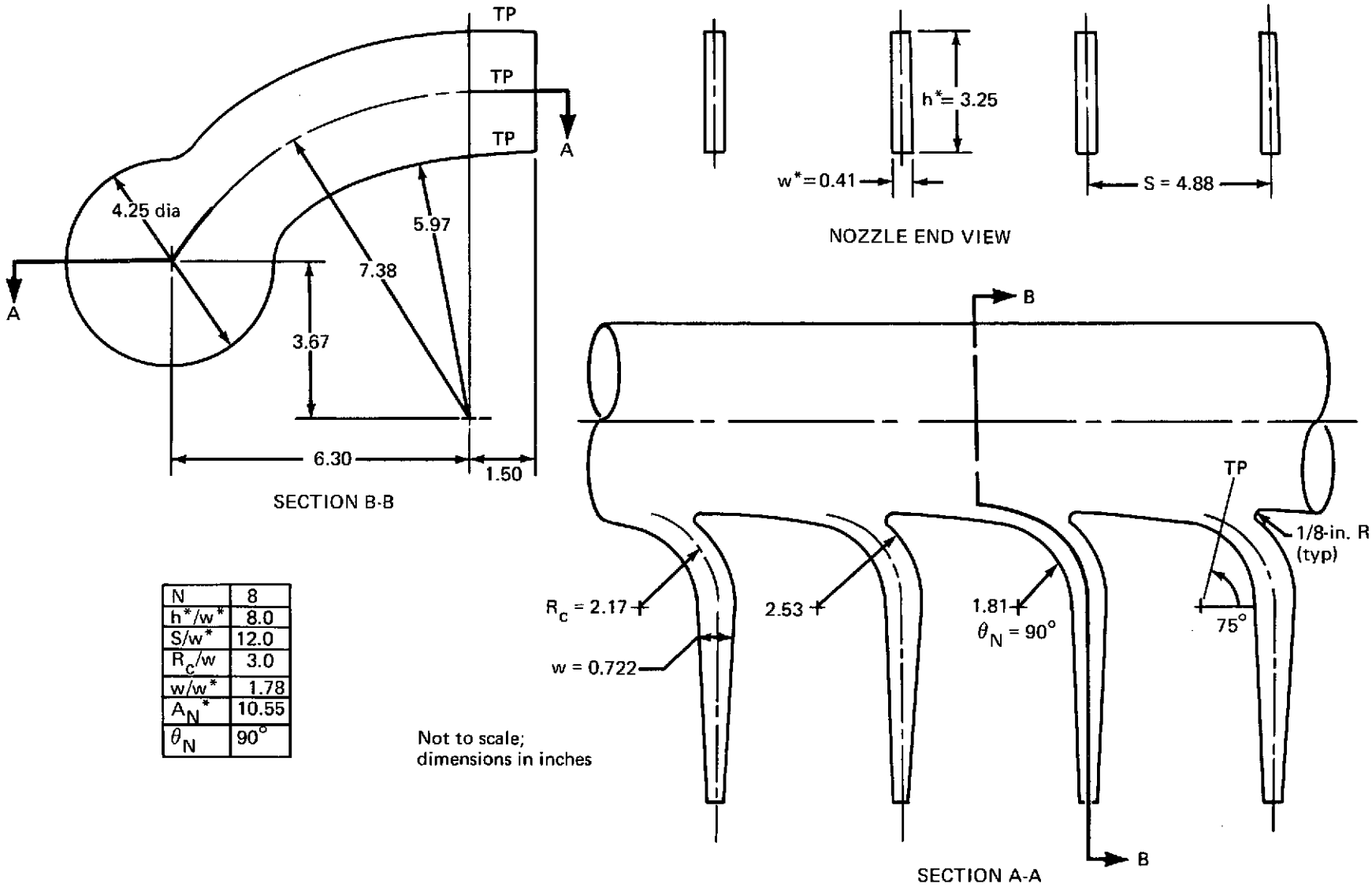

N	8
h^*/w^*	8.0
S/w^*	12.0
R_c/w	3.0
w/w^*	1.78
$A_N{}^*$	10.55
θ_N	90°

FIGURE 20.—WING-DUCT NOZZLE ASSEMBLY DNA-1 DESIGN DETAILS

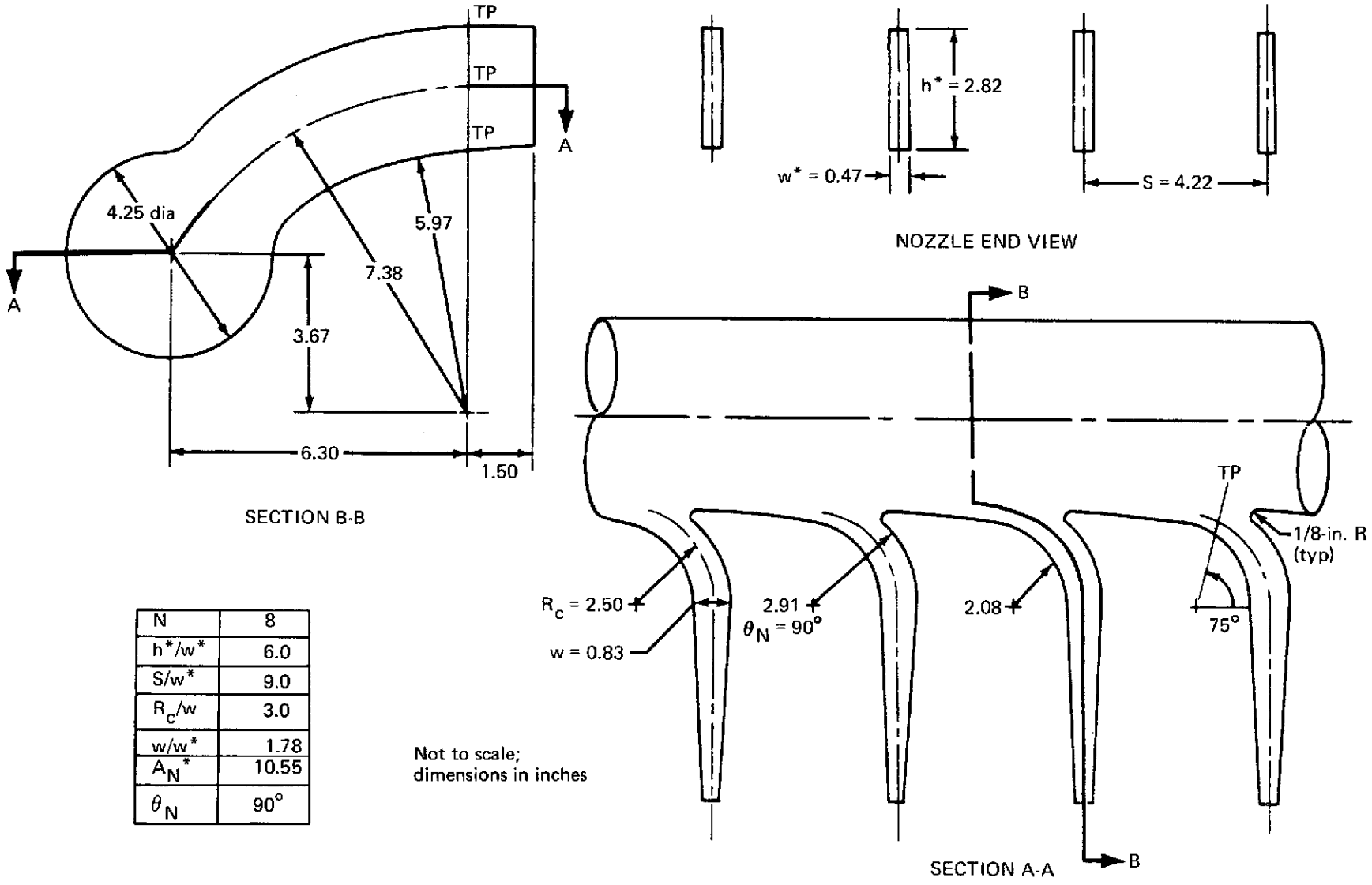

N	8
h*/w*	6.0
S/w*	9.0
R_c/w	3.0
w/w*	1.78
A_N*	10.55
θ_N	90°

Not to scale;
dimensions in inches

FIGURE 21.—WING-DUCT-LOBE NOZZLE ASSEMBLY DNA-2 DESIGN DETAILS

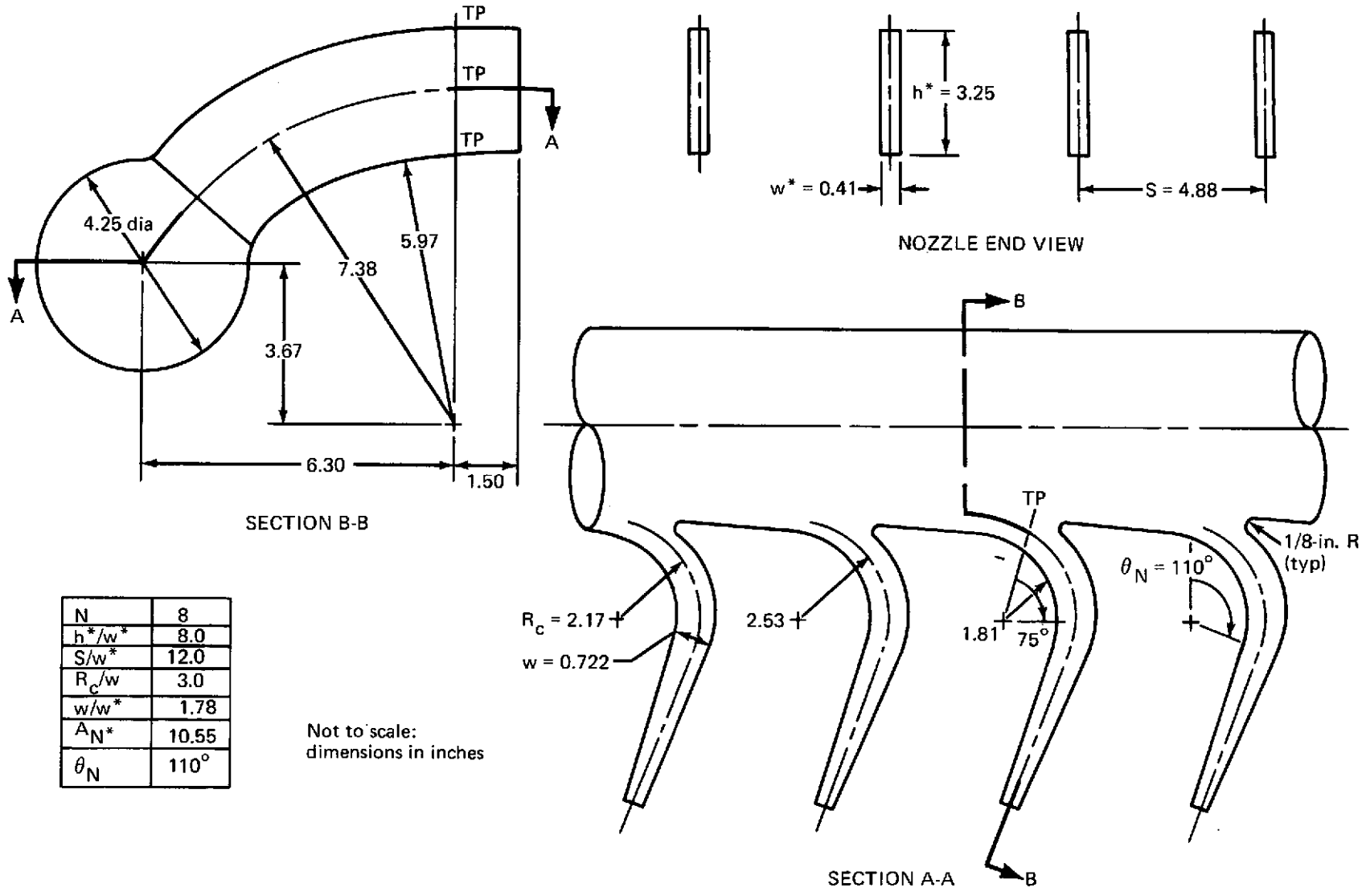

N	8
h*/w*	8.0
S/w*	12.0
R_c/w	3.0
w/w*	1.78
A_N*	10.55
θ_N	110°

Not to scale:
dimensions in inches

FIGURE 22.—WING-DUCT NOZZLE ASSEMBLY DNA-3 DESIGN DETAILS

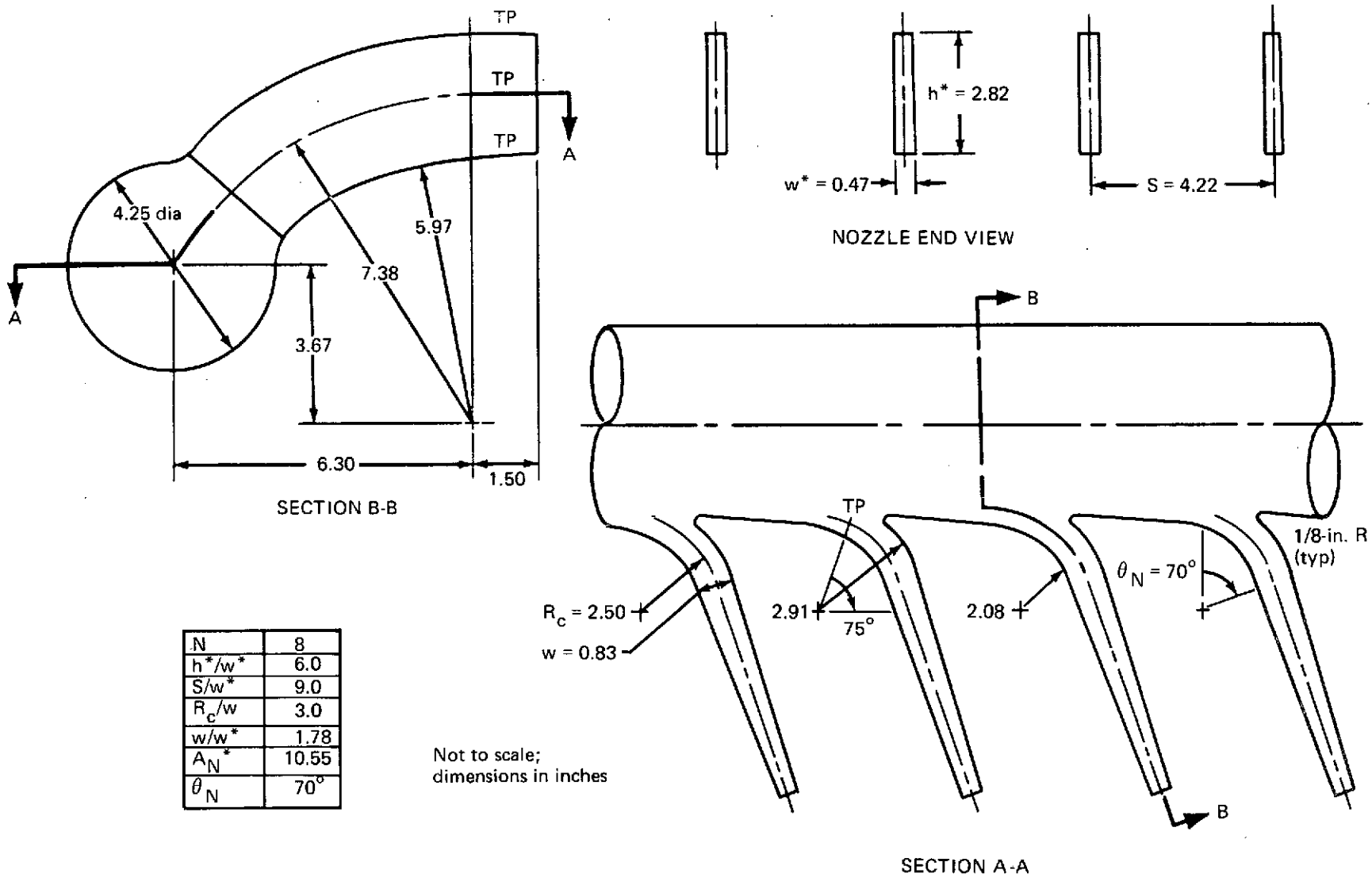

N	8
h^*/w^*	6.0
S/w^*	9.0
R_c/w	3.0
w/w^*	1.78
A_N^*	10.55
θ_N	70°

Not to scale;
dimensions in inches

FIGURE 23.–WING-DUCT-LOBE NOZZLE ASSEMBLY DNA-4 DESIGN DETAILS

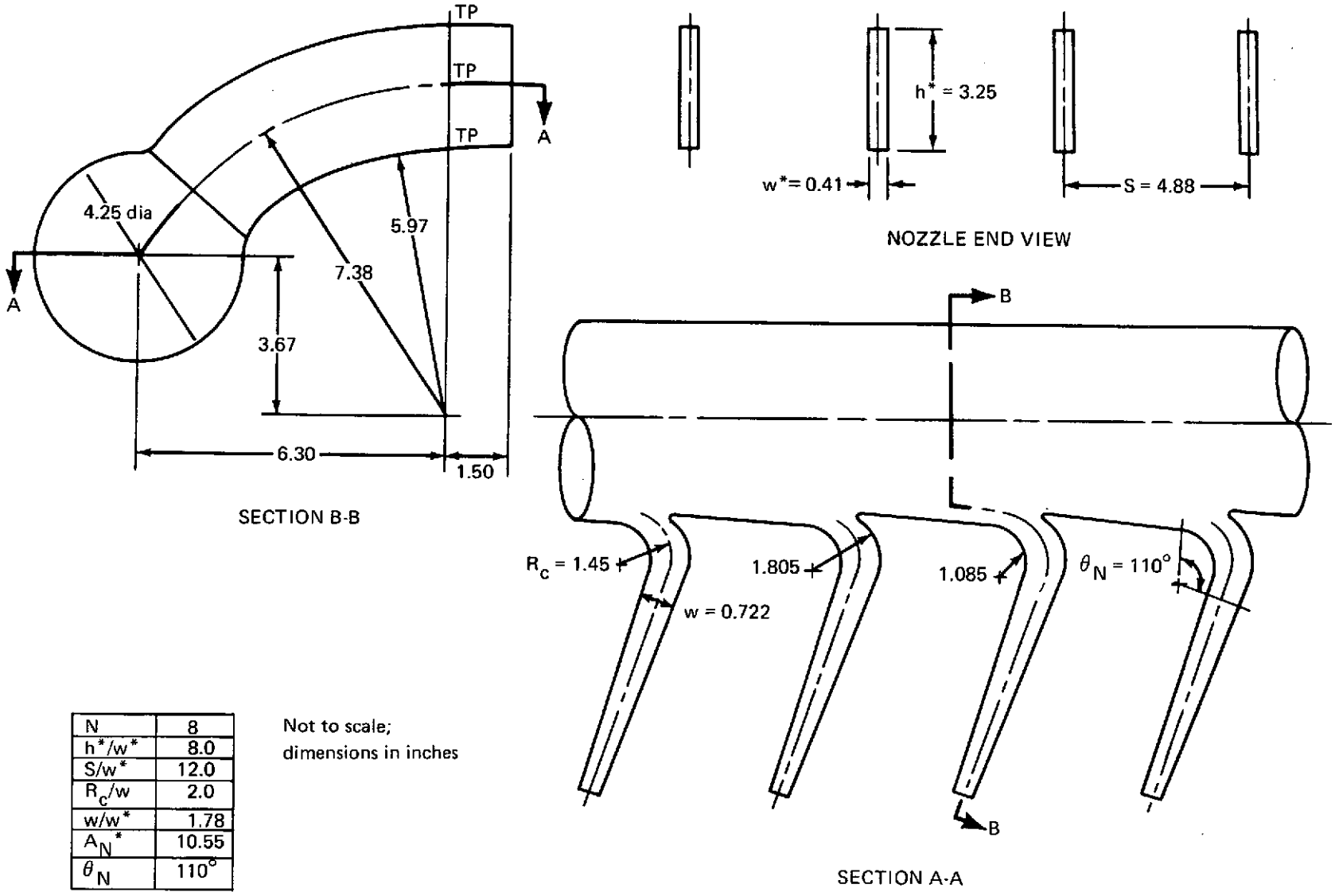

N	8
h^*/w^*	8.0
S/w^*	12.0
R_c/w	2.0
w/w^*	1.78
A_N^*	10.55
θ_N	110°

Not to scale;
dimensions in inches

FIGURE 24.—WING-DUCT NOZZLE ASSEMBLY DNA-5 DESIGN DETAILS

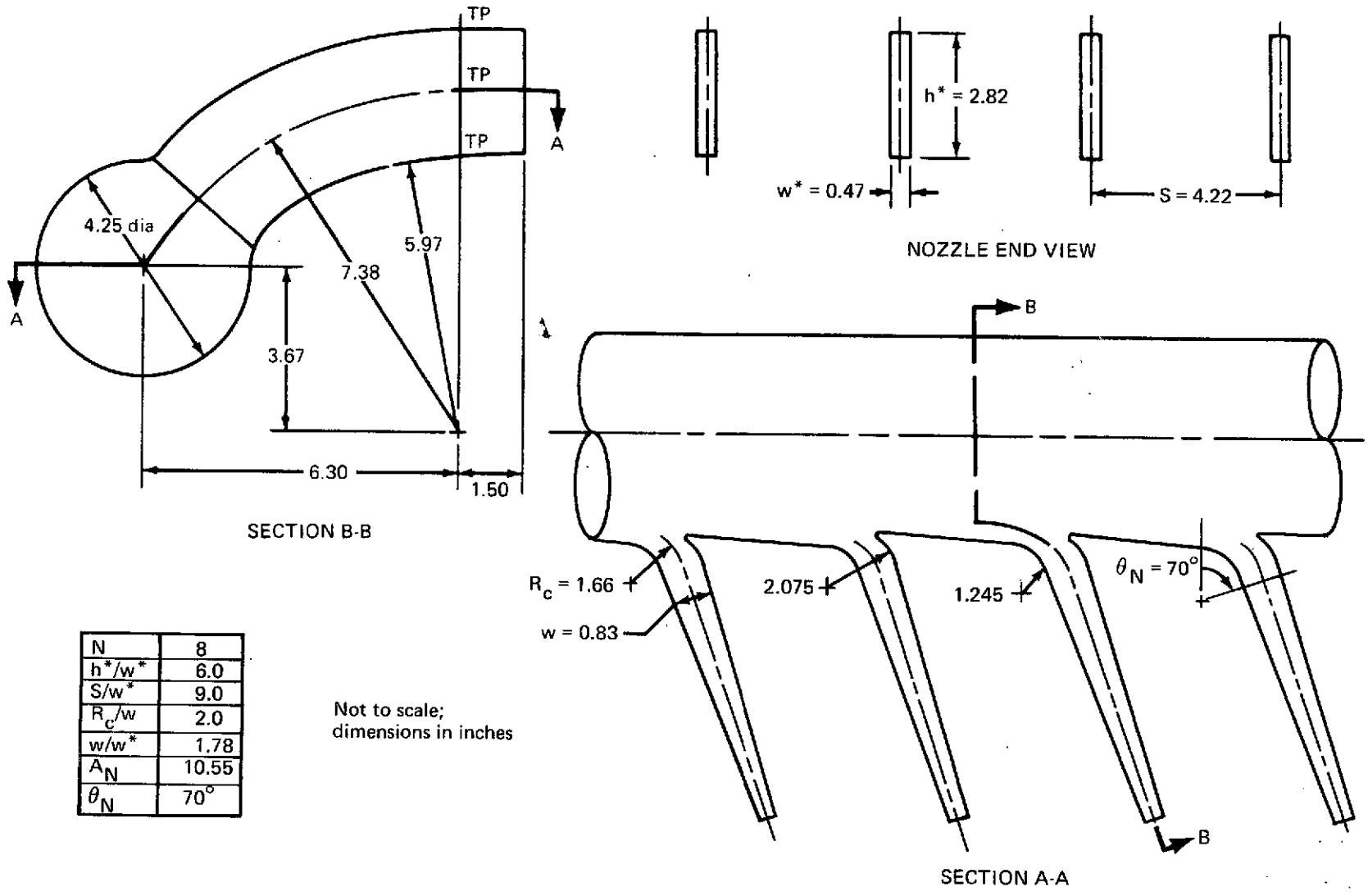

N	8
h^*/w^*	6.0
S/w^*	9.0
R_c/w	2.0
w/w^*	1.78
A_N	10.55
θ_N	70°

Not to scale;
dimensions in inches

FIGURE 25.—WING-DUCT-LOBE NOZZLE ASSEMBLY DNA-6 DESIGN DETAILS

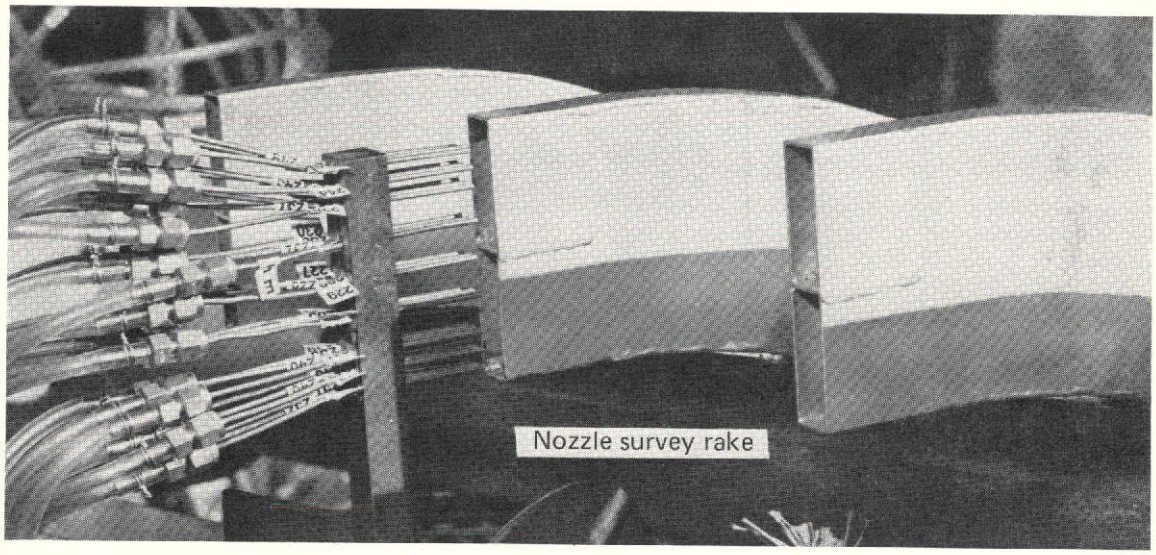

NOZZLE ASSEMBLY FRONT VIEW

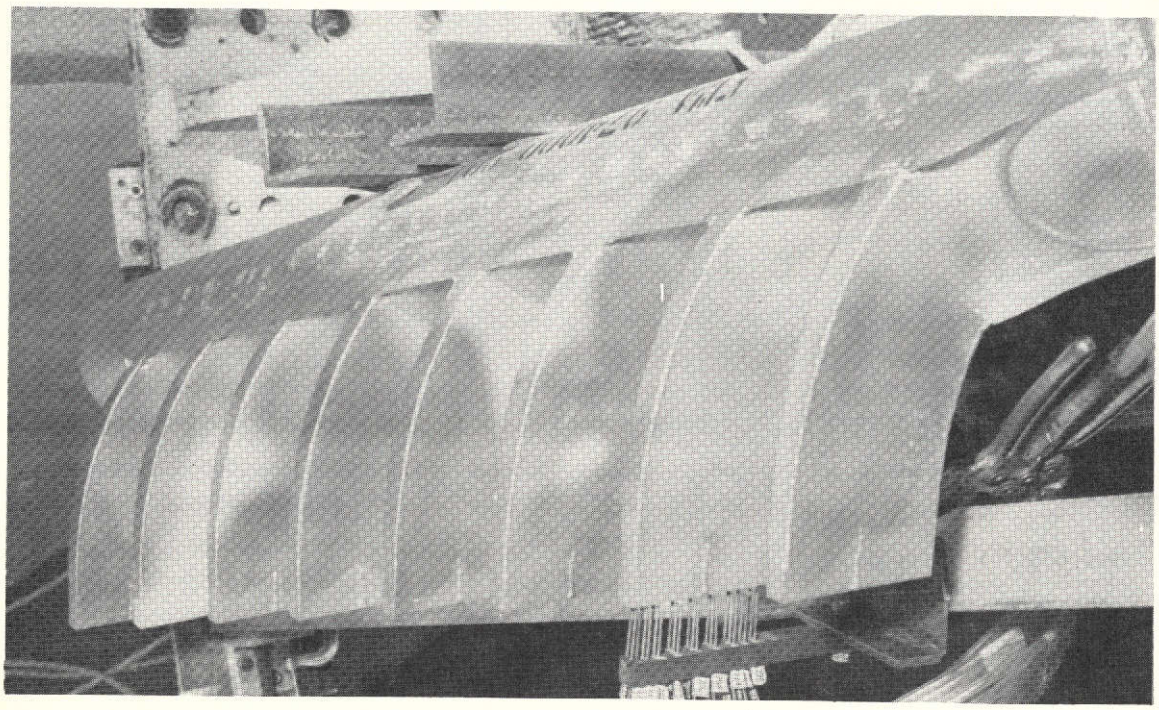

NOZZLE ASSEMBLY TOP VIEW

FIGURE 26.–NOZZLE ASSEMBLY INSTRUMENTATION

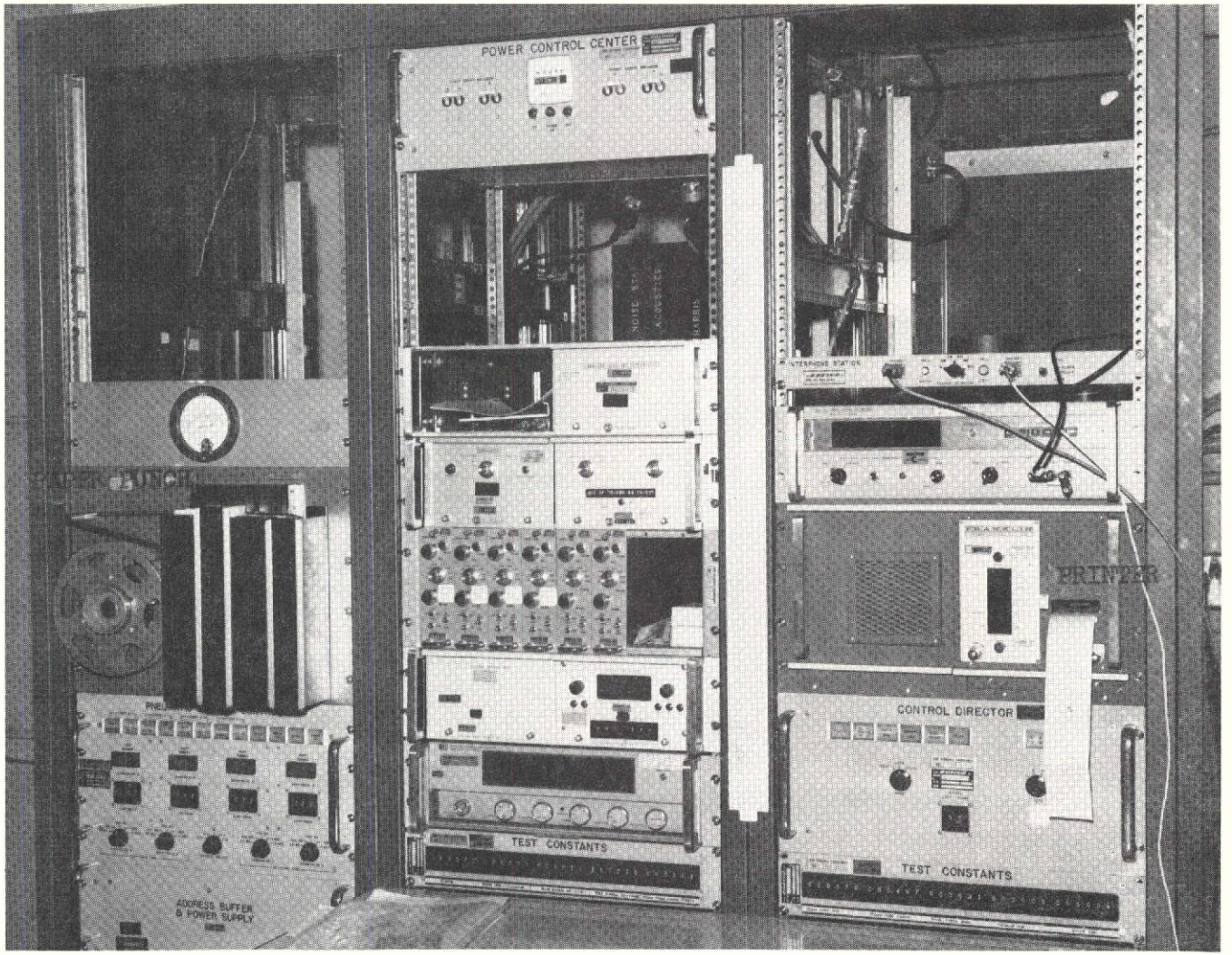

FIGURE 27.—STANDARD DIGITAL DATA SYSTEM

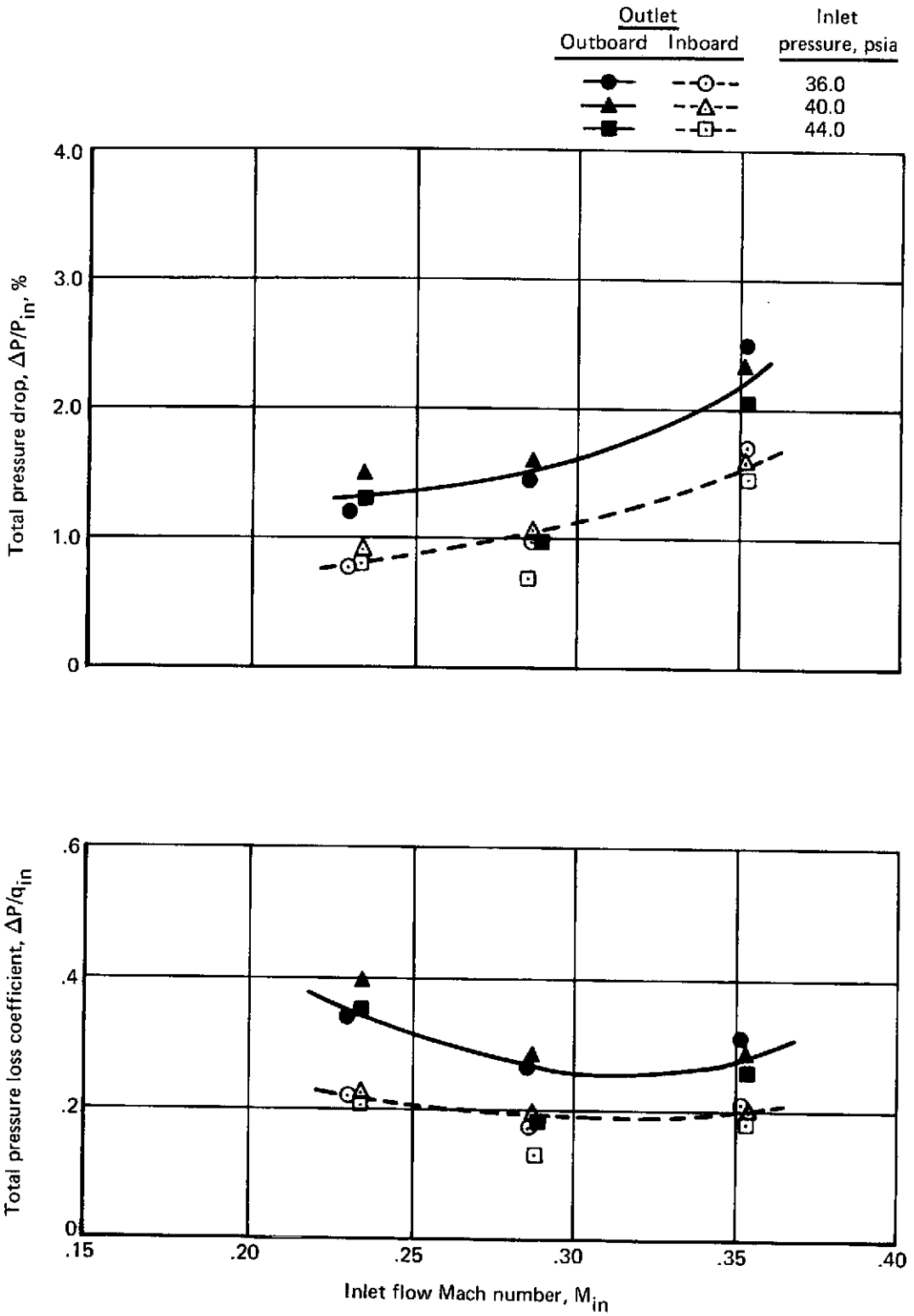

FIGURE 28.–PRESSURE LOSS, CONFIGURATION Y-1

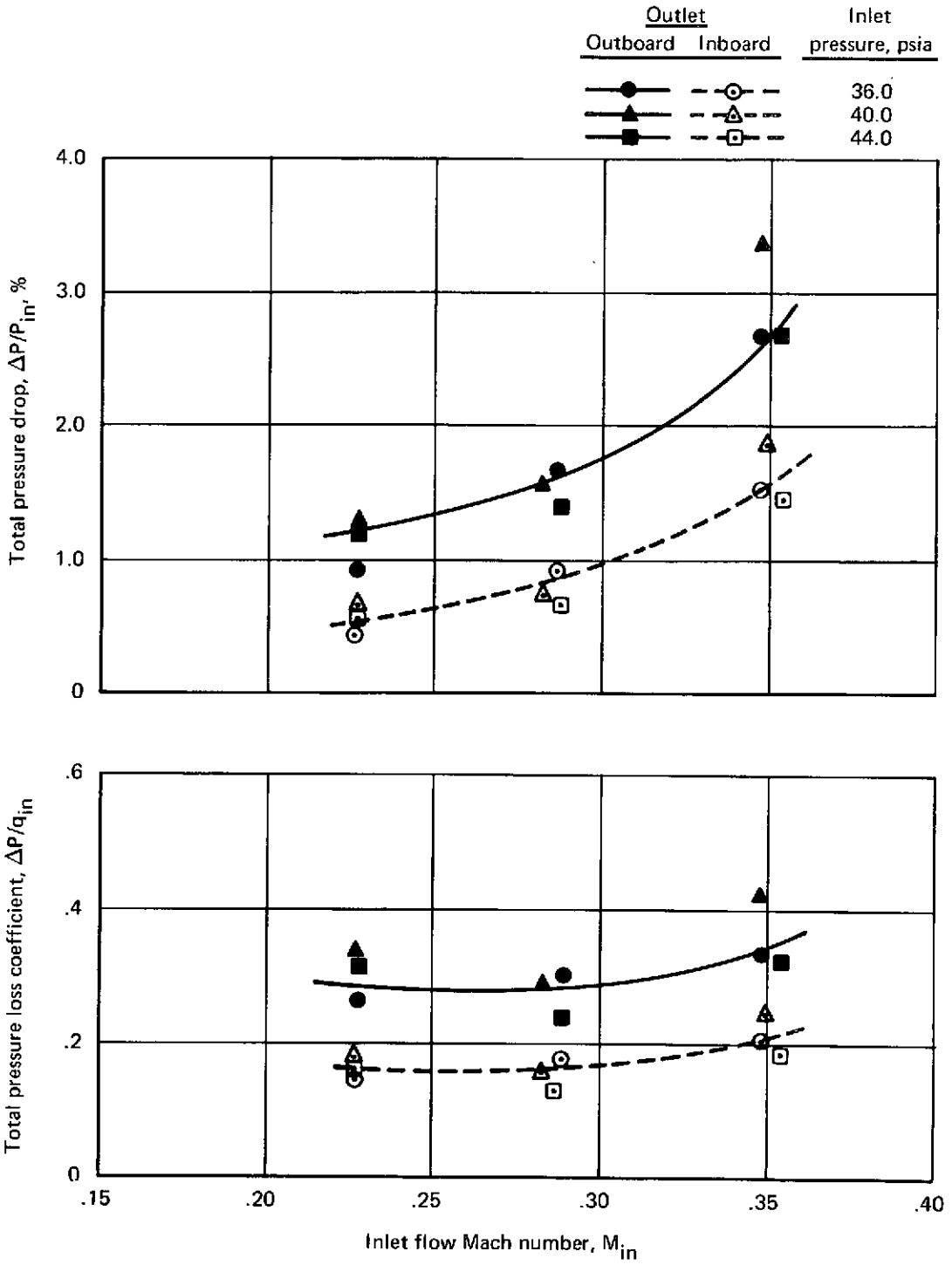

FIGURE 29.–PRESSURE LOSS, CONFIGURATION Y-2

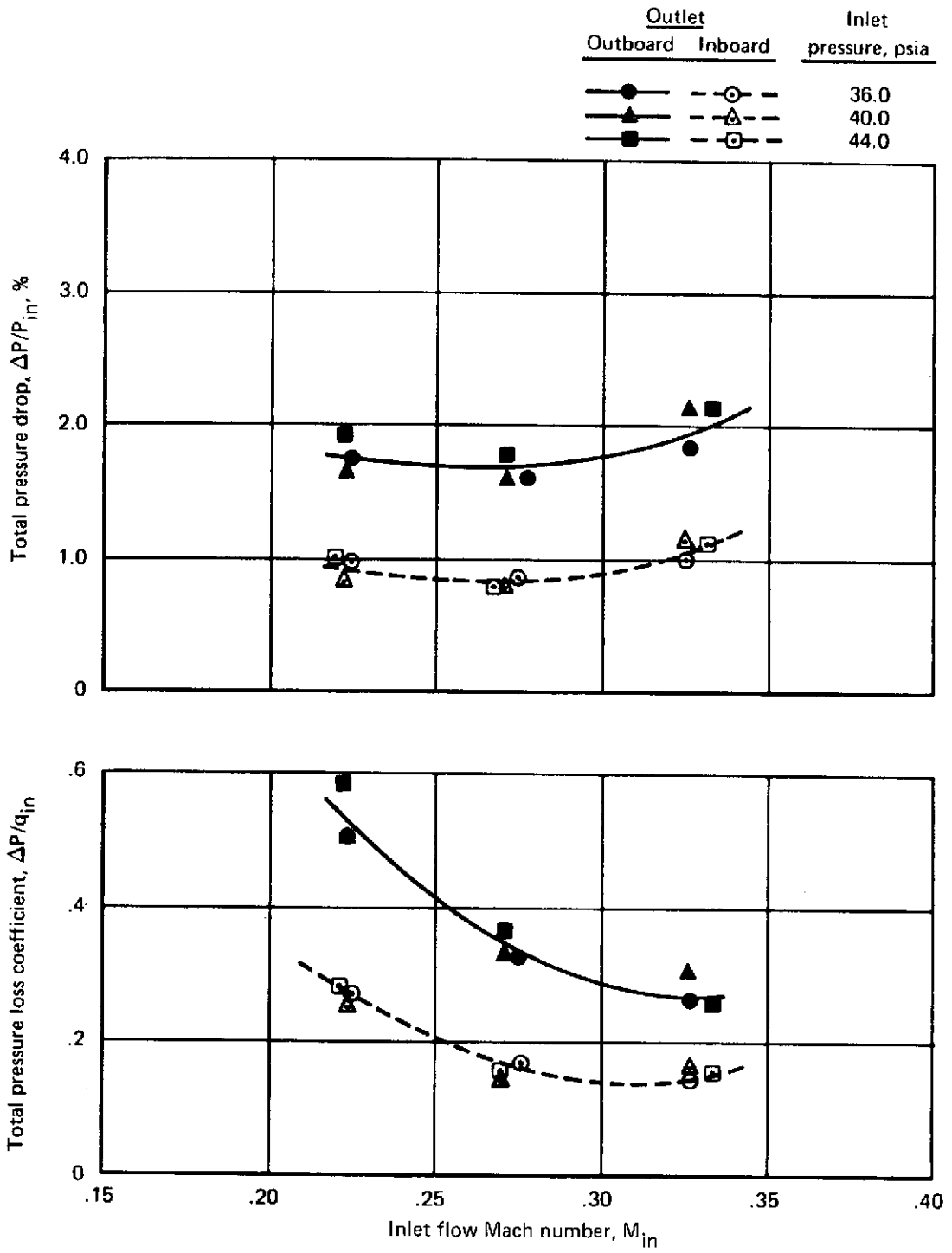

FIGURE 30.–PRESSURE LOSS, CONFIGURATION Y-3

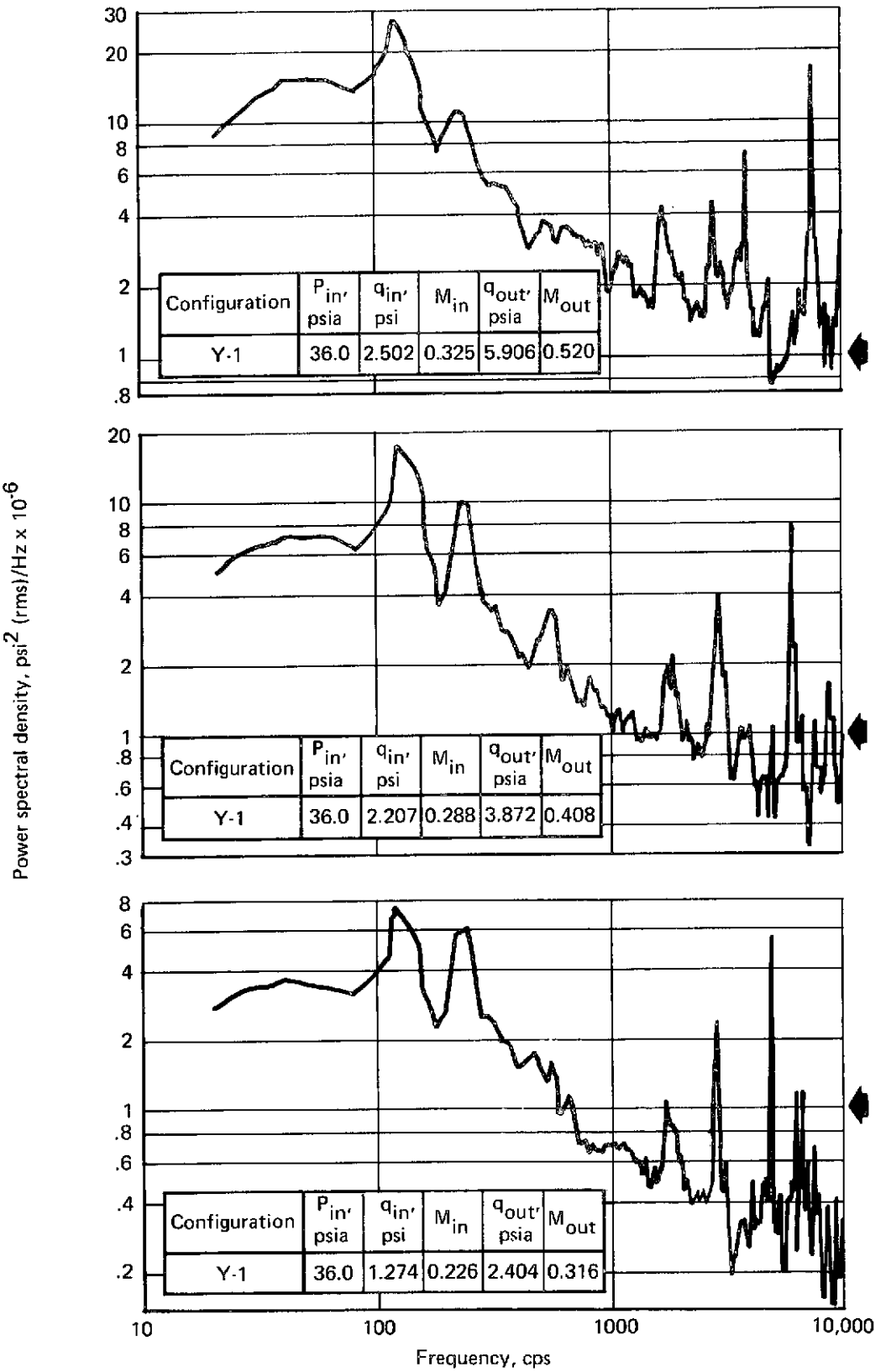

FIGURE 31.—EFFECT OF INLET MACH NUMBER ON POWER SPECTRAL DENSITY (TEST POINT 3)

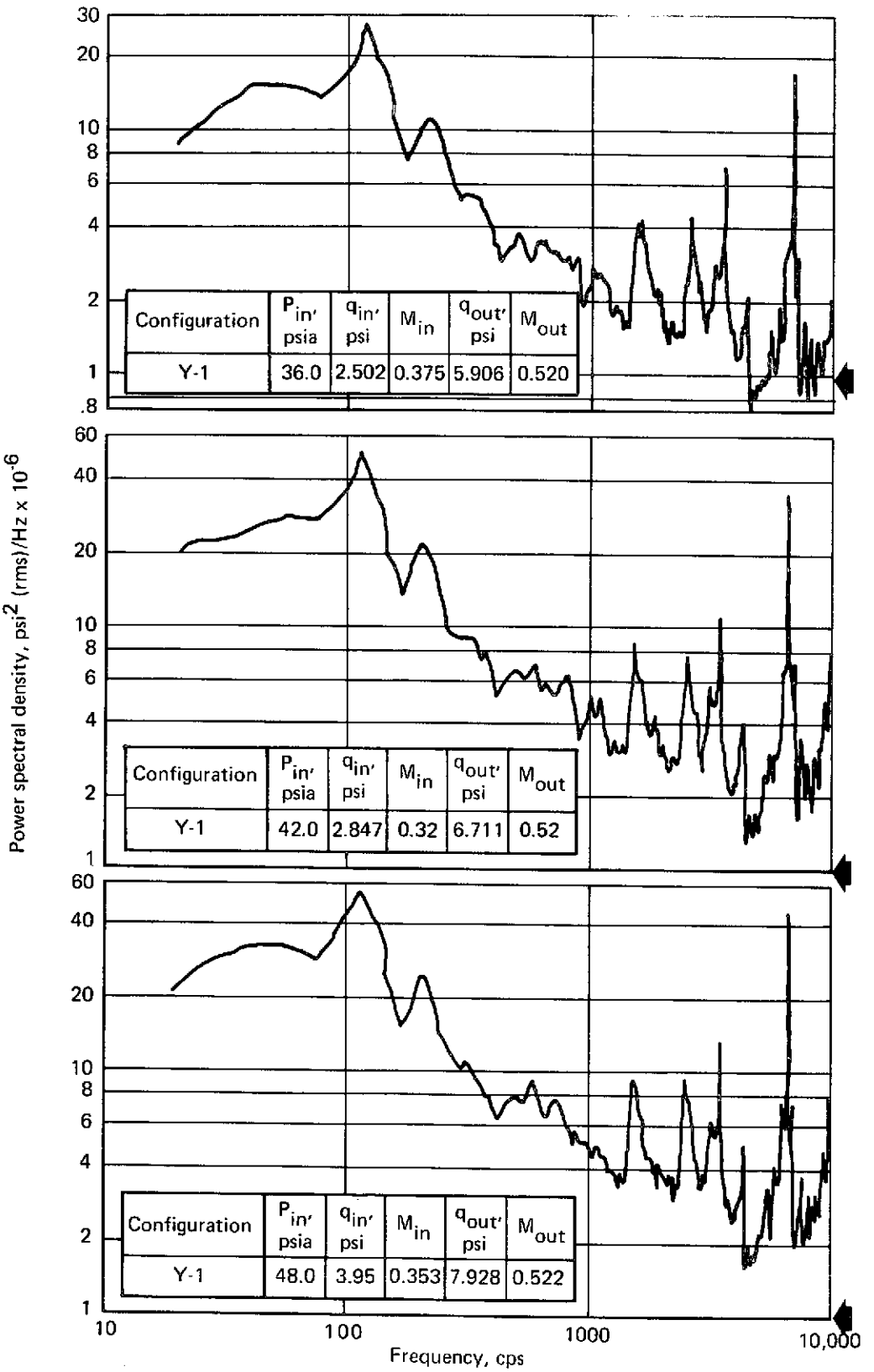

FIGURE 32.–EFFECT OF INLET PRESSURE ON POWER SPECTRAL DENSITY (TEST POINT 3)

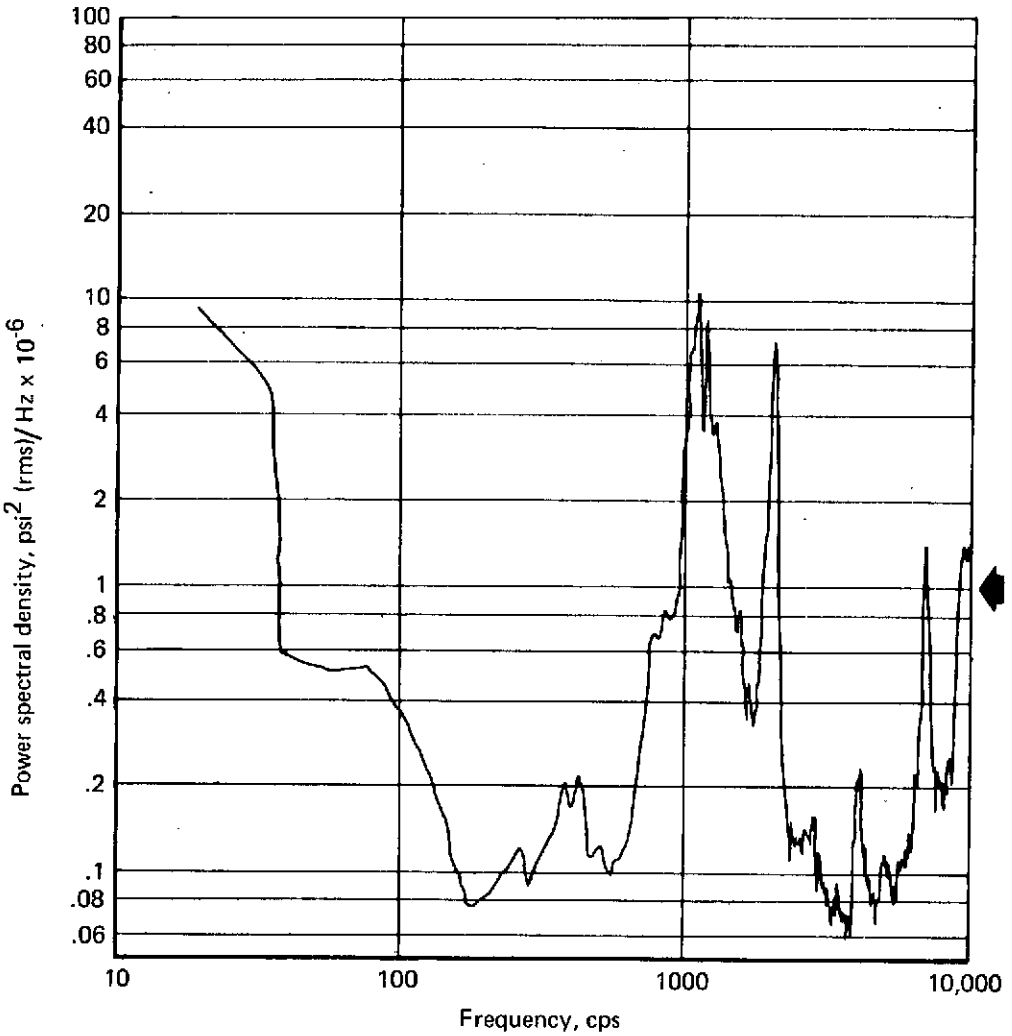

FIGURE 33.–SPECTRUM AT MUFFLER INLET (TEST POINT 1), 22 PSIG

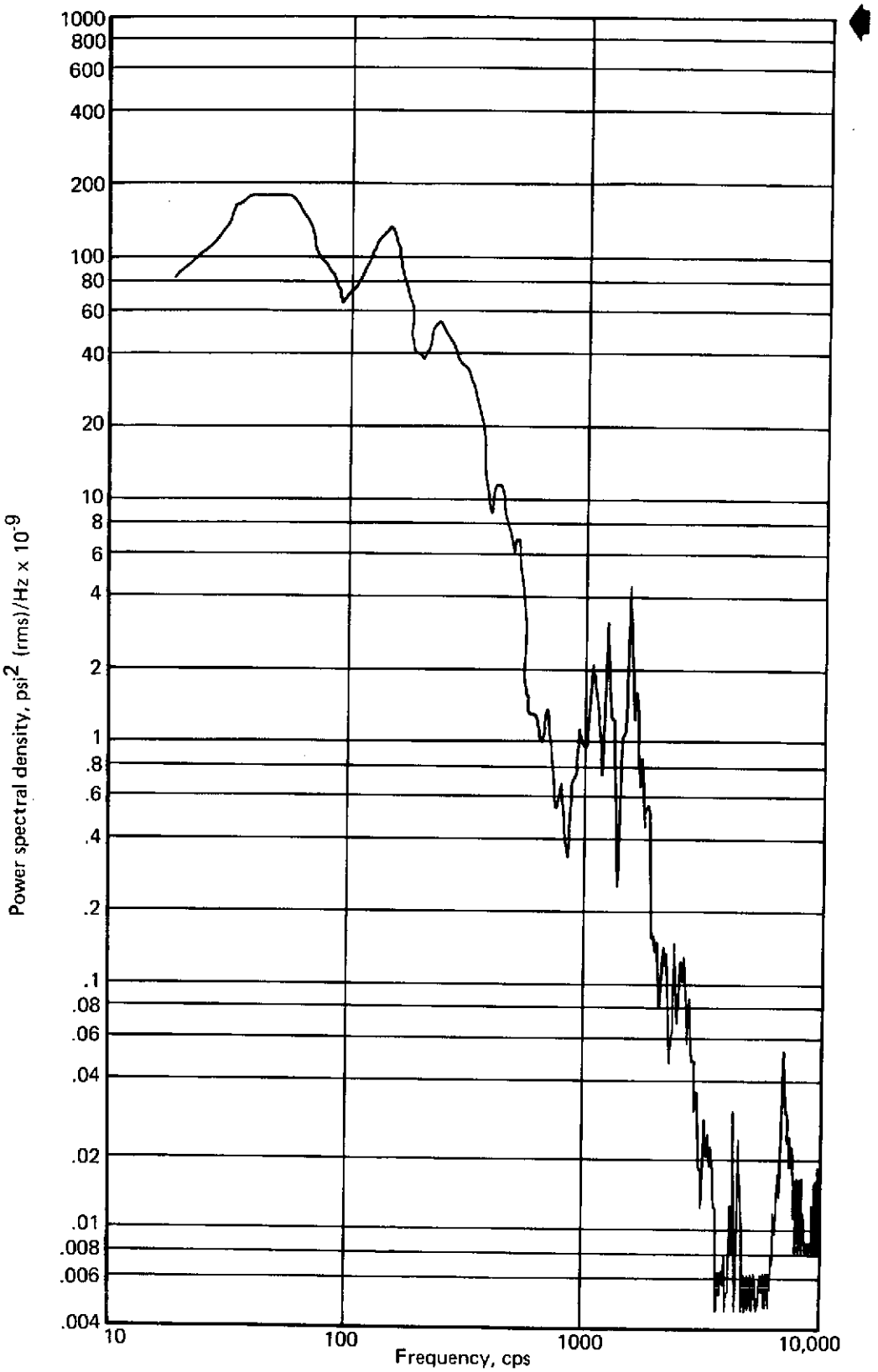

FIGURE 34.—SPECTRUM AT MUFFLER EXIT (TEST POINT 2), 22 PSIG

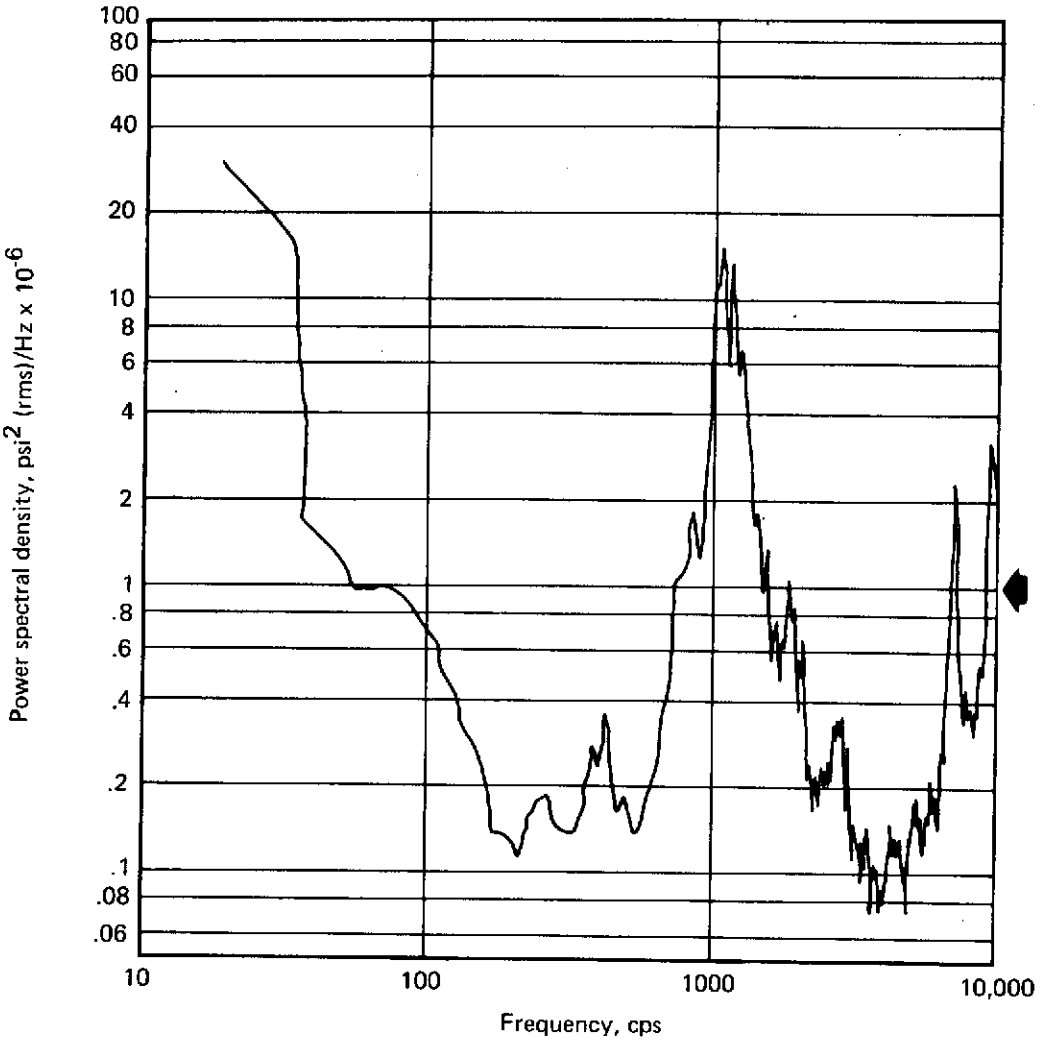

FIGURE 35.—SPECTRUM AT MUFFLER INLET (TEST POINT 1), 34 PSIG

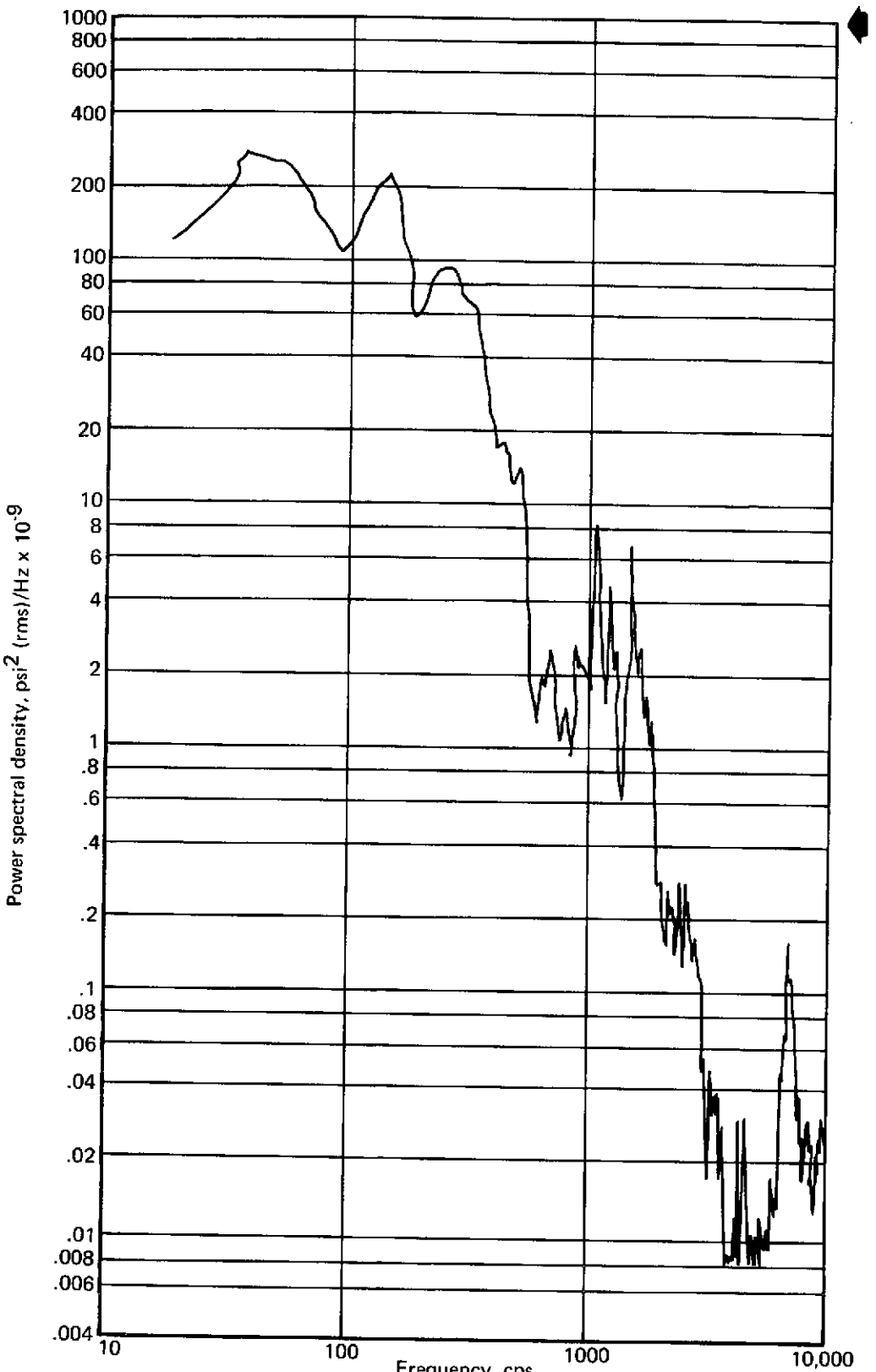

FIGURE 36.—SPECTRUM AT MUFFLER EXIT (TEST POINT 2), 34 PSIG

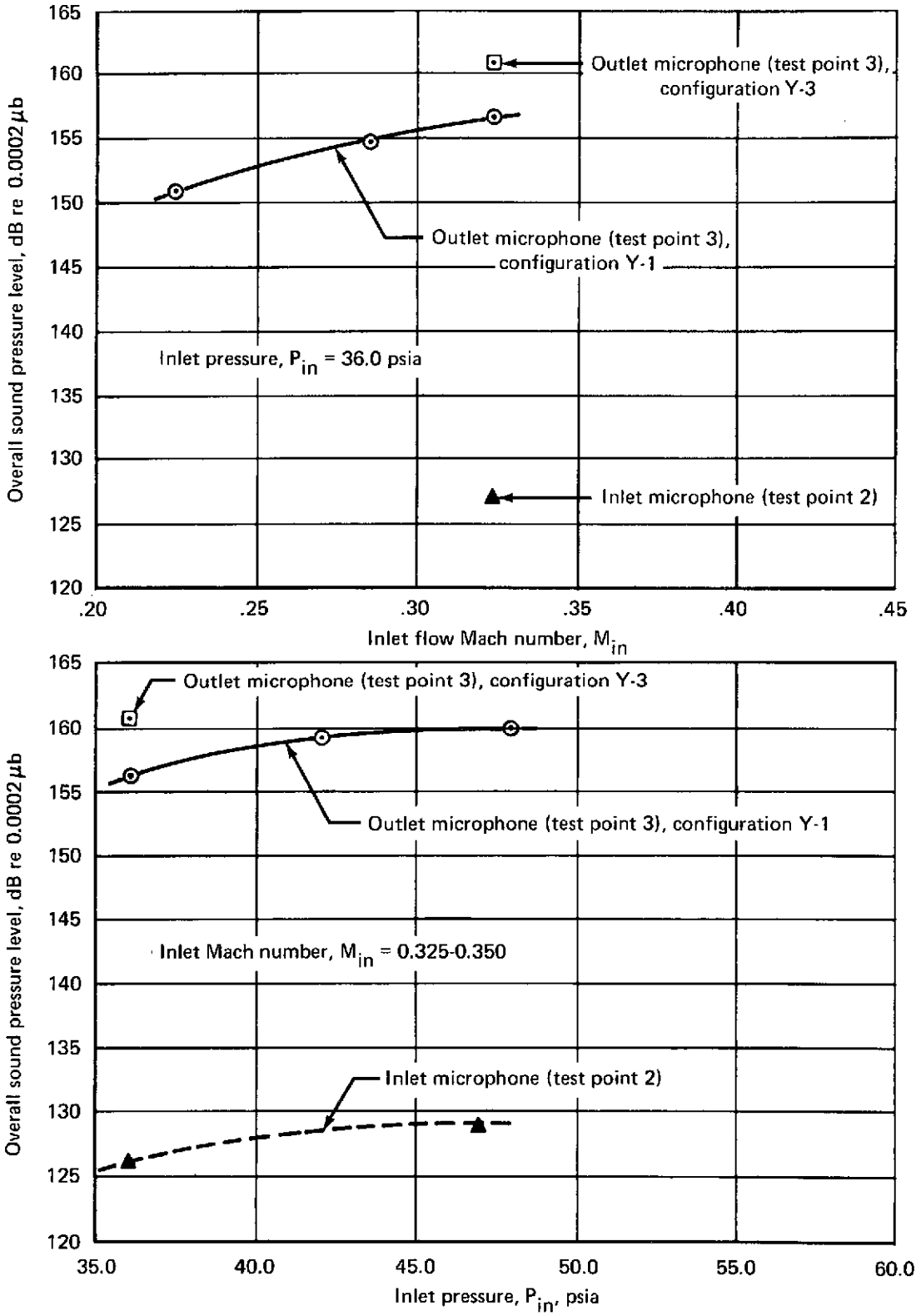

FIGURE 37.–EFFECT OF INLET MACH NUMBER AND INLET PRESSURE ON OVERALL SOUND PRESSURE LEVELS

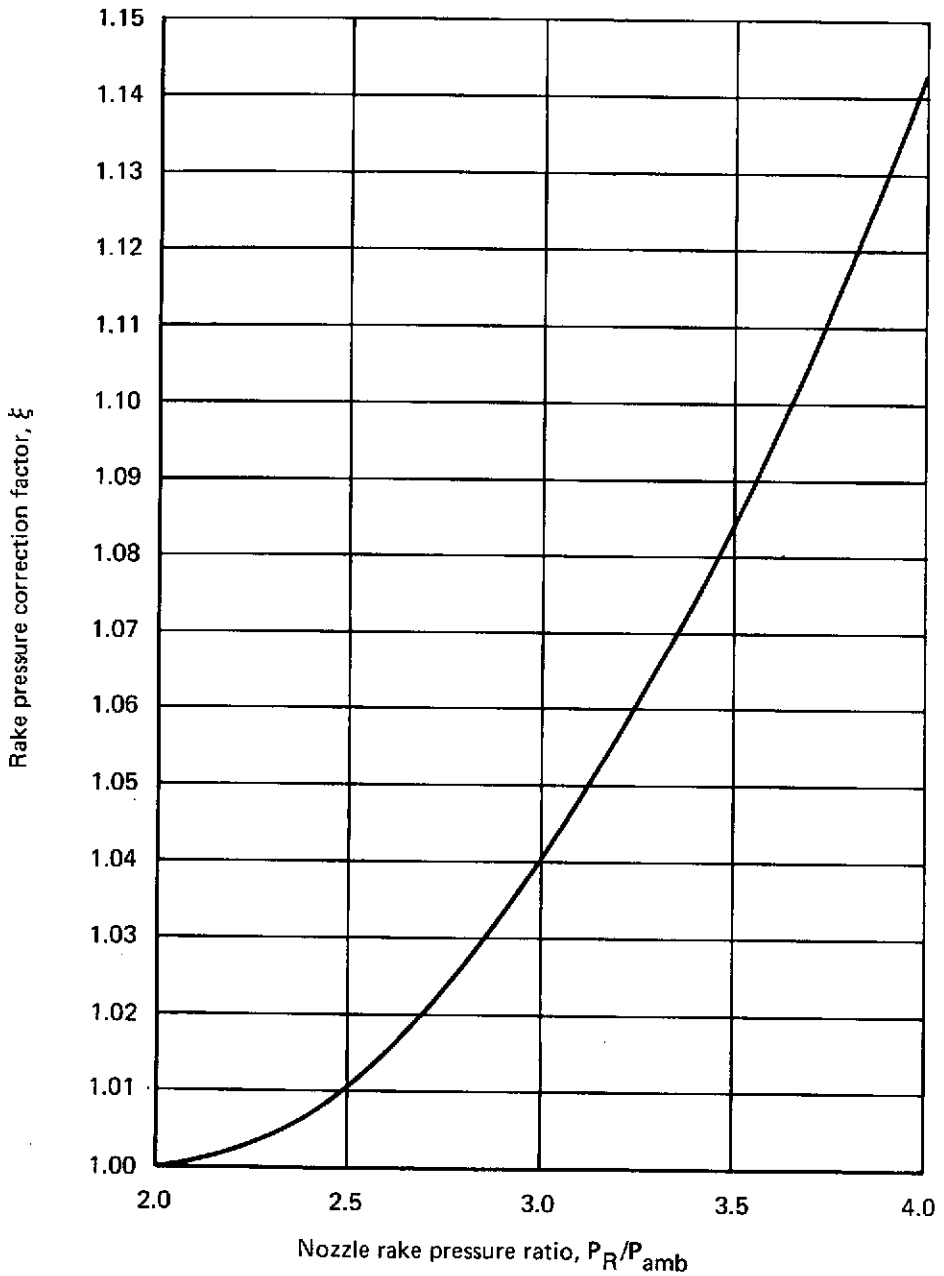

FIGURE 38.—COMPRESSIBILITY CORRECTION FACTORS

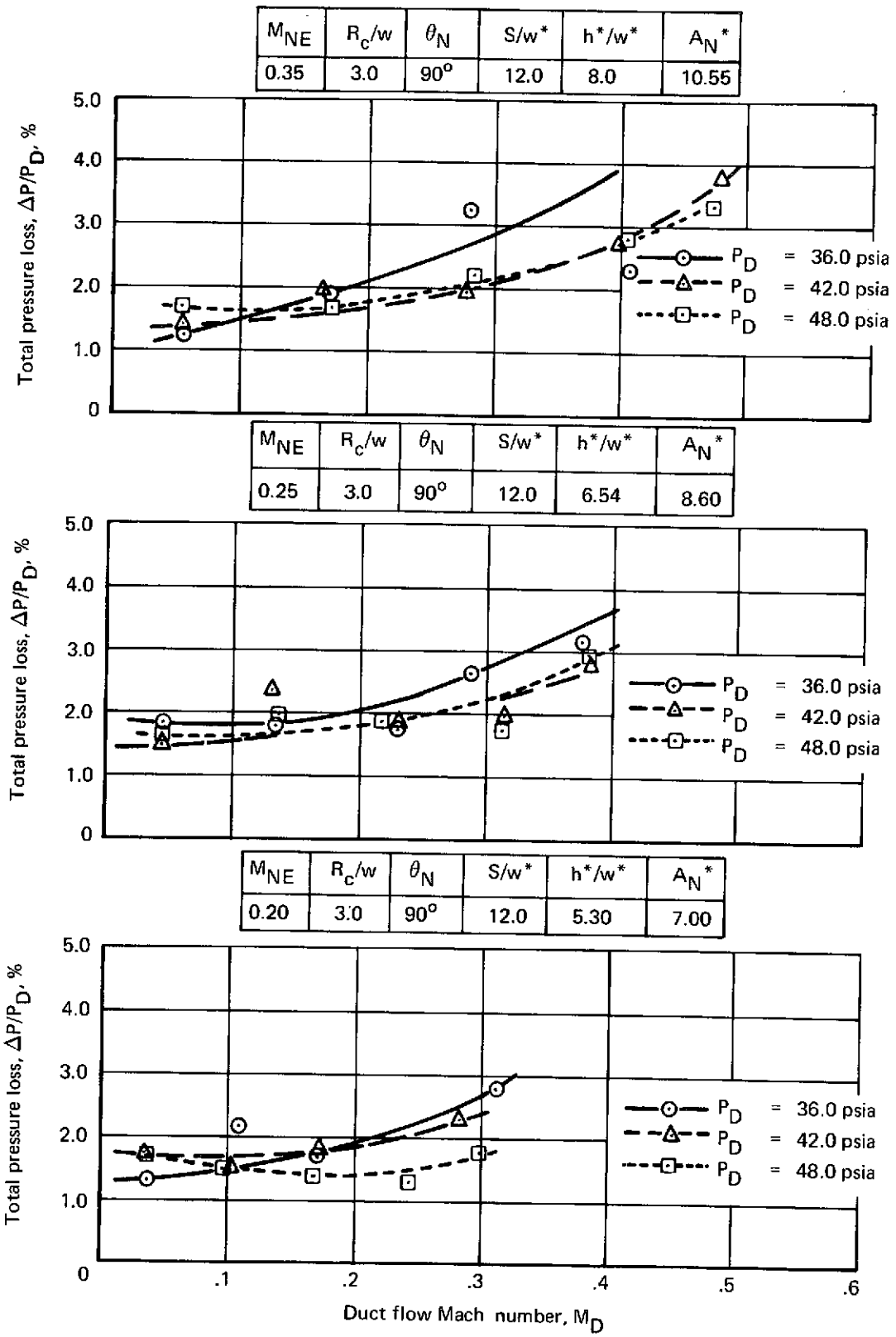

FIGURE 39.–PRESSURE LOSS CHARACTERISTICS–DNA-1

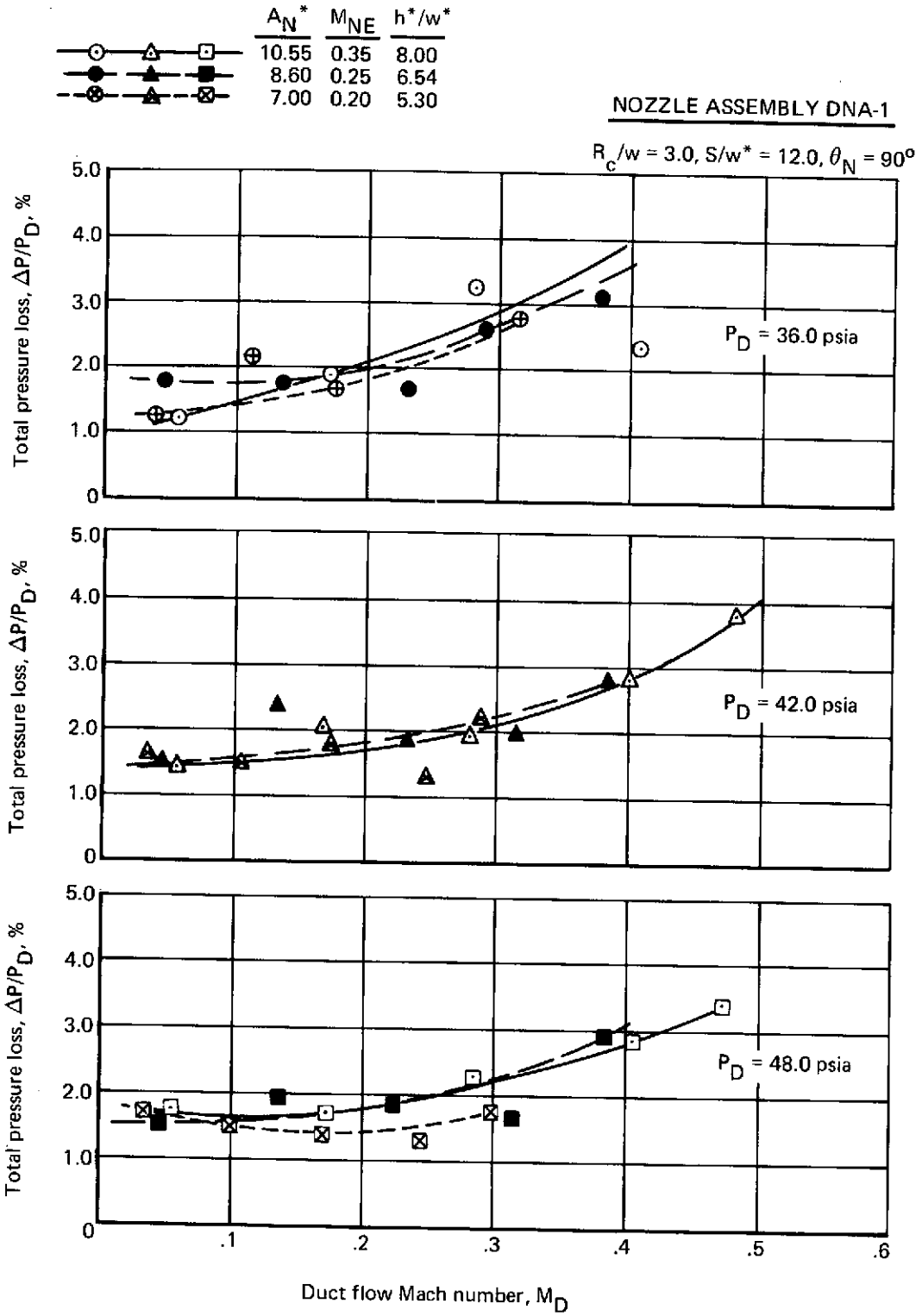

FIGURE 40.—ADDITIONAL PRESSURE LOSS CHARACTERISTICS—DNA-1

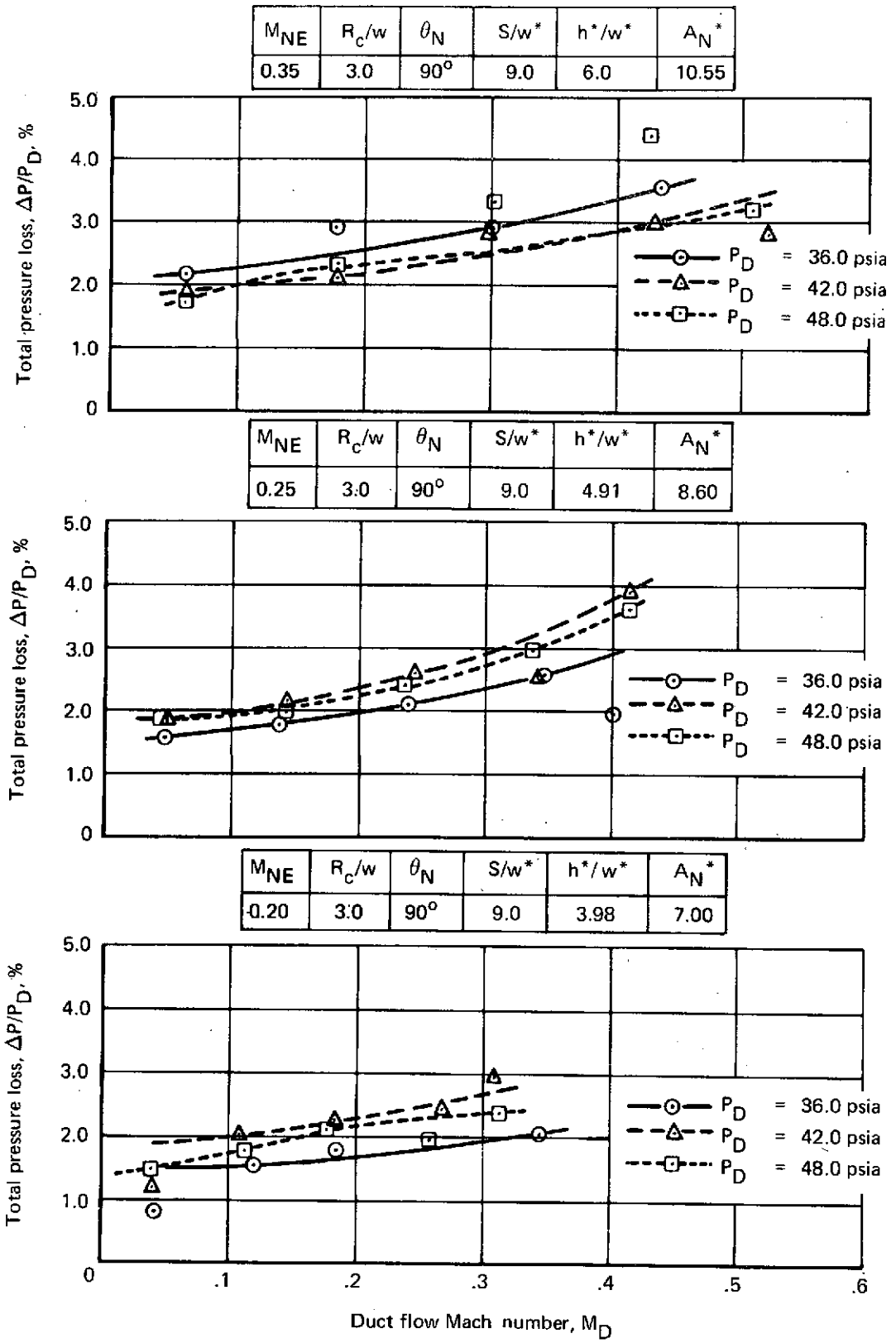

FIGURE 41.–PRESSURE LOSS CHARACTERISTICS–DNA-2

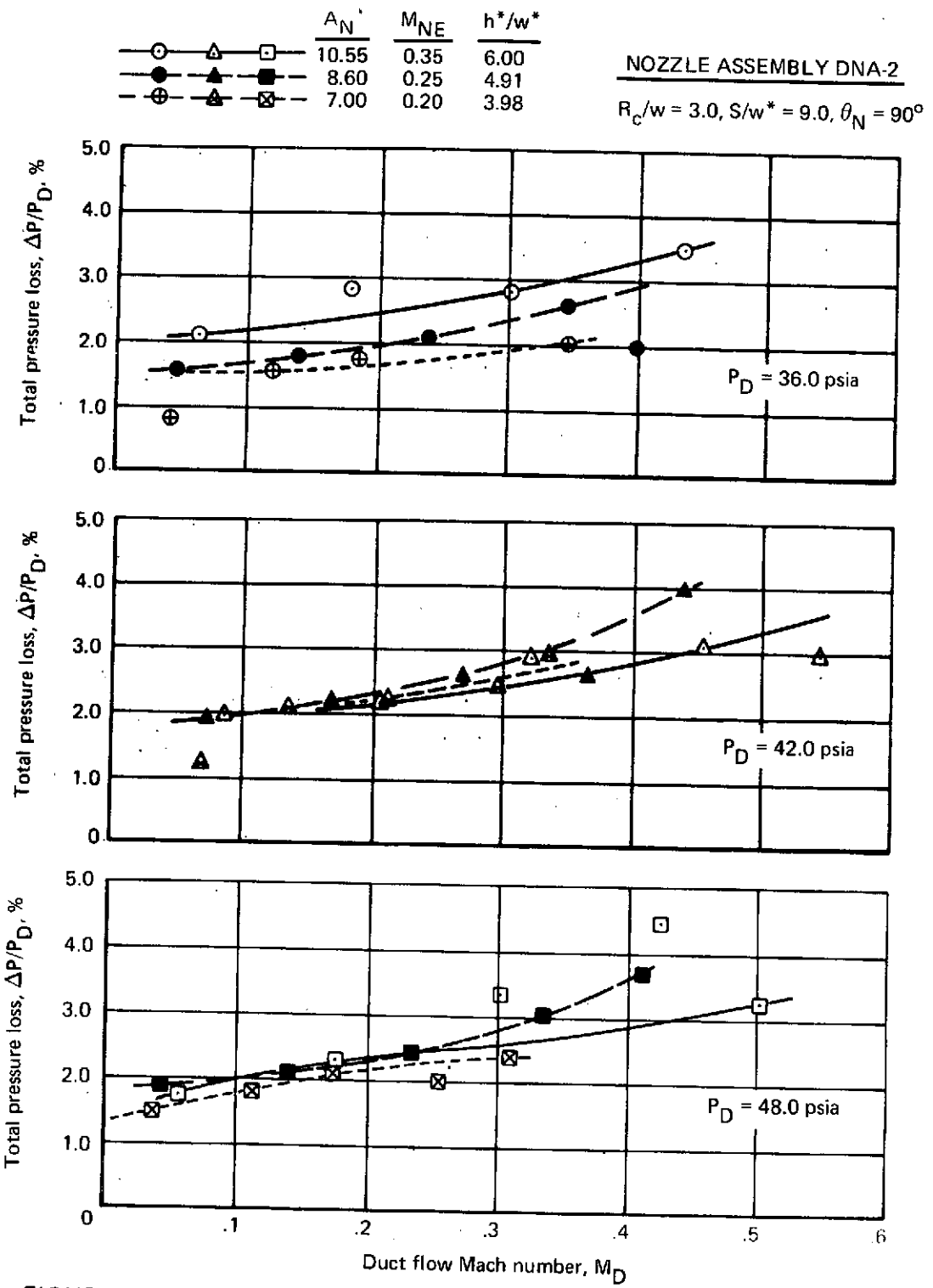

FIGURE 42.–ADDITIONAL PRESSURE LOSS CHARACTERISTICS–DNA-2

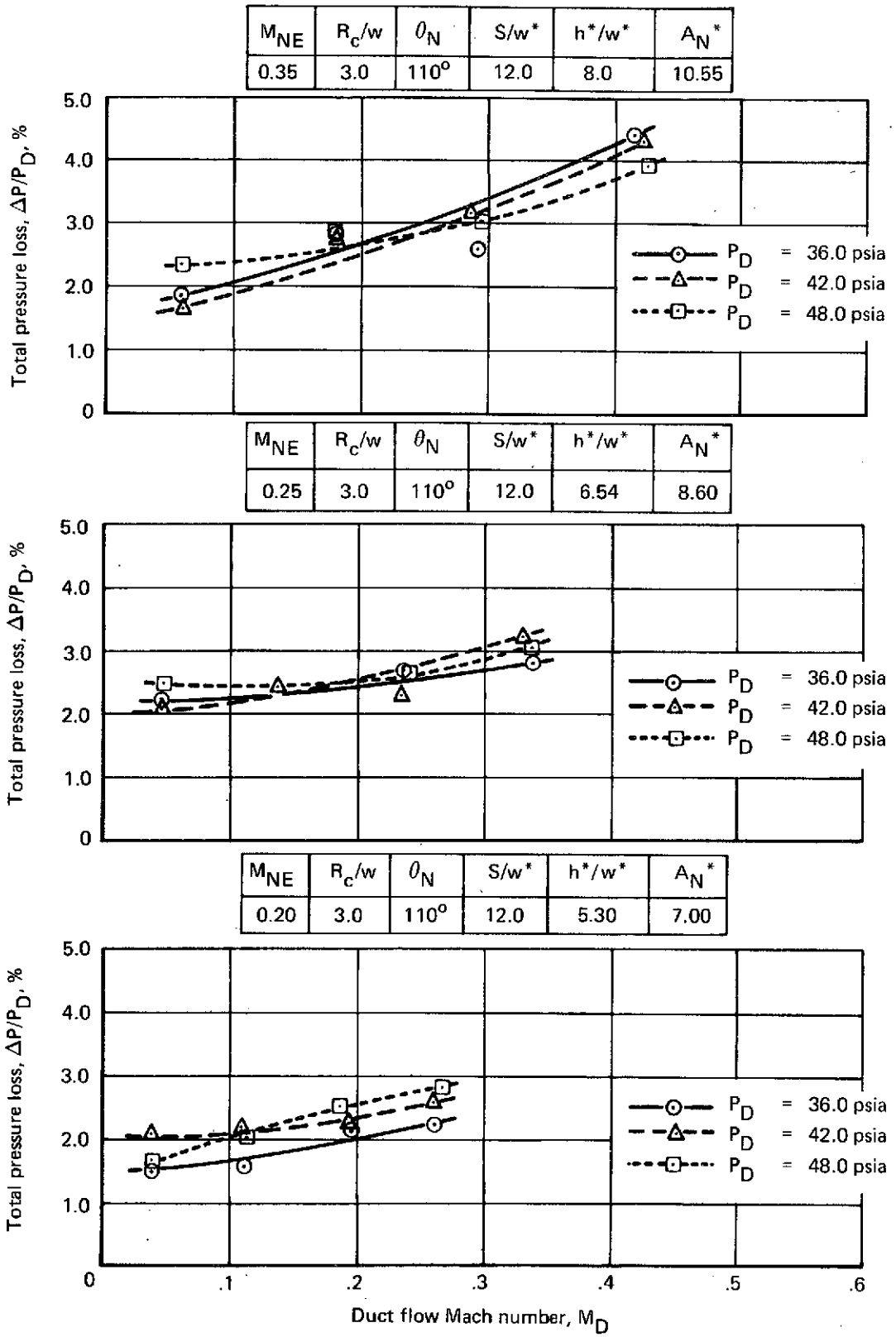

FIGURE 43.–PRESSURE LOSS CHARACTERISTICS–DNA-3

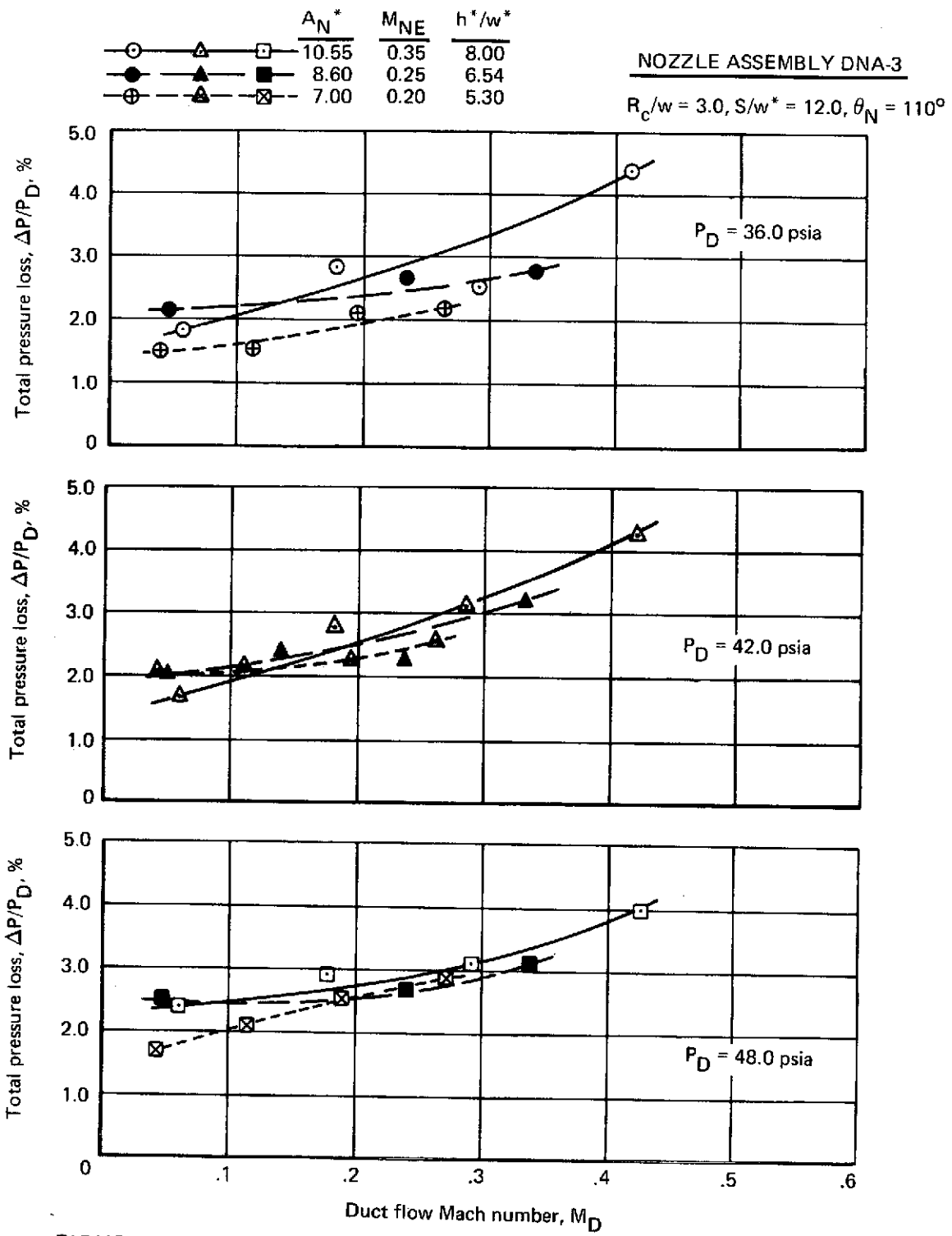

FIGURE 44.–ADDITIONAL PRESSURE LOSS CHARACTERISTICS–DNA-3

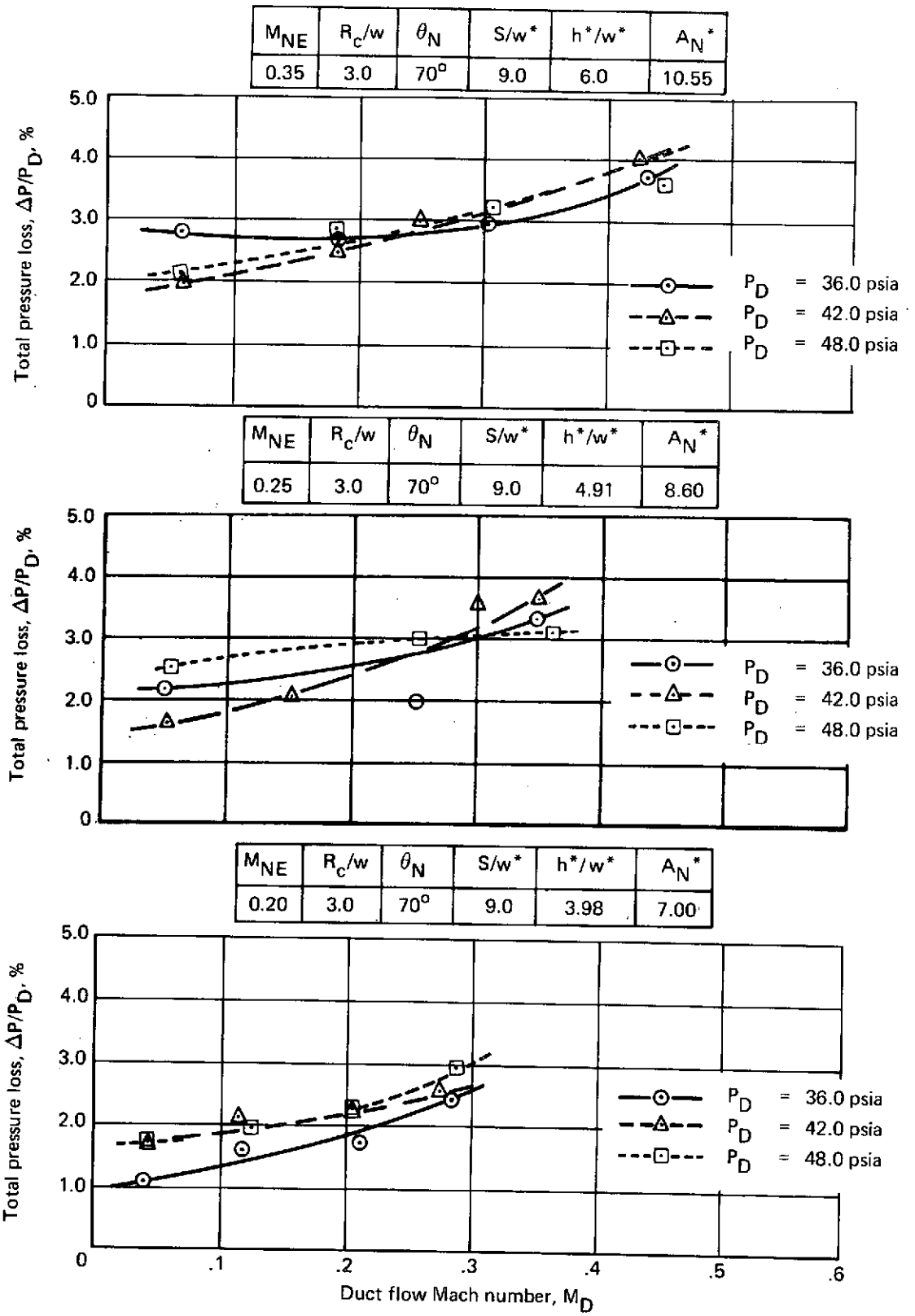

FIGURE 45.–PRESSURE LOSS CHARACTERISTICS–DNA-4

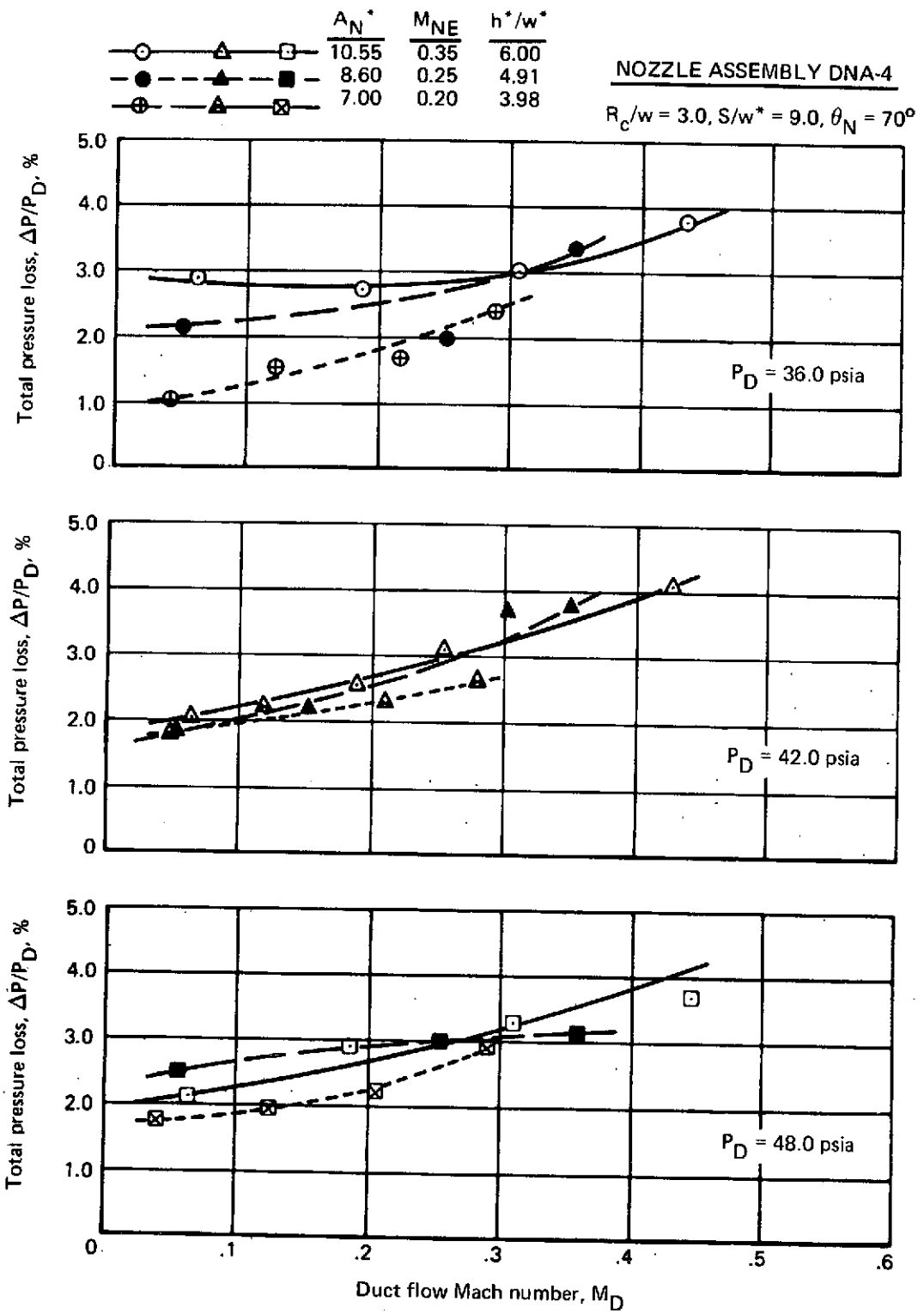

FIGURE 46.–ADDITIONAL PRESSURE LOSS CHARACTERISTICS–DNA-4

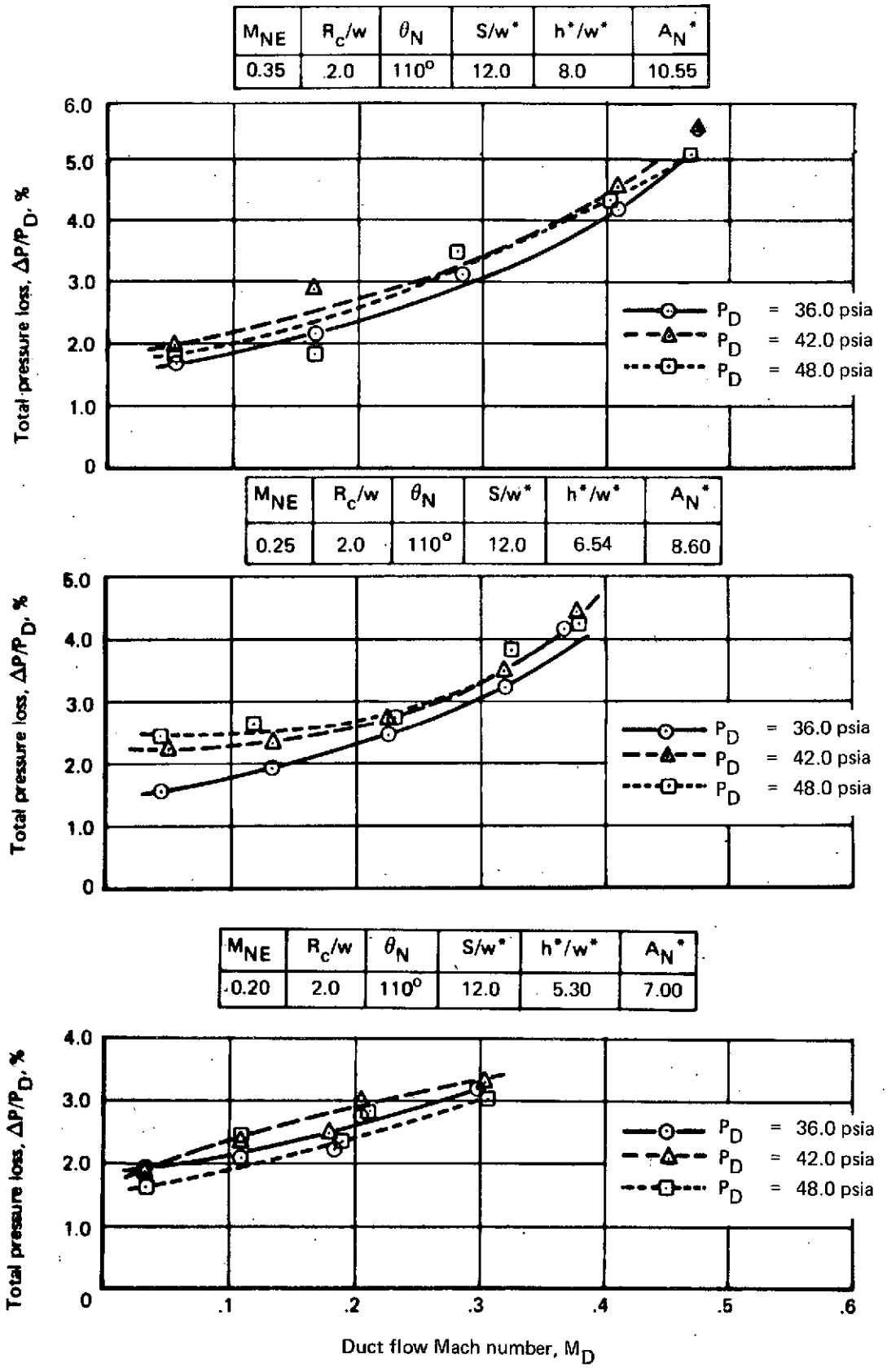

FIGURE 47.–PRESSURE LOSS CHARACTERISTICS–DNA-5

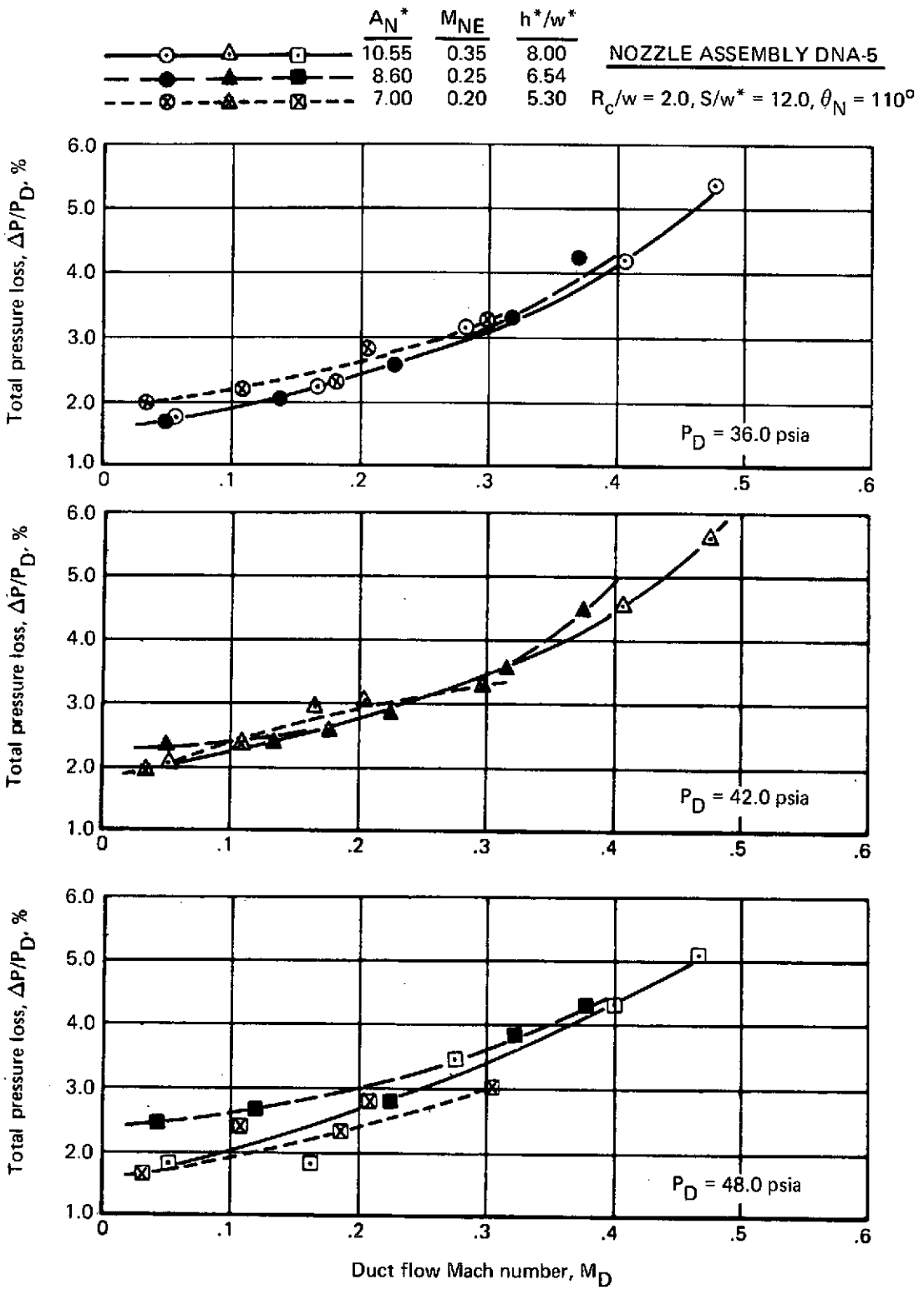

FIGURE 48.–ADDITIONAL PRESSURE LOSS CHARACTERISTICS–DNA-5

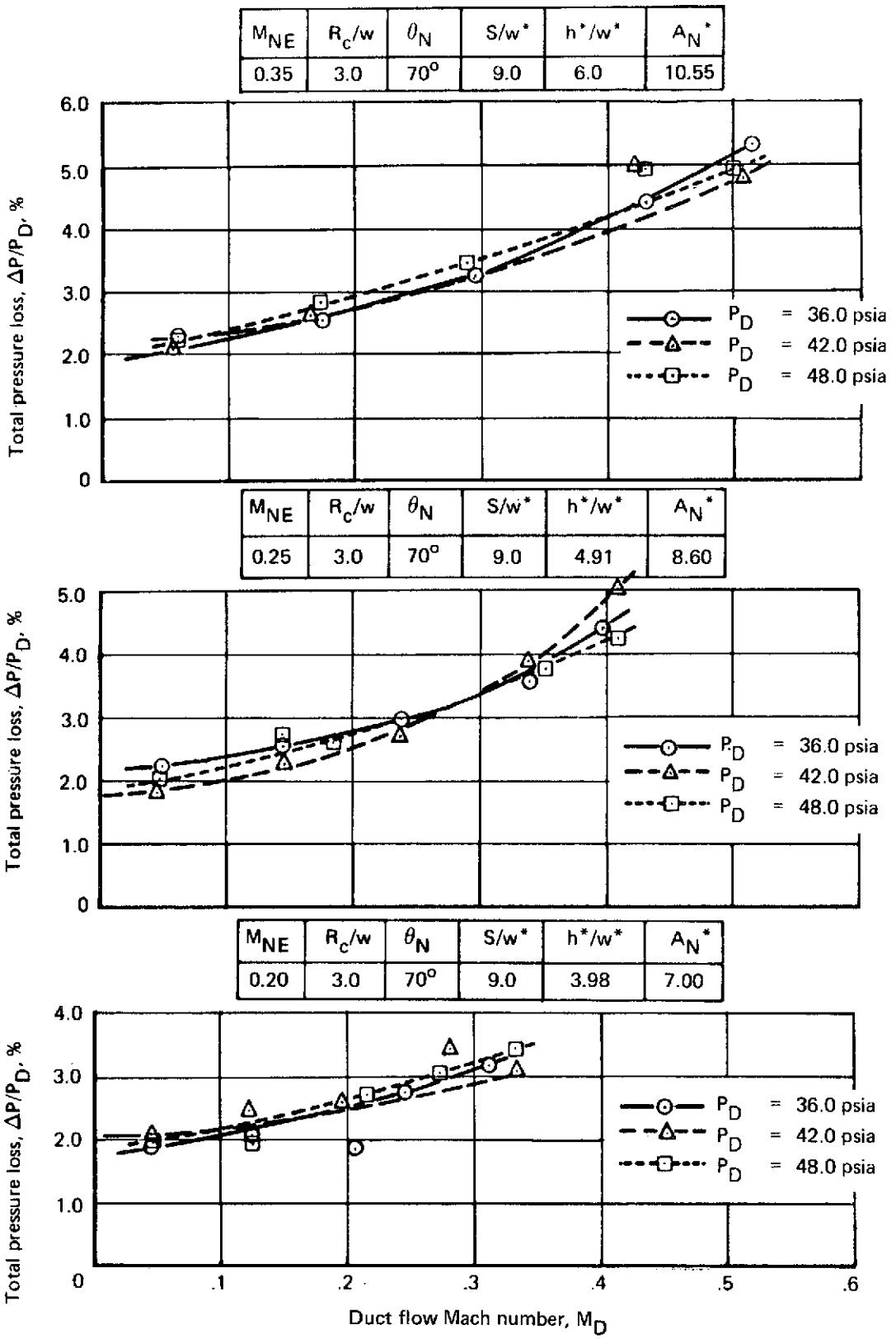

FIGURE 49.–PRESSURE LOSS CHARACTERISTICS–DNA-6

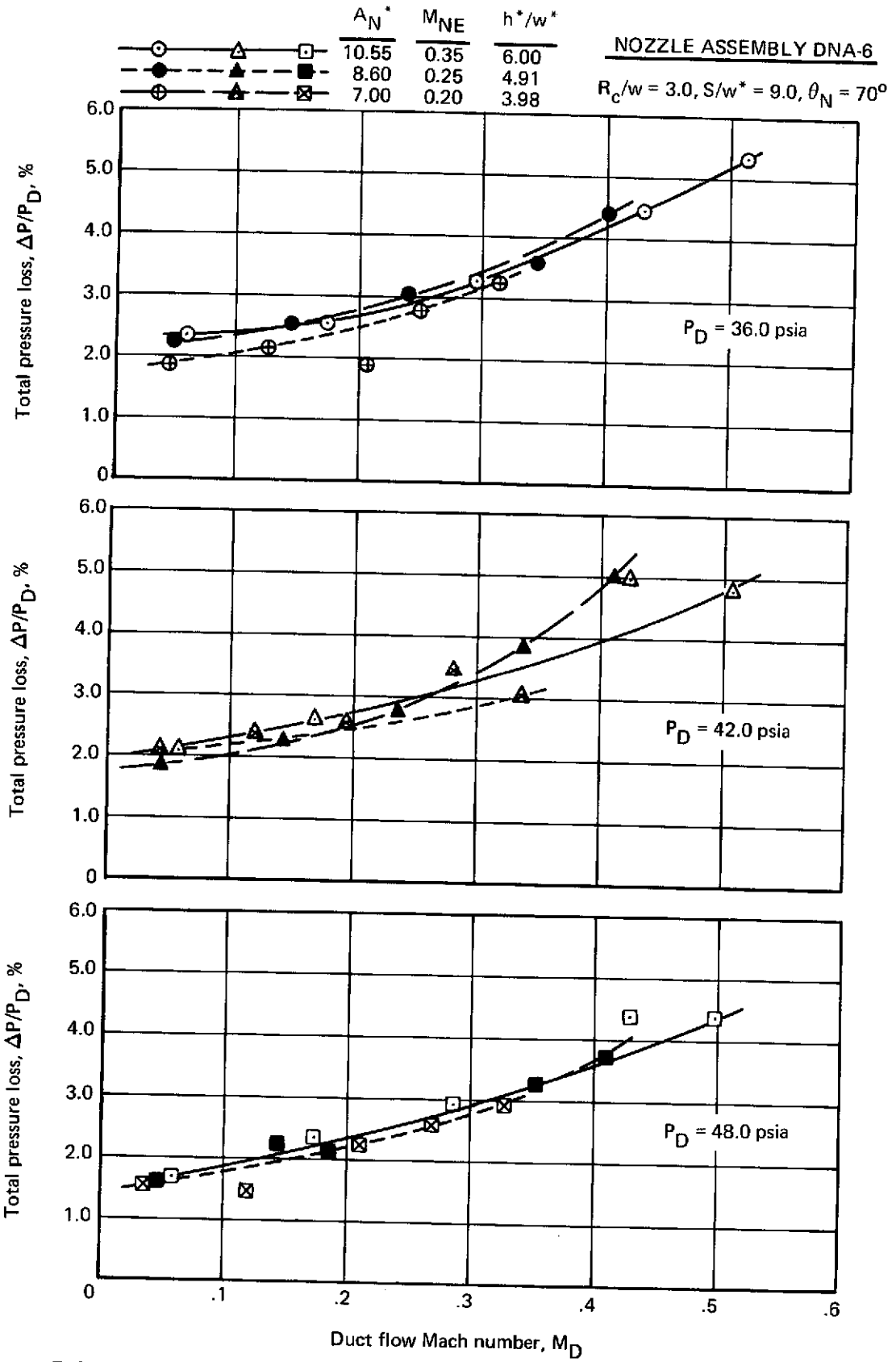

FIGURE 50.–ADDITIONAL PRESSURE LOSS CHARACTERISTICS–DNA-6

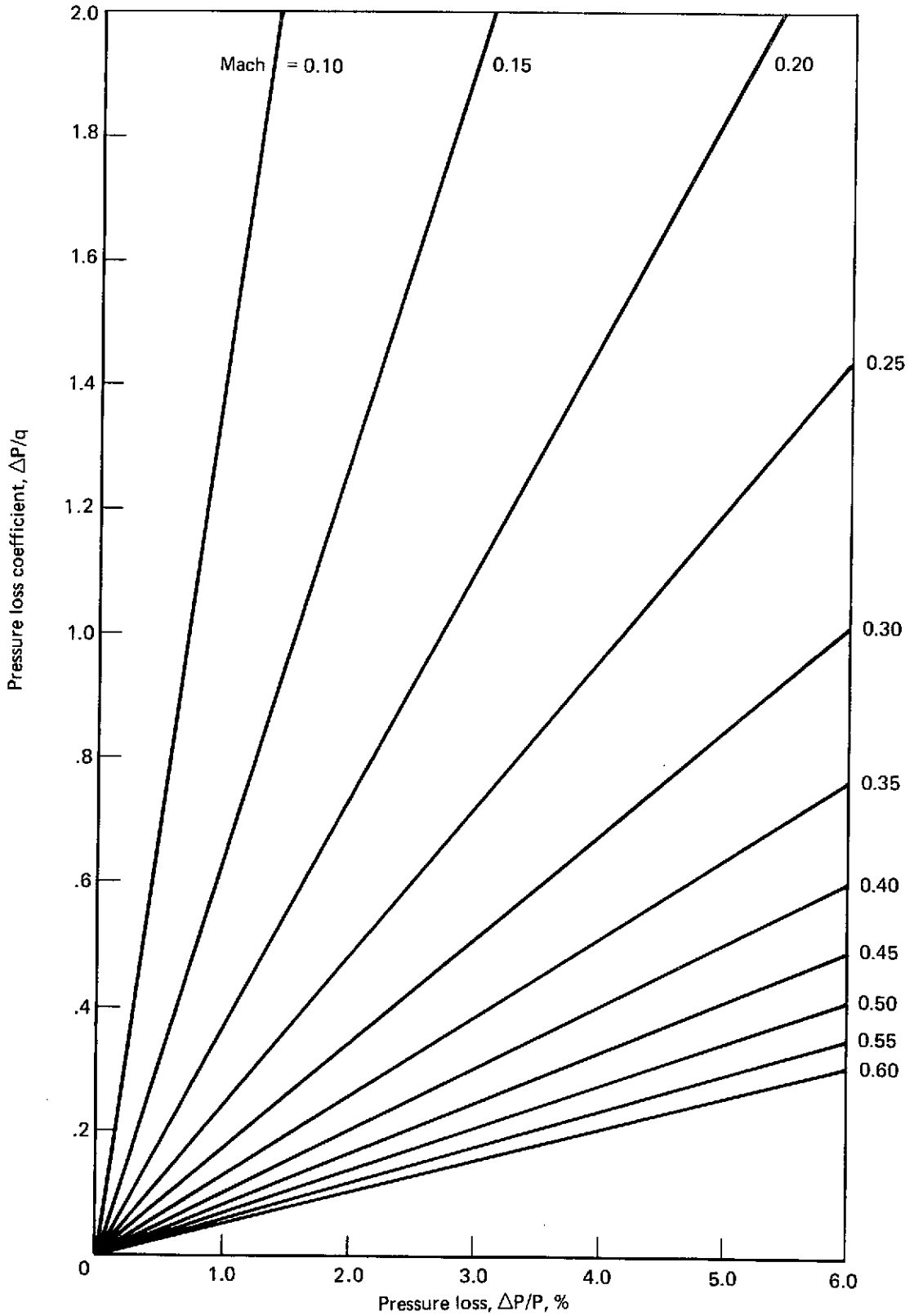

FIGURE 51.–PRESSURE LOSS COEFFICIENT/PRESSURE LOSS CORRELATION

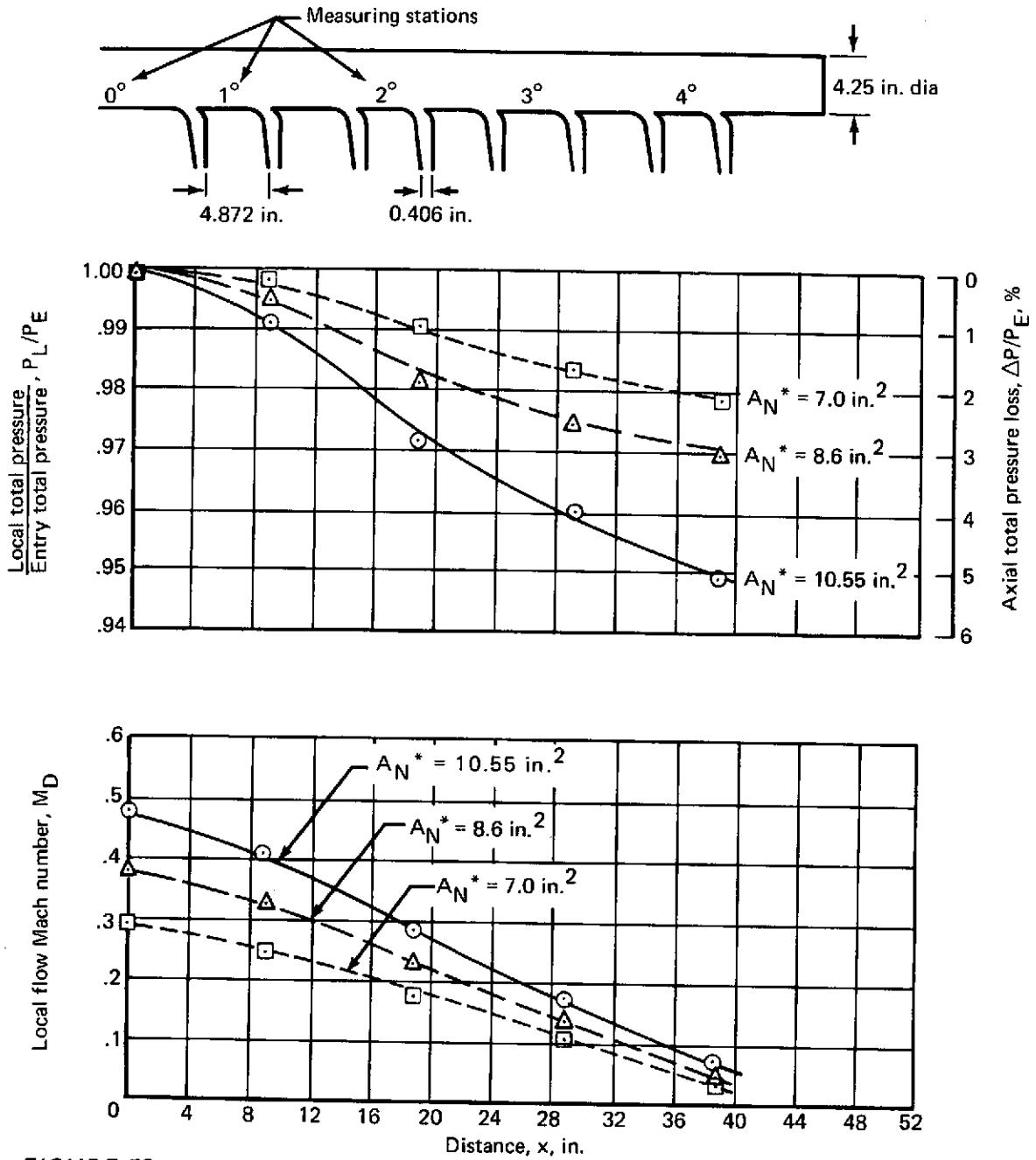

FIGURE 52.–AXIAL PRESSURE AND MACH NUMBER DISTRIBUTION FOR SET 1 DUCT NOZZLE ASSEMBLIES (DNA-1, -3, AND -5)

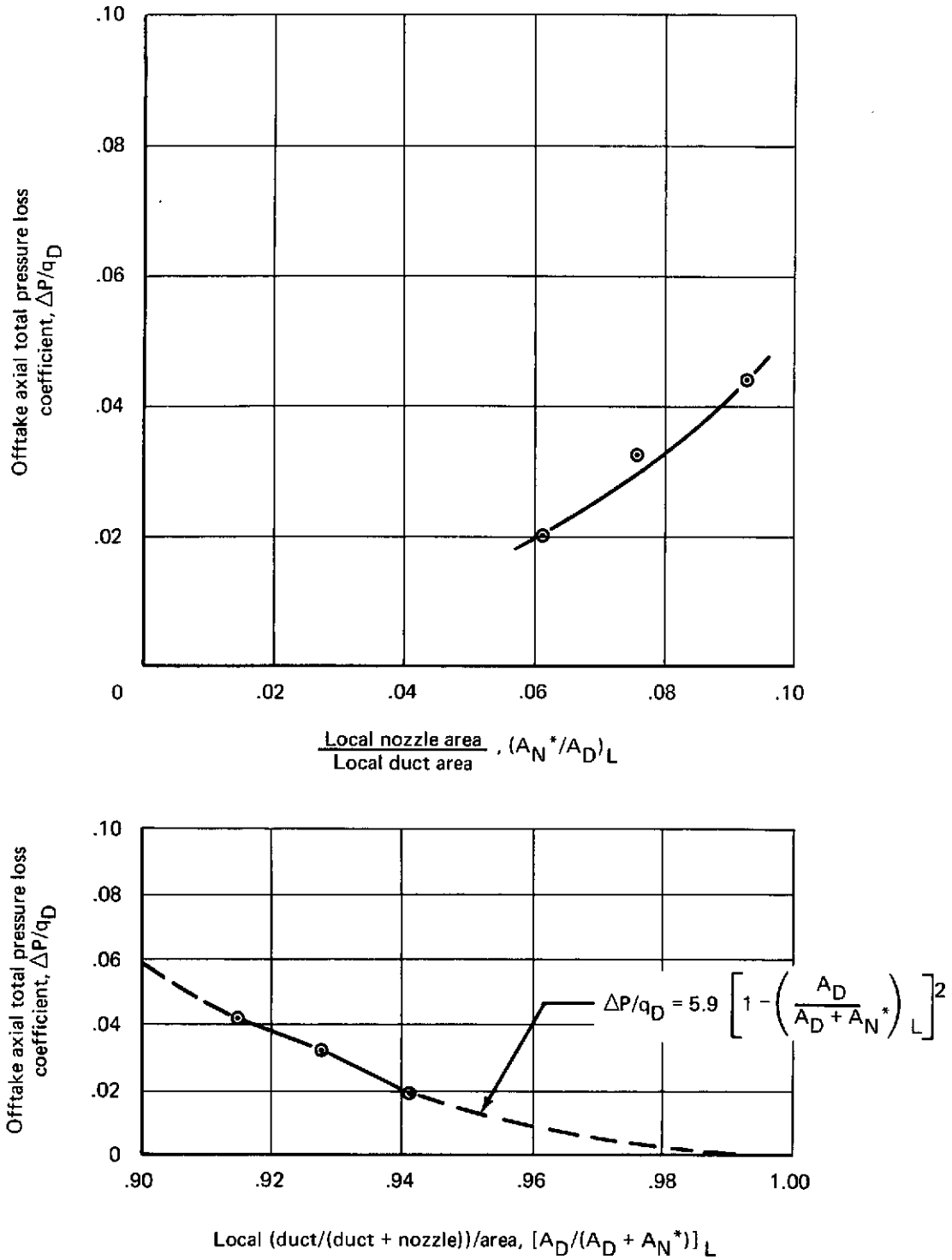

FIGURE 53.—OFFTAKE AXIAL PRESSURE LOSS COEFFICIENT